NTNU – Trondheim
Norwegian University of
Science and Technology

Polymer-Nanoparticle Hybrids For Drug Delivery Applications

Muhammad Awais Ashfaq
Alvi

Chemical Engineering
Submission date: July 2015
Supervisor: Wilhelm Robert Glomm, IKP
Co-supervisor: Sulalit Bandyopadhyay, IKP

Norwegian University of Science and Technology
Department of Chemical Engineering

Abstract

Combination of nanoparticles (NPs) and pharmaceutically active compounds like drug molecules are very effective in drug delivery systems due to their superior performance and selectivity. These advanced nanostructured drug carriers are also employed to deliver nucleic acids and proteins to the diseased site. Drug targeting and release to the infected site have now become popular both in *in vitro* and *in vivo* research areas. Multifunctional NPs used in drug delivery applications offers several advantages such as increase stability of NPs, modify optical, magnetic, electronic properties as well as incorporate biocompatibility and stimuli responsive behavior within a single framework.

Several studies have been done with inorganic NPs and polymeric NPs and combination of these, for example conjugation of thermoresponsive polymers with gold nanoparticles (Aunps) were studied and properties of these constructs were compared with the free polymer drug carrier system.

System used in this work is comparatively unique and different in the sense that Fe@Au NPs conjugated with hydrogels have not studied prior to this study. In this research, inorganic (Fe@Au) and polymeric NPs (pNIPAm/AAc and PEG) are gelled together, to from a multifunctional drug carrier. Most important attribute which these nanoconstructs should have is stability and effective release kinetics of the loaded drug. The master thesis has focused primarily on the loading and release of drug and protein molecules. First, Fe@Au were synthesized from previously established method at Ugelstad laboratory, NTNU. These NPs were then characterized using DLS (Dynamic Light Scattering), zeta-size, UV-vis (Ultra-violet spectroscopy) and S(T)EM. In order to investigate the variations of the sizes and zeta potentials as a function of temperature and pH (in case of size) as well as structural framework and UV-vis spectra of formed NPs respectively. Thereafter these NPs were coated with pNIMPm/AAc hydrogels (which were optimized previously at Ugelstad laboratory, NTNU), PEG and the combination of these polymers. Coated sample were also characterized with the same techniques as used for Fe@Au NPs. Loading studies were performer with three drugs L-dopa, coumarin and cytochrome c and estimated with UV-vis using calibration curves for the drugs. Drug loading was optimized and concentration of drug and NP which gives maximum loading efficiency was used for the release studies. Release of the loaded drugs were observed at high temperature (40^oC) and low pH (3.5). Drug release was also measured with UV-vis.

Two methods were used for coating of Fe@Au NPs, method 1 and method 2. Method 2 provides better loading efficiencies compared to method 1 and therefore used in this study. Size of pNIMAm/AAc based hydrogels decreased at higher temperature due to transition from hydrophilic to a hydrophobic state. VPPT for heating and cooling shown by hydrogels alone is 38^{o}C, which indicated their reversibility. Size increased for Fe@Au NPs coated with the hydrogel probably due to the cross-linking effect provided by Fe@Au NPs. VPTT is observed when for heating and cooling is calculated as 39.8^{o}C and 39.5^{o}C for coated samples. Fe@Au_PEG_Hydrogel system shows appreciable reversibility with VPPT values for heating and cooling reported as 37.1 ^{o}C and 36.7 ^{o}C. pH Effect on size is similar to temperature effect. Cytochrome C loading shows high loading efficiencies of 31.66 % and 32.57 % for Fe@Au_Hydrogel and Fe@Au_PEG_Hydrogel respectively. Highest release of 87.20 % was obtained from Fe@Au_Hydrogel system, while Fe@Au_PEG_Hydrogel system shows fastest release rate. In case of Cytochrome C, both highest and fastest release were given by Fe@Au_PEG. However, Fe@Au_PEG_Hydrogel system also shows almost identical $t^{1/2}$ in comparison to Fe@Au_PEG.

Polymer-NPs hybrids shows promising loading and release of the drugs with change in temperature and pH. Which highlight their superiority as a drug carrier compared to only polymeric and inorganic system. Further studies with these systems can be developed in which two drugs at the same time can be loaded and released from this nanocarrier system.

Acknowledgement

Foremost, I would like to express my profound gratitude to my supervisor Professor **Wilhelm Robert Glomm** for his exceptional supervision, valuable research guidance and continuous support at every stage of the project.

I would like to extend my whole-hearted thanks to my co-supervisor **Sulalit Bandyopadhyay** for his motivation, encouragement and unparallel support in every field, whether it's experimental work, results analysis or report writing at all levels of the project. His exceptional support can not be gratituted in terms of words.

Thanks a lot to my advisor **Birgitte Hjelmeland McDonagh** for enlightening me with her immense knowledge and valuable suggestions at various stages of the project.

My deepest gratitude for my **family** for their endless love, support & encouragement and who have been the pillars of my success in all that I have achieved so far.

I do extend my sincere thanks to my friends **Ata ul Rauf Salman** and **Anuvanash Sharma** for their support, suggestion and help throughout the course of work.

I would also like to extent my thanks to NTNU Nano-Laboratory and SINTEF for funding this research work.

Finally, I must thank **God** for bestowing upon me his blessing and giving me the strength for making this attempt a fruitful one.

"I declare that this is an independent work according to the exam regulations of the Norwegian University of Science and Technology (NTNU)."

Contents

List of Figures

List of Tables

Dedicated to Nature,

Its Creator
and My Family...

Chapter 1

Introduction

1.1 Nanoparticles

Nanoparticles (NPs) can be defined in terms of diameter as the particles which have dimensions in the range from 1 to 100 nanometers [1]. NPs have gained immense attention of researchers in recent years due to their size dependent properties.

Nanotechnology is the science that addresses the process which occurs at molecular and atomic levels. It concerns with the design, synthesis and characterization of nanostructures by regulating the size and shape at nano scale. Nanomaterials have a high surface area to volume ratio which finds applications in different fields like catalysis, drug delivery, imaging and so on. Magnetic, thermal and electrical properties of these nanomaterials also vary from the bulk properties due to transition to the nano regime. For example, the melting point of gold changes from 200 ^{o}C to 1068 ^{o}C at nanoscale [2].

Latest therapeutic and diagnostic concepts in the medicine field are mostly based on nanotechnology because of better performance [3]. NPs are getting great attraction particularly in the field of drug delivery, due to their unique properties and very few side effects [4]. It is expected that the global market for drug delivery will rise from US$ 131.6 billion in 2010 to US$ 175.6 billion by 2016, that is rise in the market value at a compound annual growth rate of 5 %. Furthermore, this increase will be continuous and the market value will reach a value of US$ 225.8 billion by 2020 [5] as illustrated in Figure 1.1 a) and b).

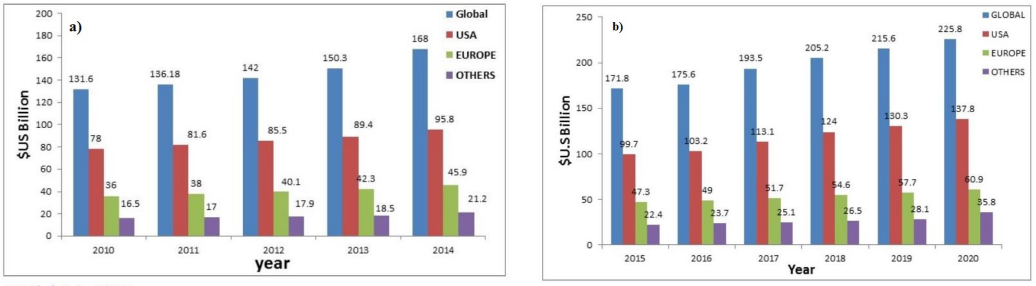

FIGURE 1.1: a) Worldwide Drug Delivery Market 2010-2014 b) Worldwide Drug Delivery Market 2014-2020 [5]

Currently, there are around 30 drug delivery products in the market for cancer treatment, with a total annual income of about US 33 billion. About 15 % increase in growth is expected on an annual basis. In 2011, the global market for NPs in drug development and drug delivery was worth around 17.5 billion and it is expected to rise to 53.5 billion in 2017. Moreover, in 2021 it is expected that the market value will increase to 136 billion (cancer treatment) [6]. Figure 1.2 shows the global market trend nanotechnology in drug delivery for cancer treatment.

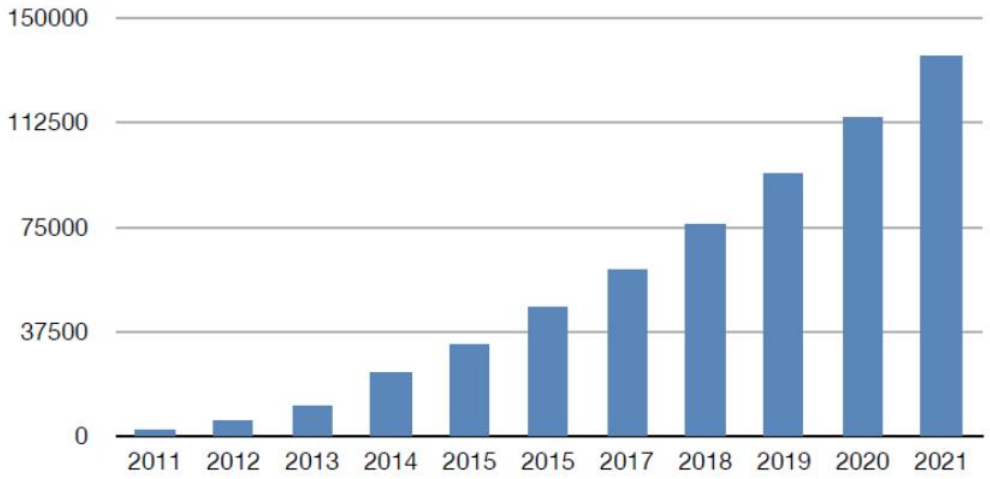

FIGURE 1.2: Global Market trend for Nanotechnology in Drug Delivery for cancer treatment [6]

Several processes are used for nanomaterials fabrication. Synthesis methods vary because of a number of factors like approach used (top-down/bottom-up), phase of synthesis (gaseous/aqueous phase), type of nucleation (heterogeneous/homogeneous), media used for synthesis (bulk/emulsion), and type of core/shell (magnetic or other), type of material (organic/inorganic). In this chapter, different types of NPs, both inorganic and polymeric, will be first discussed in terms of their synthesis and properties. Then, the

suitability of such with respect to drug delivery applications will be discussed. Thereafter, a detailed insight would be given into various modes of drug delivery. Finally, an overview of release kinetics models will be given.

1.2 Inorganic NPs

Depending on the end use, inorganic NPs can be synthesized using different methods. Further, the choice of method depends on intended particle size, shape, distribution, surface functionality and so on [7]. Among various kinds of inorganic NPs, metallic core-shell NPs have gained immense attention in the recent years, owing to their multifunctional properties, stemming from different counterparts.

1.2.1 Synthesis Methods for Core-Shell NPs

Synthesis of core-shell NPs is a two-step process, in the first step, core is formed, while in the second step, shell formation takes place. Two routes (i) pre synthesized and (ii) in-situ synthesis are normally employed depending on the availability of core. In pre synthesized process, core and shell synthesis take place separately. First, core particles are produced and afterwards, clean and dried particles are put in a separate reaction mixture to produce the shell. However, in case of in-situ production method, reactants used for shell formation are added to the already synthesized core [8]. Both routes face problems of agglomeration of particles, incomplete coverage of the core, and poor control over the reaction rate [9]. Some of the synthesis methods which are widely used to produce such NPs are discussed in the following sub-sections.

1.2.1.1 Solution Based Synthesis

Solution based synthesis of NPs is generally based on the reduction of metal complexes in dilute solution. Different methods have been established to start and control the reduction reactions [10]. The sequence for the formation of NPs by this method is shown in Figure 1.3.

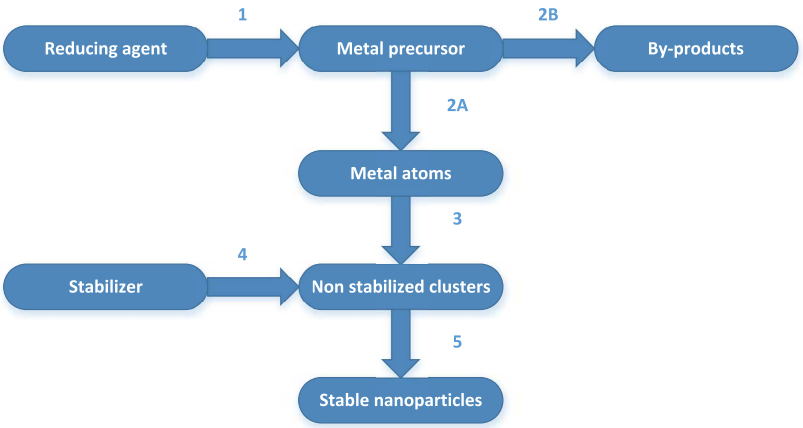

FIGURE 1.3: Sequence for the formation of NPs in solution based synthesis [11]

Aqueous medium, use of surfactants and reducing agents all are important and play major roles in the preparation of metallic NPs. Different kinds of metal precursors, reducing agents and stabilizing agents are used, also the strength of the reducing agent plays critical role in controlling the reaction rate and particle size [8].

Metal precursors used are combinations of elemental metals, inorganic salts and metal complexes, for example, Ni, Ag, Co, Fe, Ni, $HAuCl_4$, H_2PtCl_6, $RhCl_3$ and $PdCl_2$ [10]. Mostly used reducing agents are sodium borohydride [12], hydrazine, sodium citrate, hydrochloride (salt formed by reaction of hydrochloric acid with base) , citric acid, carbon monoxide, sodium carbonate and sodium hydroxide [10]. Stabilizers like polyvinyl ether, polyvinyl alcohol and sodium polyacrylate are used to stabilize formed NPs [13].

Reducing agent has a significant effect on the size and size distribution of the NPs. Small NPs are generally formed by strong reduction reaction as they promote fast reaction rates [10]. Narrow or wider size distribution of particles can be achieved with slow reaction rates depending on the formation of new nuclei or secondary nuclei. The strength and concentration of the reducing agent dictates the supersaturation. Higher supersaturation leads to the formation of a large number of nuclei, and hence small sized NPs [10].

NPs are stabilized with different polymers that provide steric stabilization and prevent agglomeration of the NPs. Interaction of polymer stabilizers with the surface of solid particles is highly dependent on the type of polymer, solvent, surface chemistry of NP and temperature. Stabilizing agents also provide functionalization of NPs like polarity change, solubilisation and capacity to encapsulate new molecules. NPs can be functionalized with more than one type of ligand, these are called multifunctional nanoparticles. Multifunctional nanoparticles are very popular in drug delivery systems [10].

1.2.1.2 Electrotemplating

In this method, electrolysis process is utilized in which anode is made of (required) metal and cathode is inert. Solution of stabilizer is electrolysed. Oxidation of anode material causes its dissolution under specific conditions of electrolysis. Movement of cations towards cathode causes the reduction, nucleation and stabilization. Current density can be used to change the size of the NPs prepared by this method. Formation of bi metallic nanoparticles can occur by employing pair of anodes of different metals. Sometimes it is difficult to cause the oxidation of anode metal, this problem can be solved by introducing metal as an inorganic salt [11].

Electrochemical process is also used to produce NPs from polymers and dispersions of NPs in aqueous medium. In a relatively new method, deposition of NPs (which were first added in aqueous phase) is done on conductive polymer using required electric field [11].

Electrochemical synthesis of NPs has become important especially in the preparation of composites of metal particles and conducting polymers as core-shell constructs. NPs in polymer matrix increase the mass transfer parameters of the nano-composites because electron tunnelling distance is shortened. Properties like this make polymer/stabilized metallic NPs an important class of materials [11].

1.2.1.3 Sol-gel

Sol-gel is an extensively used process for the preparation of metal oxide NPs; it is a wet chemical method. This process involves hydrolysis and polycondensation of precursors like metal alkoxides or chlorides, leading to the formation of solid-phase network (dispersion of oxide particles in a solution) [8][14].

Solvent removal or chemical reaction is used to dry or gel the sol. Precursors can be hydrolyzed with an acid or base but in most cases, water is used. There are three different routes into which sol gel process can be divided (i) gelation of colloidal powder solutions (ii) hydrolysis and polycondensation of metal salt precursors succeeded by aging and drying under ambient conditions and (iii) hydrolysis and polycondensation of metal precursor succeeded by hypercritical drying of the gels [15].

To form a sol or colloidal suspension, the precursor goes through a series of polymerization and hydrolysis reactions. Hydrolysis and condensation rates can change the properties of end product, for example, slow and controlled hydrolysis rates give small particles[16][17]. Temperature and pH also affect the particle size. Iron oxide supported

on silica gel[17] and magnetite [18] have been prepared very often by this method. Schematic representation of sol-gel process is shown in Figure 1.4.

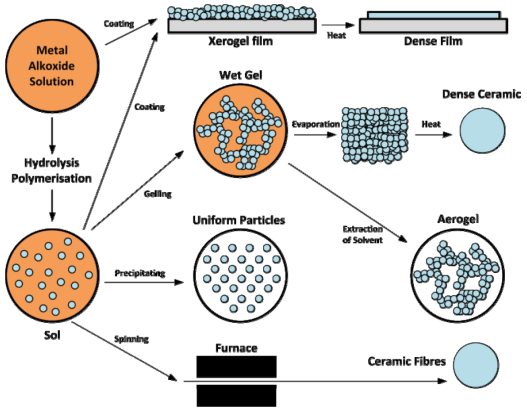

FIGURE 1.4: Schematic representation of sol-gel process [19]

1.2.1.4 Micro-emulsion based synthesis

In this method, two immiscible liquids are dispersed to form a thermodynamically stable, isotropic system. Interfacial film of surfactant molecules is used to stabilize the micro domain of two liquids [20]. Water phase is dispersed as micro-droplets having 1-50 nm diameter. A monolayer of surfactant molecules in the hydrocarbon phase surrounds these micro-droplets. Molar ratio of water to surfactant is used to estimate the size of the reverse micelles and hence the size of the NPs [21]. Water in oil micro emulsions, one having the reducing agent while the other having the metal precursor, are mixed, resulting in continuous collisions. This leads to coalescence of the micro-droplets leading to reaction and formation of NPs [22]. The NPs are separated from the excess surfactants by adding solvents like acetone or ethanol followed by centrifugation steps. Thus, microemulsions are used as nano-reactors for the synthesis of NPs as their sizes limit the growth of the NPs [23]. Figure 1.5 depicts the steps involved in the synthesis of NPs by micro-emulsion based synthetic route.

This method has been widely used to produce metallic cobalt, cobalt/platinum alloys and cobalt/platinum NPs coated with gold in reverse micelles of cetytrimethlyammonium bromide, using 1-butanol as cosurfactant and octane as the oil phase [25].

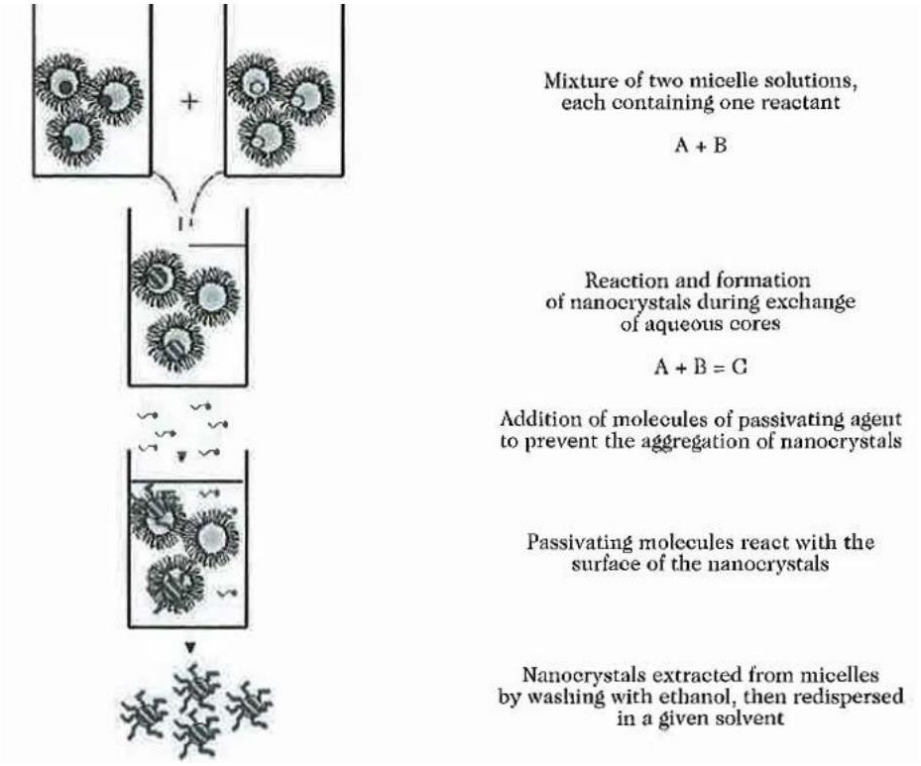

FIGURE 1.5: Steps involved in the synthesis of NPs by micro-emulsion based synthetic route [24]

1.2.2 Magneto-plasmonic NPs

Recently, innovative multifunctional NPs have gained great consideration, because they have the capability to import distinct functionalities to attain collegial therapeutic treatment. Multifunctional NPs are fabricated to co-transport multiple cargo molecules, and at the same time, they assist in the delivery of drug through NP surface-cell interactions, serving both in therapy and diagnosis[26]. Combining material properties of constituting metals in core-shell NPs is one such example.

1.2.2.1 Magnetic NPs and Superparamagnetism

Magnetic NPs are playing a critical role in the broad spectrum of bio-medical applications, such as biomedical sensing, targeted drug delivery, and ultra-sensitive disease detection. Due to small particle size, there is an enhancement in reactivity and they have strong magnetic properties because of superparamagnetism and surface effects. Further, they can reach the site of concern more precisely owing to their size and functionalization. These particles can be coated with biological molecules, thereby promoting interactions with biological systems[26][23].

As mentioned above, magnetic NPs have strong magnetic properties due to superparamagnetism, so it is important here to give a brief overview of superparamagnetism.

In paramagnetic phase, material shows randomly oriented magnetic dipoles that arrange in a straight line and along its direction under the influence of external magnetic field. When magnetic field is removed, high thermal energy decouples all the spins. While in case of superparamagnetism, material shows magnetic effect in which all the spins are always collinear to each other but anisotropic energy is not high enough to keep them aligned along stable magnetocrystalline direction. As a result, superparamagnetic material displays constant and collective fluctuations of its spins. This means that these dipoles move collectively in a random way and are always aligned parallel to one another. Spins align in the same direction only when external magnetic field is applied in a certain direction. Superparamagnetic response of the material is dependent on the relaxation time and measuring time of the technique [27]. The main difference between superparamagnetic and paramagnetic material is that the transition for superparamagnetic material happens below the Curie temperature. Figure 1.6 shows the difference between superparamagnetic and ferromagnetic particles.

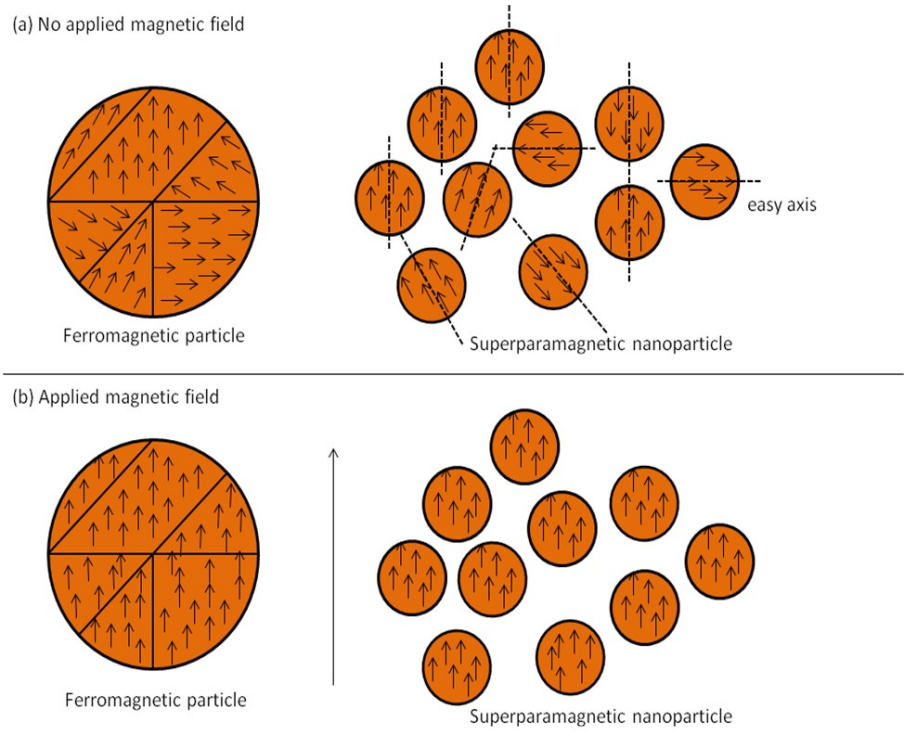

FIGURE 1.6: Superparamagnetic versus ferromagnetic particles in (a) the absence and (b) the presence of an external magnetic field [28]

Coating of magnetic NPs with noble metals like gold is done to utilize the optical properties of the gold NPs.

1.2.2.2 Coating of magnetic NPs and localized surface plasmon resonance (LSPR)

Coating of magnetic nanoparticles (MNPs) with biocompatible materials like silica and gold is gaining importance in the development of MRI contrast agents for drug delivery. Coating with precious metals offers several advantages. For instance, gold has low reactivity and it is considered an inert coating. A gold layer prevents chemical degradation of magnetic cores and also forbids release of potentially toxic components. Adding gold offers additional advantage of forming self assembled monolayers (SAMs) on the surface of MNPs using alkanethiols. Gold coating also improves the ability of NPs to attach with functional ligands and functional chemistries are improved drastically as compared to MNPs[29].

As mentioned above, chemical inertness of gold offers several advantages, but on the other hand, this chemical inertness is disadvantageous in a sense that it is difficult to form gold shells over MNPs. Advanced methods offer a way to form gold-coated iron NPs. These methods include reverse microemulsions, combined wet chemical methods and laser irradiation [29].

One of the most exploited properties of gold NPs is LSPR. Conduction band electrons on the surface of noble metal NPs undergo polarization when they absorb light. This polarization is triggered by the electromagnetic field of the incident light. Polarized electrons go through collective oscillations due to positive ions in the metallic lattice. These oscillations are called surface plasmon oscillations. Surface plasmon oscillations have the same frequency as the incident light that is why this phenomena is also called surface plasmon resonance and in case of NPs, these surface plasmons are confined and the phenomenon is thus known as LSPR. Intensity and position of LSPR is affected by the shape, size and material of the NPs. For spherical gold NPs, the wavelength at which LSPR happens is around 520 nm which falls in the visible region [30]. Figure 1.7 illustrates how LSPR occurs in noble metals.

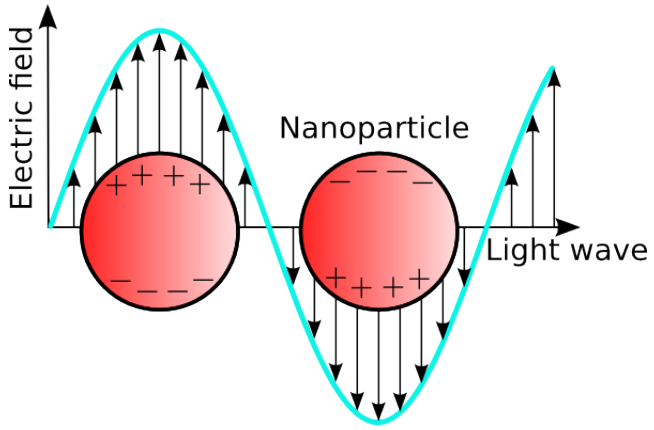

FIGURE 1.7: Light causes the electrons of the NPs to delocalize forming an electric field opposite to that of the wave [31]

MNPs can also be coated with different kinds of polymers to introduce multifunctionality,

1.2.2.3 Polymer coating of MNPs

MNPs utilize their high surface energy to agglomerate. Salts or electrolytes which are present in biological solutions can neutralize the charges present on the surfaces of NPs. This neutralization can cause agglomeration of the NPs. In addition to this, surfaces of MNPs are subjected to opsonisation -the first step during their clearance by reticuloendothelial system (RES) when they are injected into the body. To effectively escape the uptake by the RES and maintain longer plasma half-life, as well as to prevent agglomeration, it is important to coat the surface of MNPs. Some common coating schemes of MNPs are represented in Figure 1.8 [29]. Surface properties like surface charge and chemical functionality are also modified with these coatings. Few important parameters which should be kept in mind with respect to polymeric coating of MNP systems are types of chemical structure of the polymer (hydrophobic/hydrophilic, biodegradation), molecular weight of the polymer, conformation of polymer, degree of particle surface coverage and the manner in which polymer is attached. These factors can affect the performance of MNP systems .Polymers can be attached to the surface of particles in a number of different arrangements, for example, in the form of end-grafted brushes, or as completely encapsulated polymers shells. These different orientations along with molecular weight can affect antifouling characteristics of NPs and their hydrodynamic sizes [29].

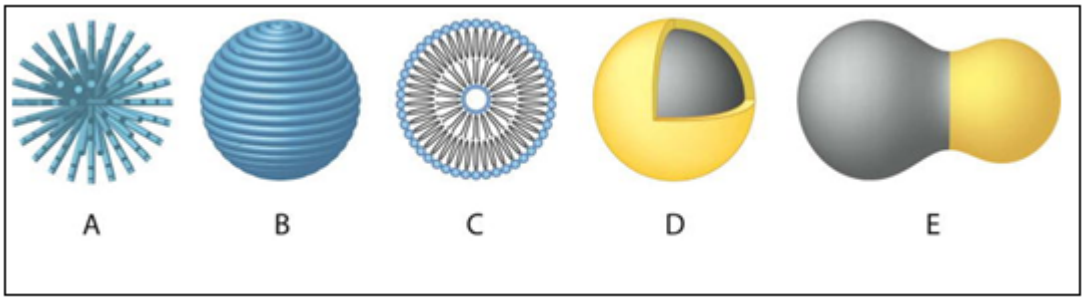

FIGURE 1.8: Magnetic nanoparticles coating schemes: (A) Coated with End-grafted (B) Encapsulated in polymer coating (C) Liposome encapsulated (D) Core-Shell (E) Heterodimer [29]

1.3 Polymeric NPs

On the other hand, polymeric NPs have shown superior characteristics as a medium for delivery of drugs, biomolecules and genes. These polymeric NPs are generally known as polymeric colloidal particles because their size range falls within the colloidal regime [32, 33]. Biocompatibility, low toxicity and biodegradability of polymeric NPs are their prominent features which are utlized in drug delivery strategies. In addition, these polymeric NPs can be easily functionalized to produce multifunctional vectors for advanced drug delivery applications. It is important to mention that size, shape and surface properties of the NPs can be customized, along with degradation kinetics and mechanical properties [34].

Polymeric NPs have the ability to entrap and adsorb both hydrophilic and hydrophobic molecules with ease and provide intended results. These NPs are also very stable [35]. Molecules like proteins, peptides are protected from degradation because of drug entrapment with polymeric NPs. Apart from this attribute, they also facilitate controlled drug release and site-specific drug targeting [36]. Furthermore, nano scale polymeric NPs are able to cross extra and intercellular barriers. These systems can cross endothelium and deliver the entrapped drug to the tumor site [36, 37].

Normally, two types of polymeric NPs are widely considered in regards to drug delivery - nanospheres and nanocapsules. In nanospheres, drug molecules are dispersed homogeneously in the polymer matrix. On the other hand, nanocapsules are typical vesicular systems constructed of polymers in which the polymer wall surrounds a core where the drug molecule is entrapped [36]. A number of different processes are developed to synthesize polymeric NPs. Most common of these processes are spray-drying, salting out, nano-precipitation and emulsion-based methods [38]. Size and surface of the produced

NPs will be dependent on the method employed for their production and the given process can dictate the properties and features of NPs. In addition to that, in order to get the required characteristics of the formulation, it is important to have a good understanding of the different experimental variables [38, 39]. In the following sub-sections, a brief overview of different kinds of polymeric NPs is being presented.

1.3.1 Polymeric Micelles

Polymeric micelles are termed as self-assembled particles that have gained popularity as spherical nano-scale carriers for delivery of drugs, proteins, genes and imaging agents [40]. These structures are constructed by self-assembly of amphiphilic block or graft copolymers in aqueous solution. Size of polymeric micelles is in the range of 10 to 100 nm with hydrophobic a core and a hydrophilic surface [41, 42]. The core-shell structure comprises a shell of hydrophilic polymer chains which surrounds the inner hydrophobic core. Hydrophobic or water insoluble drugs are delivered by using polymeric micelles because they can be encapsulated in the hydrophobic core of the micelles. Figure 1.9 shows the hydrophilic shell in these structures that prevents the deterioration of the micelles in the aqueous dispersion [41–43].

These systems can increase the bio-availability of the drug as they prevent the physically entrapped drug from hydrolysis and enzymatic degradation which ultimately prolong the blood circulation times of the micelles [40, 44]. Low toxicity is also a positive attribute of these systems [44].

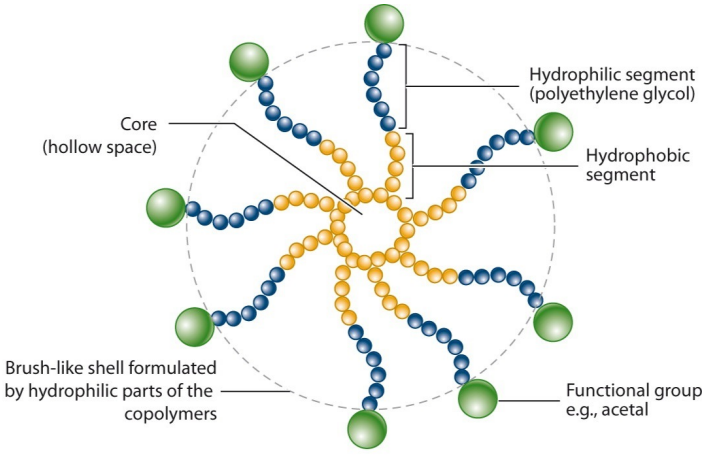

FIGURE 1.9: Micelle structure [43]

1.3.2 Dendrimers

Dendrimers are synthesized by convergent or divergent polymerization of branching units. This results in structures made of a hydrophilic surface and a hydrophobic central core as shown in Figure 1.10 [45]. Dendrimers can be produced from a branching monomer, central core and functionalized peripheral groups and they are generally called hyperbranched nanocarriers. In the case of divergent polymerization, formation starts from the core element, while in convergent polymerization growth starts from the peripheral branching units [45].

Low viscosity, hyperbranched molecular structure, macromolecular size and multiple end groups which can be functionalized are key physico-chemical properties of the dendrimers [45]. Wong et al. (2012) [46] describes the controlled release of loaded cargo from these systems by altering the de-polymerization of dendrimers.

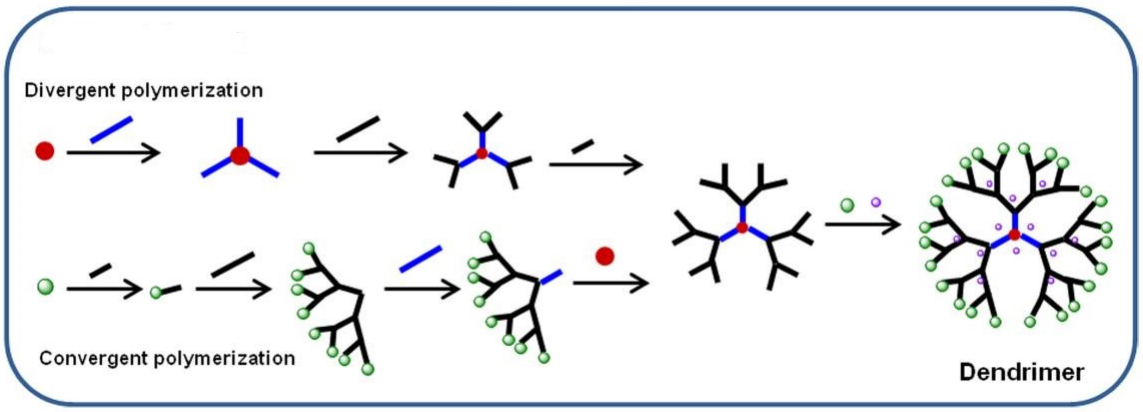

FIGURE 1.10: Formation of dendrimers by convergent and divergent polymerization [45]

Drug molecules can be delivered to specific sites by using dendrimers either by incorporating it in the core and branches, or by conjugation to terminal groups [45]. Dendrimers also find their application as diagnostic tools because of their capablity to protect imaging agents, reducing their toxicity and also upgrading the specificity of imaging agents [47].

1.3.3 Hydrogels

Hydrogels comprise hydrophillic organic polymer components that are cross-linked into a network by either covalent or non/covalent interactions [48, 49]. They show swelling-collapse behavior in aqueous media upon water ingestion or as a function of temperature

and/or pH. In these structures, large solvent contents induce fluid-like properties while cross-linking provides the dimensional stability. Many research groups are now focussing on fabrication of more complex polymer constructs (hydrogel based) to obtain highly functional nanomaterials. This interest is developed to create impact in the fields like *in-vivo* diagnostics, drug/gene delivery and optical materials [50]. These materials are intended for biocompatibility, biodegradation, encapsulation, biorecoginition, environmentally switchable payload release and/or directed self-assembly. Utilization of stimuli-sensitive polymers in nanostructured hydrogels enables them to sense and respond to the local conditions. For instance, it is conceivable to envision the formation of a hydrogel molecule that embodies and protects a pharmacologically dynamic protein, just releasing it when the molecule "detects" the vicinity of a specific infection state [50].

Hydrogels can be classified from numerous points of view, yet discussion here will be limited to only classification based on the type of cross-links. Important attributes of the cross links is the maintenance of a network structure of the hydrogels and to avoid the disintegration of the hydrophilic chains [50].

1.3.3.1 Physically Cross-linked Hydrogels

Hydrogels (both synthetic and natural) in this class have prompted the idea of reversible or degradable polymers that experience a shift from a three-dimensionally stable structure to a polymer solution. These hydrogels have been frequently utilized to embody proteins [51], cells, or drugs [52] and afterwards release them by dissolution of the hydrogel structures. Hydrophobic interactions, hydrogen bonding, or ionic interactions fall under the non-covalent attractive forces between the polymer chains and are responsible for the cross-linking in physically cross-linked hydrogels [50].

1.3.3.2 Chemically Cross-linked Hydrogels

Chemically cross-linked hydrogels are normally more stable than the physically cross-linked hydrogels on the grounds that they are formed by covalent bonds [53]. Hydrogels formed by such cross-links have a perpetual structure unless chemical liable bonds have been deliberately added to the system to make the hydrogels degradable. Monomers are polymerized in the presence of the cross-linking moieties to form chemically cross linked gels. Different physical properties, for example, the swelling limit of hydrogels can be controlled by controlling the amount of cross-linker utilized [53].

Hydrogels can likewise be categorized taking into account their size as either macrogels [54, 55] or microgels [56, 57]. Size can vary from millimeters and bigger in case

of macrogels and they are termed as bulk gels, while microgels are colloidally stable hydrogels, and their size can shift from several nanometers to micrometers. Moreover, hydrogels can also be categorized as non-responsive and stimuli-responsive hydrogels. Non-responsive hydrogels, as the name indicates, are just the materials which swell upon water ingestion, while the stimuli responsive gels swell as a function of changes in the environment [50, 58, 59]. Hydrogel can respond to temperature [55], pH value [57], ionic strength, light, electrical field and biomolecules. The responsive property of the hydrogels is acquired from the nature of the polymer utilized as a part of forming the gel and/or any post-polymerization adjustments that are made [50]. In the next section, a brief overview of stimuli-sensitive polymers and differences between micro and nanogels will be highlighted.

1.3.3.3 Stimuli-Sensitive Polymers

The utilization of the stimuli-sensitive polymers in manufacturing hydrogels has prompted numerous intriguing applications such as targeted drug delivery. Poly(N-isopropylacrylamide) (pNIPAm) which is constructed from the monomer N-isopropyl-acrylamide (NIPAm) has been extensively studied as a stimuli-sensitive polymer [60]. Heskins et al. has observed that the phase transition of pNIPAm is endothermic and is driven by entropy. Owing to this, pNIMAm is extensively employed to produce responsive hydrogels [61].

Balance between solvent-solvent, solvent-polymer, and polymer-polymer interactions has a relation with the behaviour of any polymer in the solvent [50]. It is possible to switch the polymer solvation by either strengthening one of these interactions or by weakening another. Figure 1.11 depicts this.

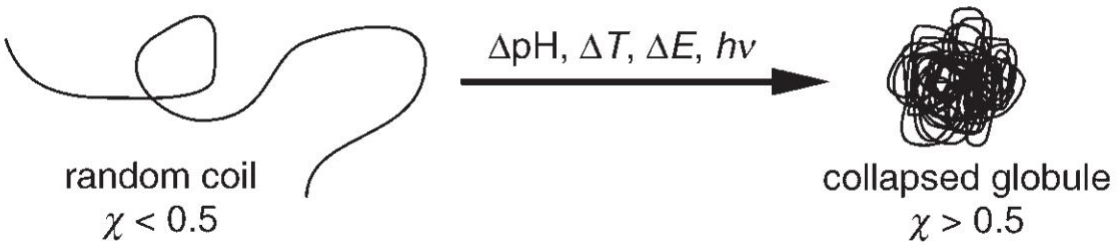

FIGURE 1.11: Changes in solvent properties induce phase transition in stimuli-sensitive polymers [50]

Amide-chains in the pNIPAm form hydrogen bonds with the water, on the other hand, the isopropyl groups gather as side chains prompting hydrophobic structuring of the

water. This structured water prompts polymer-polymer interactions due to hydrophobic effect which is entropically driven [60]. When the polymer-solvent interactions are greater than the polymer-polymer interactions, pNIPAm will have random-coil structure. There will be a breakage of hydrogen bonds at high temperature leading to entropically driven release of the bound water, which results in the formation of globular polymer structures. At this point, hydrophobic interactions between polymer-polymer dominate the polymer-solvent interactions which cause phase separation of the polymer phase. The temperature at which this phase separation happens is called lower critical solution temperature (LCST). Study of pNIPAm phase transition by Wu et al. stated that transition from random coil state to globular form is not first order, rather, there are other thermodynamically stable conformations present intermediately [62, 63].

1.3.3.4 Microgels and Nanogels

Colliodally stable hydrogels in the micro and nano size range are termed as micro and nano gels respectively. Properties of micro or nano gels are almost identical to that of macrogels except for size related properties. Microgels also have other attributes of colloidal dispersions, like zeta potential, and can frame ordered colloidal phase along with the properties mentioned above [50]. Studies performed by Wu et al. have indicated differences in the phase behavior of the macro- and microgels, for example volume phase transition temperature (VPTT which is defined as volume phase transition of polymer gels at and above their phase transition temperature) of microgels is a bit higher than the LCST of pNIPAm.

In addition to this, transition region in case of micro/nanogels is less sharp than that of the macrogels [64]. The possible reason for this kind of transition is due to more heterogeneity in the structures of the microgels compared to macrogels. Microgels have regions of long and short sub chains, therefore when temperature is raised above the VPTT, the areas with the longer subchains undergo collapse at lower temperature compared to the areas with shorter subchains. It can be inferred from the discussion above that phase transition from a microgel is a combination of the phase transitions of diverse sub-networks in the system, this particular behavior is also shown by the core-shell structured microgels [65].

1.3.4 Synthesis Methods for Hydrogels

There are several techniques to synthesize hydrogels, the most widely used will be discussed here. It is important to mention here that the method used to synthesize nanogels is purely dependent on the end use and required application of the produced nanogels.

1.3.4.1 Emulsion and Precipitation Polymerization

Surfactant-free emulsion polymerization or precipitation polymerization is the most widely used method to produce thermosensitive hydrogel systems. In this technique, NIPAm and the cross-linker commonly, N,N- methylenebisacrylamide (BIS), are dissolved in water. After purging the solution with N_2 gas and heating above the pNIPAm LCST(reaction temperature being normally around 70 ^oC), ammonium persulfate (APS) or potassium persulfate (KPS) type initiators are added to this solution. This process can provide particles with narrow size distribution if performed precisely [50]. High temperature is required in this method to form sulfate radicals which are responsible for the initiation of polymerization. This method is based on homogeneous nucleation. After initiation, sulfate radicals react with NIPAm monomer which is followed by radical propagation and chain growth. As the polymerization temperature is greater than the LCST of the polymer, chains collapse upon themselves after reaching a critical length to form precursor particles, that is why this method is also called precipitation polymerization. Growth of precursor particles takes place by aggregation either with other particles or with growing monomer. The hydrogels are stabilized with the charge from initiator after they have attained a critical value. Figure 1.12 depicts the possible mechanism for precipitation polymerization.

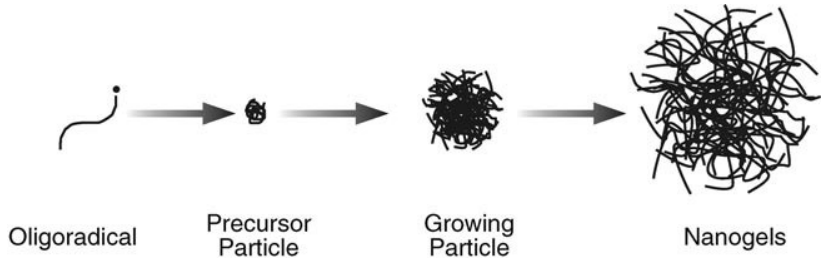

FIGURE 1.12: Suggested mechanism for precipitation polymerization of nanogels [50]

Precise size control of the hydrogels can be achieved very easily. For instance, smaller hydrogels can be produced by stabilizing the precursor particles in the earlier stages of the reaction. Sometimes it is reasonable to add ionic surfactants to the system to transmit colloidal stability during the earlier stages of the reaction as there is insufficient charge accessible from the initiator to stabilize small precursor particles. On the other hand, to get larger particles, surfactant concentration can be decreased [50]. Percipitation polymerization is also useful to add co-monomer in the hydrogel. pH responsive hydrogels are formed by co-polymerization of ionic monomers like acrylic acid (AAc) with pNIPAm [57, 66, 67].

1.3.4.2 Core-Shell Structured Systems

There are two kinds of core-shell hydrogels; one in which both core and shell are made of hydrogel-like materials and the other in which core is not made with hydrogel while shell is constructed from hydrogel. In the second class, polystyrene, silica or gold is normally used as a core. In the first case, two-stage polymerization protocols have been used to produce these kinds of hydrogels [57]. In these strategies, radial distribution of the functional groups in the particles is allowed by adding polymer shell having the same or different structure as that of the core into the preformed core particles. In a common synthesis approach, shell monomer solution is added to the heated (at 70 ^{o}C) preformed pNIPAm core particles. After reaction is completed, resulting mixture is allowed to cool and thereafter separated by filtration. Mechanism followed by this reaction is somehow similar to that for the core hydrogels. As the reaction occurs at a temperature higher than VPPT of the core particles, the particles which are formed are in collapsed form. These hydrophobic collapsed particles attach to the growing oligomers, resulting in the production of shell [50]. Core-shell particles which are formed by this approach can show very exciting properties [56, 68, 69]. These particles can demonstrate multiple phase-transition behaviours with temperature and/or pH as shell can be constructed utilizing distinctive co-monomers [57, 68, 69].

1.3.5 Swelling properties of hydrogels

Monomer used to synthesize hydrogel will decide the nature of the produced hydrogels. When hydrogels are produced by using pNIPAm, they show thermoresponsive behaviour similar to pNIPAm. Hydrogels display volume phase transition temperature (VPTT) at around the LCST of pNIPAm [70]. When temperature is raised above the VPTT, hydrogels undergo transition from a hydrophilic state which is the swollen state to a hydrophobic or the compressed state. Cross-linking density, hydrophobic-hydrophilic balance, ionic strength and solvent composition are typical factors which can influence the VPTT of the gels.

Hydrogels depict pH-dependent swelling when they are synthesized from ionic monomers. Acrylic acid is the most widely used ionic monomer. The gel swells at pH $>$ pKa of the acid co-monomer, due to de-protonation of acrylic acid segments which prompts Coulombic repulsion (electrostatic repulsion) between the carboxylate anions. This repulsion increases the osmotic pressure inside the particles which leads to increase in the swelling of the polymeric system. Therefore, equilibrium gel-swelling volume is a balance between the osmotic pressure of the polymer system which is administered by polymer-solvent interactions, and the elastic properties of the polymer network [71].

1.4 Advantages of NPs

Radical change in novel drug delivery systems is driven by the persistent development of the pharmacological and therapeutic properties of the drug. This rising need of drug delivery systems is tackled by analysing a broad spectrum of therapeutic nanocarries due to their improved performances [6]. NP based drug delivery systems have certain advantages such as longer circulation half-lives, minimum side effects and better pharmacokinetics [2].

Nanoscale size delivery systems are popular among formulation scientists. The most significant reason for their popularity is the increase in the surface area because the ratio of number of molecules to the total number of molecules or surface atoms is increased. This increased surface area is helpful in binding, and in adsorption of drugs, probes and proteins [2].

Another important advantage of NPs is the easy control of their size, morphology and surface charge. NPs can be modified with different systems which can alter the particle degradation and hence drug delivery and targeting properties. Ability of NPs to release drug is dependent on their size and proper surface modification [72].

The transport mechanism is also guided by the NP properties and their surface modification Endocytosis is a more effective transporting mechanism than passive targeting in which case, NPs extravasate through leaky vasculature around tumour tissues. On the other side endocytosis is based on activation energy where there is interaction and collision between the NPs and cells. In order to facilitate greater interaction with the negatively charged cell membrane, NPs should be modified with positive charge. It is concluded from the above discussion that size, surface charge and hydrophobicity of NPs are important for the uptake of drugs incorporated with NPs. Size is also important for intracellular uptake within the cells [73].

Moreover, NP based drug delivery systems increase dissolution rate of drug, decrease drug dosage and help avoid early loss of drug by rapid clearance and metabolism [2]. Figure 1.13 summarizes the significant advantages of NP based drug delivery systems.

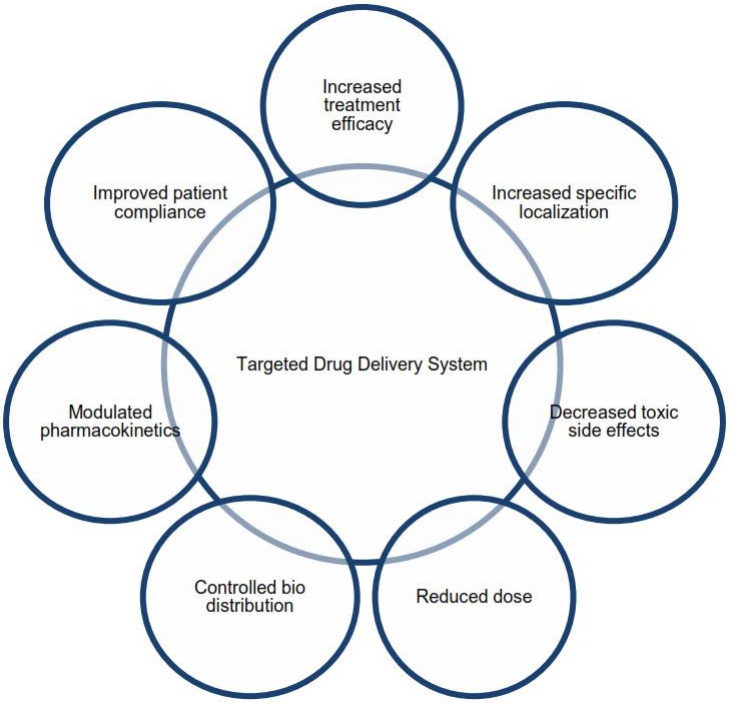

FIGURE 1.13: Advantages of NPs based drug delivery [6]

1.5 Surface Modification of NPs

Surface modification of NPs has several advantages, most important of them are (i) controlling the growth of NPs by stabilizing the NPs and directing their shapes during the growth process (ii) incorporating functional groups on the surface (iii) enhancing applications of NPs by increasing their solubilisation in different solvents (iv) modifying the optical, electronic, spectroscopic and chemical properties of the NPs, whereby allowing wide scale application possibilities (v) altering the capability of NPs to target the desired chemical, physical, or biological environments, (vi) improving chemical and mechanical functioning for example shielding against oxidation (vii) decreasing toxicity [74].

For example, in case of cancer treatment, multifunctional NPs can be employed to co-deliver proteins, small molecule drugs and genes like DNA and siRNA which are therapeutic agents [75–77]. These multifunctional NPs carrying vector molecules like peptides having capability of identifying tumor cells, have the ability to pass through cancer cell barriers due to permeability and retention (EPR) effect [78–80]. Further, they can preferably stay within target cells for longer periods. As a result of this effect, these NPs have the ability to deliver more drug to the cancer cells. Surface modification

can also equip NPs with imaging modalities which provide diagnostic capacities like optical and magnetic resonance imaging [81–83]. In addition to this, surface functionalization with ligands can particularly pin point the receptors on the surface of the cell for targeted drug delivery. This is very helpful in cancer treatment [84–86]. Compact layer of endothelial cells which surrounds the brain that is blood-brain barrier (BBB), can be crossed by functionalized NPs to deliver specific payloads [87, 88].Figure 1.14 a) and b) represent multifunctional NPs.

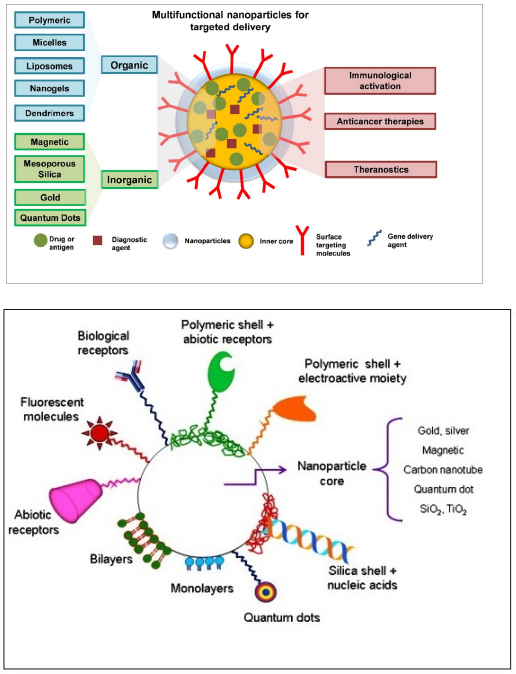

FIGURE 1.14: a) Figure illustrating targeted drug delivery and bioimaging functionalities of multifunctional NPs [89] b) Multifunctional NPs, surface modification with different functional particles [74]

Surface functionalization with PEG is very helpful in avoiding immunogenic reactions which refers to bio-acknowledgment and elimination of nanocarriers by the immune system. This surface functionalization with PEG enhances the circulation time of the drug and decreases the clearance rate by deceiving the phagocytic cells of the immune system like macrophages, liver cells and spleen red pulp macrophage cells whereby, giving stealth properties to NPs. These cloaking properties forbid the adsorption of opsonins at the NP surfaces [90]. Enhanced immunogenicity of NPs through functionalization is depicted in Figure 1.15

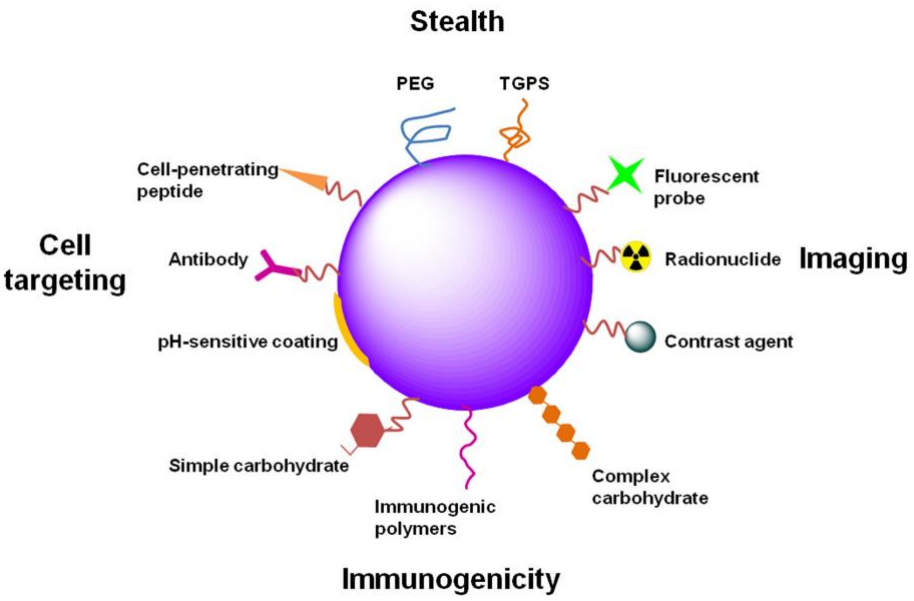

FIGURE 1.15: Enhanced immunogenicity of NPs through functionalization [90]

1.6 PEGylated NPs

As mentioned previously, coating of magnetic and polymeric NPs with hydrophilic polymers like PEG, offers several advantages. PEGylation is an extensively used procedure to enhance the half-life time of nanocarriers, through cloaking properties and steric stabilization. Surface functionalization of nanosystems is done with PEG by either conjugation, grafting or adsorption [90]. Foreign particulate matter in body fluids are instantly covered with immunoglobulins igG and igA and the supplement proteins C3b C4b opsonins, this process is called opsonization. Opsonins stamp the particular substance for phagocytosis through their acknowledgment by Fc receptors (protein present on the surface of cells which enhance the protective functions of the immune systems) on phagocytic cells, for example, macrophages. To avoid the adsorption of opsonins at the surface of NPs, they are functionalized with PEG. Hydrophilicity of the PEG makes this possible by attracting water molecules to NP surface which ultimately contributes to invisibility of NPs to phagocytic cells [90]. This enhances the particle circulation time. Moreover, owing to inflammatory reactions caused by the tumor, pathological tissues have large permeability; this enhanced life time of NPs in plasma contributes towards more accumulation inside the tumor and more effective drug release. The vicinity of the polymer at the surface can likewise stablize particles, abstain them from agglomeration, provide better bioavailability and reduce toxicity [91]. Efficiency of internalisation of drug carrier is enhanced by modification with PEG, for example PEG-coated MNPs

are effectively internalized by cells through endocytosis. Also surface functionalized gold NPs coated with PEG provide effective internalization in endosomes and cytosol [29, 92, 93]. Effect of PEG functionalization is shown in Figures 1.16 a) and b).

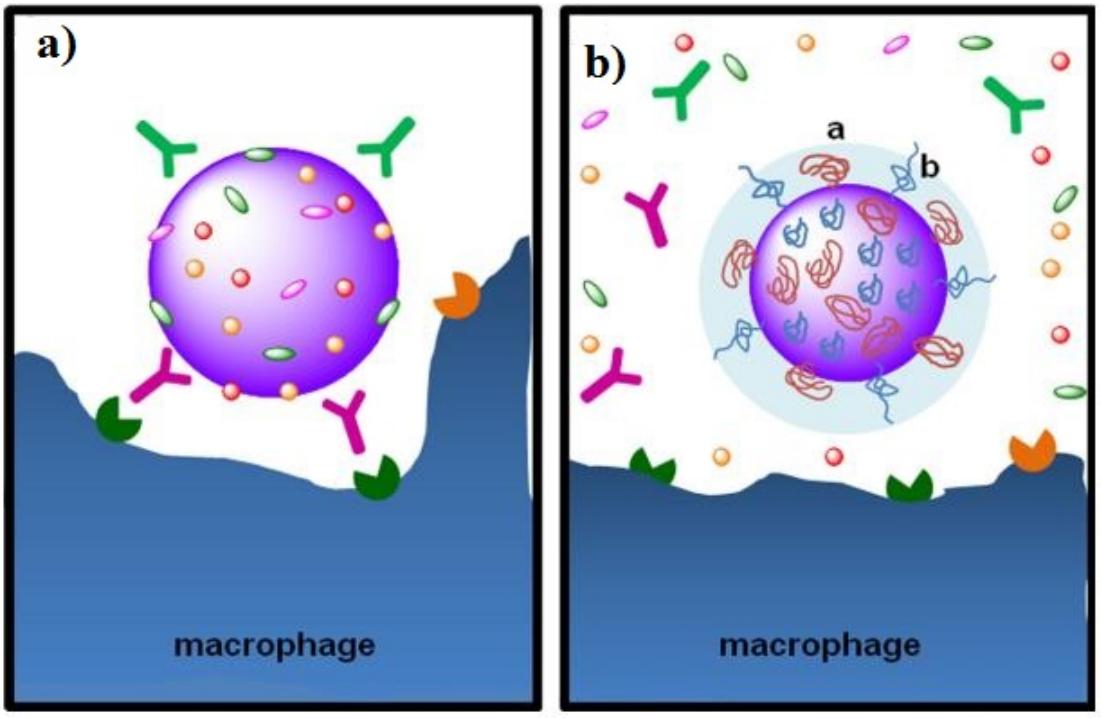

FIGURE 1.16: Effect of PEG functionalization on NP (A) Process of opsonization (B) PEG functionalized NP [90]

PEGylated nanogels have also shown reduced protein adsorption on their surfaces. Non-PEGylated nanogels have shown greater protein adsorption in their collapsed state as compared to the swollen state because nanogels become hydrophobic in their de-swollen state above VPPT, resulting in hydrophobic adsorption of proteins [94, 95]. However, surface modfication of nanogels with PEG reduces the protein adsorption at collapsed state. PEG integrated to PNIPAm has indicated reversible temperature dependent swelling/de-swelling transitions. It is additionally vital to mention that introduction of PEG expands the microgel VPTT, for example, 40 wt % PEG incorporation to the BIS cross linked pNIPAm, shifts the VPTT from 31 ^{o}C to 36 ^{o}C [95]. In addition to this, phase transition phenomena occurred over a wider temperature range. PEG incorporation to the nanogels enhances the hydrophilic composition of the nanogels, therefore more thermal energy is required by the particles to experience phase separation from the aqueous environment which is the suggested reason for the above phenomena [95].

1.7 Polymer-NPs Hybrids

Combination of inorganic and polymeric NPs offers great advantages in drug delivery application. Hybrids of polymeric and inorganic NPs offer magnetic, optical, thermal and pH responsive behaviour and steric stability in a single drug carrier. Basic aim of this research is to highlight the superiority of polymer-NP hybrids as drug carriers.

1.8 Administration Routes of NPs

In pharmacology, the path through which a drug, fluid or any other substance enters the body is called route of administration. Route of administration can significantly influence the pharmacokinetic properties such as adsorption, distribution, metabolism and excretion of a drug [6]. Different routes of drug administration are shown in Figures 1.17 (a) and (b). Toxicity might vary with different modes of administration of the drug [96]. Also, some routes might not be feasible for particular drug delivery scenarios. For instance, oral delivery of drug incorporated in the NPs gives better bioavailabilty and biodistribution for insulin loaded NPs; but in case of oral protein and peptide delivery, poor oral bioavailabilty is still an issue. Oral administration of polyacid should be protected from low pH in the stomach, because low pH will influence the drug release rate and swelling of drugs; whereas, higher, pH in small intestine will ease drug release in gastrointestinal tract due to dissociation of acid at higher pH [97, 98].

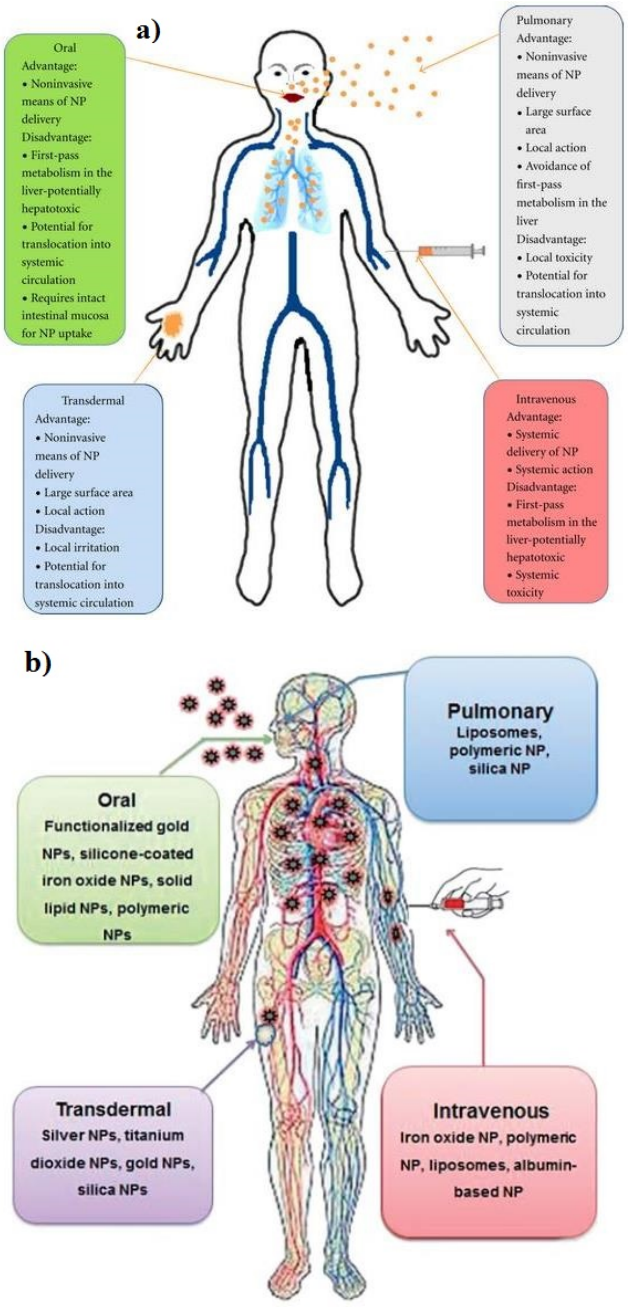

FIGURE 1.17: a) Routes of NP administration and their advantages and disadvantages [96] b) Important routes of drug administration based on NPs [99]

1.9 Non Targeted Drug Delivery

In this type of drug delivery, drug is not targeted to the specific cells. Drug is introduced in-to the body using conventional methods of drug delivery.

1.10 Targeted Drug Delivery

It is very important that drug carriers should have specific quality to avoid the release of drug to the healthy cells which can cause serious side effects. Drug carrier should be specific so that it will attack the specific site in the body to cure the damaged cells. Important to consider in the design of drug carriers is how they will be received by the cells with which they need to interact. Today most of the research in the field of drug delivery systems is focused on targeting drugs to the diseased site [50, 100]. Targeted drug delivery reduces the toxic effects caused by the drugs attacking the cells other than which are affected by disease. Effectiveness of the targeted drug delivery system depends on the ability to hold the drug in the polymer, to avoid disturbance to the immune system, to specifically target the cells and in the end to release the drug to the specific cells in a controlled manner. Many factors can affect the targeted drug delivery like body's response to the drug which should be considered.

1.11 Active and Passive Targeting

Targeting can be classified as active and passive. NPs having long circulation in the body are able to explore structural abnormalities in the vasculature of tumors and infectious sites. Passive targeting is mostly due to enhanced permeability and retention (EPR) effect. This effect is based on the accumulation of drug carriers to the targeted cells due to extravasation through leaky vasculature, followed by retention in the cells and final drug distribution in the cells. Passive targeting or non-specific accumulation happens for NPs having size in the range of 10-500 nm diameter. Information about the distribution of drug is required to enhance this effect [29].

Active targeting is based on the recognition of specific diseased tissue and accumulation of NPs and release of drug to the specific target site. This happens because of conjugation of targeting molecule that has high affinity to the overexpressed molecules present in affected cells. For active targeting, it is important that target and drug carriers are close to each other which cannot be achieved easily[29, 50].

In the next sections, different drugs used in this study are presented along with loading and release methods and release kinetic models.

1.12 Drugs Studied

Physico/chemical properties of three different drugs chosen based on their aqueous solubility are highlighted in the next sections.

1.12.1 L-dopa

L-Dopa (3,4-Dihydroxy-L-phenylalanine) is an amino acid and hormone, it is formed naturally in humans, animals and plants. Synthesis of L-dopa is done from amino acid L-Tyrosine. L-dopa is used to treat Parkinson's disease as it is considered a psychoactive chemical. It is also used to treat other abnormal conditions such as lower levels of neurotransmitters (Dopamine). Dopamine cannot pass through the blood-brain barrier and should be synthesized in the brain. L-dopa can cross this blood brain barrier; after crossing the barrier, it is converted to dopamine, which enhances level of pleasure inducing hormones inside the brain[101]. L-dopa therapy for the treatment of Parkinson's disease is shown in Figure 1.18.

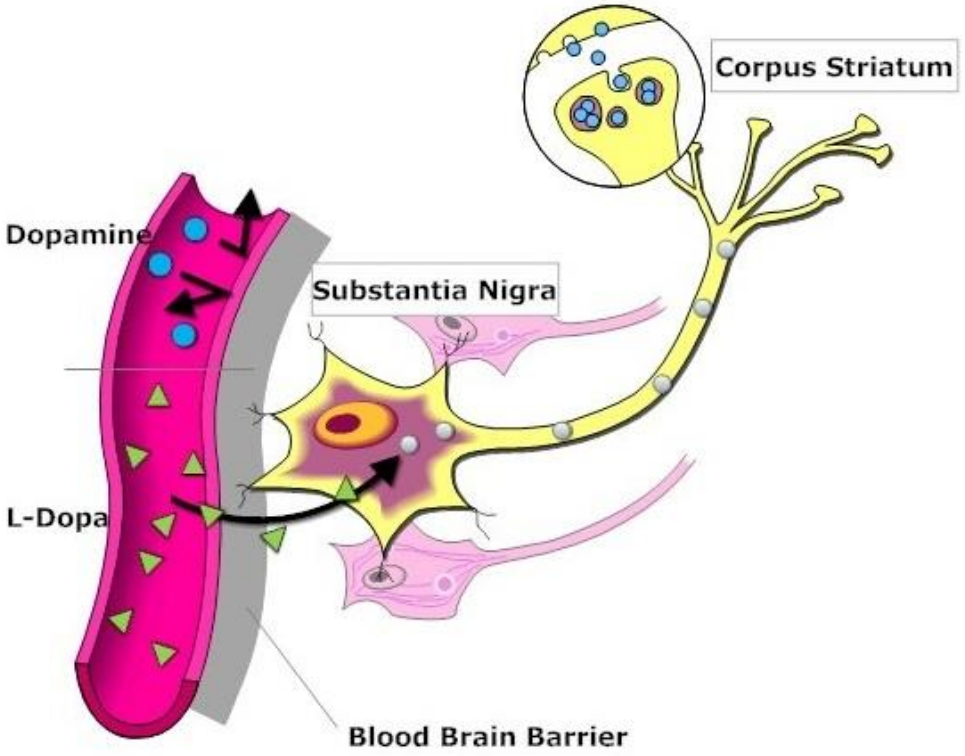

FIGURE 1.18: L-dopa therapy for the treatment of Parkison, disease [101]

NPs loaded with L-dopa can pass through blood brain barrier more efficiently and can give better results by targeting the drug to the desired site of action. Molecular weight of L-dopa is around 197.19 g/mol. It is slightly soluble in water, acids and bases while it is insoluble in ethanol. Its solubility in water is about 3.3 mg/ml[102]. Structure of L-dopa is shown in the Figure 1.19. Characteristic UV-Vis peak for this drug is reported at 281 nm.

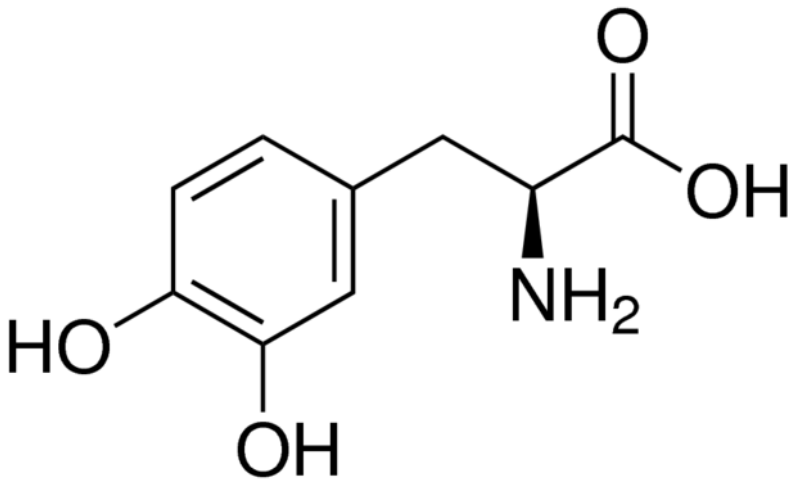

FIGURE 1.19: Structure of L-dopa [102]

1.12.2 Cytochrome-C

Cytochrome C is a hemeprotein found in plants and animals. It is associated with the mitochondria as an important part of the electron transport chain[103]. Structure of Cytochrome C also known as cyt c is represented in Figures 1.20 A) and B),

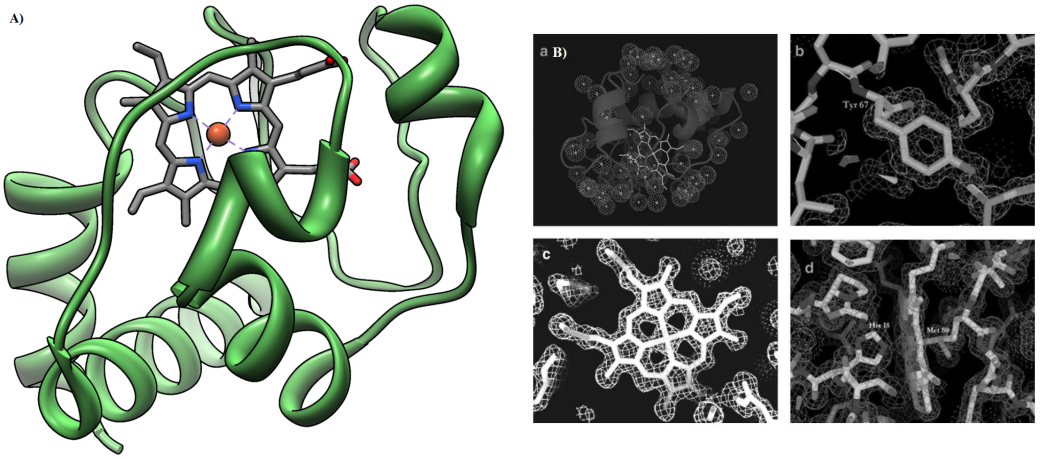

FIGURE 1.20: A) Structure of cytochrome c [104] B) 3-dimensional structure of cytochrome c a) ribbon illustration of cyt c with water molecule b)Tyrosine high resolution image c) haemo's group d) interaction of haemo's group with histidine 18 [105]

Proficiency of cytochrome C as a biological electron transporter is a result of its convenient interconversion between ferrous and ferric states. Formation of necessary electron-bridge between the oxygen and respirable substrate is attributed to this hydrophilic protein. Owing to this, it is viewed as universal link in the respiratory chain[106]. Figure 1.21 shows electron transport protein complex.

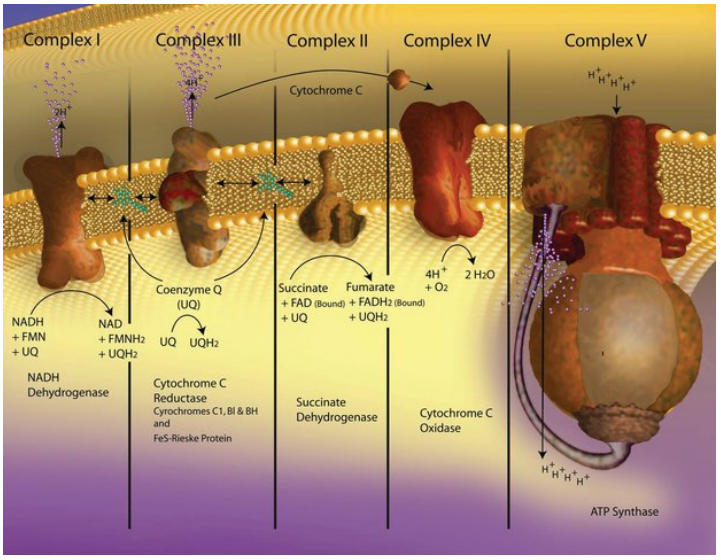

FIGURE 1.21: Electron transport protein complex [106]

Apoptosis is the programmed cell death which involves the characteristic cell changes and cell's death. Diseases like cancer, immune and neurodegenerative disorders can be possible if process of apoptosis is disturbed. Capases(cysteine proteases) are responsible for the execution of apoptosis, cytochrome c activates capases. In this pathway, a number of apoptotic stimuli cause cytochrome c discharge from mitochondria, which thus incites a progression of biochemical reactions causing caspase initiation and consequent cell death. Thus, cytochrome is important for apoptosis process[107].

Isoelectric point of cyt c is roughly at pH 10, and it is not affected by the low pH and its solubility in water is 100 mg/ml. Small size and overall positive charge of the cytochrome c is important in some applications[108]. Characteristic UV-Vis peak for this protein is reported at around 409 nm.

1.12.3 Coumarin

Coumarin(1,2-Benzopyrone or 2H-Iibenzopyran-2-one,) and derivatives of coumarin are extensively dispersed throughout the nature. Coumarin has 0.10 mg/ml solubility in water. They display fruitful and broad biological actions. The name Coumarin originated from the French word *coumarou* used for tonka bean. This is due to the presence

of the coumarin in seeds, roots and leaves of several plants especially in tonka bean in large concentrations. Natural and synthetic coumarin are widely available and can be divided into a number of subclasses. Some natural coumarin derivatives include (6,7-dihydroxycoumarin, 4), warfarin and psoralen. Mostly coumarin is classified by reviews as simple coumarin(for example, coumarin, 1), linear and angular furanocoumarins, linear and angular pyranocoumarins. Coumarin can also be classified by using biogenetic approach using number of nuclear oxygen atoms as a basis. Structure of coumarin used in the study is given in the Figure 1.22

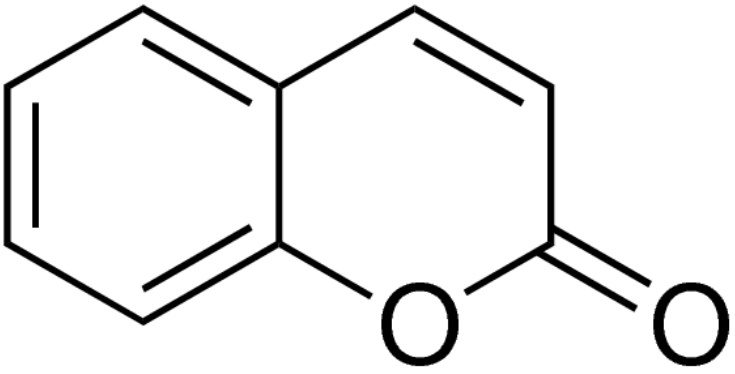

FIGURE 1.22: Structure of Coumarin[109]

Several therapeutic applications of coumarin derivatives include photochemotherapy, anti-tumor and anti-HIV cure. In addition, they are used as stimulant for the central nervous system and as antibacterials. The most fascinating application of coumarin is the striking effect against breast cancer. Recent studies on the antitumoral action of coumarin derivatives affirm that it is possible to manage coumarin-estrogen conjugates by conjugating coumarin substrate with 17β-estradiol. This conjugate exhibits growth stopping exercise in different breast cancer cell lines[110]. Characteristic UV-Vis peak for this protein is reported at around 277 nm.

1.13 Loading and Release of the drugs

Effectiveness of drug delivery systems is based on the efficient drug loading and release properties [111]. Drug loading is incorporation of the drug into/onto a nanocarrier [112]. Drug encapsulation or conjugation with the nanocarriers can shield it from inactivation and also help drug to stay active for longer periods. Furthermore, there is a decrease in the drug toxicity and flexibility in administration modes. Drug release however is opposite in the sense, that drug molecules are released from the carriers and then perform pharmacological action. Physico-chemical properties of drug and matrix, interaction

between the drug, matrix and the environment establish a relation between drug loading and release as both of these phenomena are dependent on them [111]. In order to obtain successful drug loading, it is important to have good compatibility between the drug molecule and the carrier, leading to reasonable loading degree and proper location of the drug molecules in/on the drug carrier. Payload molecules should maintain stability during loading, storage and release. This is important for the case of proteins, peptides and oligonucleotides, because these systems can lose their biological activity over time and owing to environment [113]. It is also important to mention that sustained controlled release is vital in providing required drug concentration to the target sites.

1.13.1 Loading and encapsulation efficiency

Primarily there are two methods by which drug is loaded onto the NPs, one is incorporation of the drug during the NP production while in the other method drug is adsorbed to the NPs after their formation [114, 115]. Apart from these methods, breathing in mechanism is also used for hydrogels. In this method, polymers are imbibed with a concentrated drug solution whereby the hydrogel pores are filled up with the drug solution. Drug loading can also be performed by chemically conjugating the drug with the NPs. One example of this technique is formation by solvent diffusion method of conjugated doxorubicin-PLGA and doxorubicin-loaded PLGA NPs [116].They can be calculated by using the following formulae,

$$\text{Loading efficiency} = \frac{\text{Mass of drug loaded}}{\text{Intial mass of drug}} \times 100 \tag{1.1}$$

$$\text{Encapsulationefficiency} = \frac{\text{Mass of Drug loaded}}{\text{Mass of NPs}} \tag{1.2}$$

Irrespective to the loading methods, loading efficiency and encapsulation efficiencies are two important numbers that define loading capabilities. Drug loading and encapsulation efficiencies are dependent on degree of solubility of the drug in the solution and the matrix. Drug solubility is related to molecular weight of the matrix, its composition, interaction between drug and polymer and existence of end functional groups like ester or carboxyl in drug or in matrix material [117–119]. For some systems, it is observed that as the alkyl chain length becomes longer, the attraction towards the drug is increased. Therefore, the adsorption capacity has a relation with the hydrophobicity of the polymer and specific area of the NPs [120]. In addition to that, surface-active agents and stabilizers also have an influence on the drug loading [121]. It is important to mention here that various factors are crucial for hydrogel swelling/deswelling kinetics- size, cross

linking density and network homogeneity[122–127]. Higher cross-linking density causes a decrease in drug release and swelling response. Bromberg et al. indicates with the example of poly(acrylic acid) based systems that the swelling kinetics decreases with increase in cross-linking density [124]. Swelling kinetics becomes slower and also degree of network swelling decreases as the microgels become more hydrophobic. Hydrophobic modification of the PNIPAm microgels decreases their swelling kinetics as studied by Bysell et al [94]. Moreover, ratio of cross linker and AAc has an effect on the loading of drug onto PNIPAm/AAc particles [94]. Heterogeneity of microgels is also of significance for loading and release kinetics in microgel frameworks. Studies performed by Chu et al. indicate that faster temperature response is achieved with the microgels having voids. Fine tuning of phase transition kinetics is also possible by regulating the size and count of the voids. Thus, significance of microgel polydispersity and structural heterogeneity are the driving force to establish methods which provide monodisperse and uniform microgels [128].

1.13.2 Drug and carrier Interaction

Increased interactions between drug and carrier enhance the loading and encapsulation efficiencies. Hydrophobic and non-electrostatic interactions are of vital significance for loading of amphiphilic drugs[94]. However, ionic interactions between drug and the carrier are the most popular kind of interaction. Introduction of ionic interface between drug and matrix provides improved drug loading as indicated by several studies [93, 94]. Hydrophillic interfaces have given better results for adsorption and release. Hydrophilic hydrogels provide easier loading of hydrophilic drugs and charged bio-macromolecules. Depending on the interaction strength, partially hydrophilic hydrogels will not induce conformational changes and aggregation of proteins. As a result of this, hydrophilic hydrogels enable bio-macromolecules to sustain their biological effects [93, 94].

1.14 Release of the drug

There are a number of factors which govern the drug release rate like (1) drug solubility (2) desorption of the adsorbed drug (3) diffusion of the drug from the NP matrix (4) NP matrix erosion (5) combined effect of erosion and diffusion processes. Subsequently; solubility, diffusion, and biodegradation are important parameters of the particle matrix which oversee the release process [114]. Drug release can also be influenced by the loading efficiency of drug and NP size, smaller particles will provide larger initial burst release as compared to larger particles [129]. If the drug is evenly distributed (for example in case of nanospheres), erosion or diffusion of the matrix will cause the release of the drug.

However diffusion process will be responsible for the drug release, if the diffusion of the drug is faster compared to the matrix erosion. Moreover, if the interaction between drug and particle matrix is weak and/or drug is attached to a large surface of the NPs, then burst release can occur [130]. Research studies have shown that mechanism of incorporation has an influence on the release profile. For instance, if the incorporation method is utilized for drug loading, then the framework has a comparatively little burst release and constant release attributes [131]. In contrast for coating of NPs with the polymer, the release of the drug is regulated through diffusion of the drug from the polymeric system. Coating of NPs with different layers can work as an obstruction to the drug release, causing drug diffusion and solubility in or over the polymer layer act as deciding factors. Besides, release rates can be additionally influenced by ionic interactions between the drug and subsidiary constituents. Least water soluble complex formation takes place due to interaction between the drug and subsidiary constituents, which ultimately effects (slows) the release rate of the drug with more or less no burst release effect [132].

1.14.1 Release Models

Mathematical modeling provides a platform to investigate the mass transfer mechanisms that are involved in the control of drug release [133]. There are few good reviews on mathematical modeling for drug release from bio-erodible polymeric delivery frameworks, hydrogel systems, degradation-controlled drug delivery processes [134]. The most vital systems, for drug transport from polymeric grids are diffusion, erosion and degradation [134]. Brief summary of these systems is condensed in the next sections.

1.14.1.1 Empirical Models

Power law equations can be employed to perform the modeling of the release kinetics. Use of empirical models is not very difficult and it is possible to clarify transport mechanisms utilizing proved empirical rules. Contrarily, these models do not give further bits of knowledge into more complicated transport systems. In addition, these models may come up short whenever there is a requirement for considering particular physicochemical procedures [135].

1.14.1.2 Diffusion-based Models

Drug release for slab-like planes can be modelled using the given mathematical equation based on Fick's second law of diffusion.

$$\frac{M_t}{M_\infty} = 4\left(\frac{Dt}{\Pi h^2}\right)^{\frac{1}{2}} \tag{1.3}$$

Here M_t, represents the quantity of drug released at time t, while M_∞ is the amount of drug release as time approaches infinity. Thickness of the drug delivery device is represented by h, diffusion coefficient of the drug in the polymer grid is given as D.

This equation is valid for the condition $0 \leq \frac{M_t}{M_\infty} \leq 0.6$, which accounts for the first 60 % of cumulative release.

The equation given above is applicable only when the assumption of no deterioration or mass loss of the material grids is met. In order to anticipate the release profile, it is important that diffusion coefficient (D) inside the polymer grid ought to be accessible. This problem can be resolved by using nuclear magnetic resonance, and fluorescence correlation spectroscopy to measure diffusion coefficients [136].

1.14.1.3 Degradation-based models

Model based on polymer dissolution

The process in which polymer starts to release drug to the encompassing liquid, in the vicinity of a thermodynamically suitable solvent is known as polymer disintegration or dissolution [137]. Solute diffusion as well as polymer dissolution can regulate the discharge of the drug from these kinds of polymeric frameworks. On the basis of molecular mechanism, Narasimhan and Peppas constructed a model for polymer dissolution [138]. In equation 1.4 (S-R) is gel layer thickness,

$$\frac{(S-R)}{B} - \frac{A}{B^2}\ln\left\{1 - \frac{B}{A}(S-R)\right\} = t \tag{1.4}$$

In equation 1.4 parameter A and B are given as,

$$A = D\left(v_{1,eq} - v_1^*\right)\left[\frac{v_{1,eq}}{v_{1,eq} + v_{d,eq}} + \frac{1}{v_1^* + v_d^*}\right] + D_d\left(v_d^* - v_{d,eq}\right) \tag{1.5}$$

$$B = \frac{k_d}{v_{1,eq} + v_{d,eq}} \tag{1.6}$$

The equation for cumulative release is

$$\frac{M_d}{M_{d,\infty}} = \frac{v_{d,eq} + v_d^*}{2l}.(\sqrt{2At} + Bt) \tag{1.7}$$

In equations 1.5, 1.6 and 1.7 D is define as diffusion coefficient for the solvent while D_d represents the drug coefficient for drug. While characteristic concentrations for solvent and drug are given as v_1^* and v_d^* respectively. Equilibrium concentration for drug and solvent are represented as $v_{d,eq}$ and $v_{d,eq}$ and rate of polymer dissolution is given as k_d .

Model based on Erosion

Systems in which drug release is based on the erosion of the polymeric surface, Hopfenberg's model can be suitable. In Hopfenberg's model, zero-order surface dissolution of the drug is defined as the rate limiting discharge (of the drug) step. Equation based on this model is applicable on constructs like spheres, cylinders and slabs.

$$\frac{M_t}{M_\infty} = 1 - \left(1 - \frac{k_0 t}{c_0 a}\right)^n \tag{1.8}$$

In the equation 1.8, the amount of drug released after time t is given by the ratio of M_t and M_∞. Shape factor is represented as n in the equation. Value of n varies for different shapes and n=1 for slab, n=2 for cylinder and n=3 for spherical geometries [139].

There are several shortcomings of the Hopfenberg's model. One of them is deviation of the estimated values from the equation for the cylinderical tablet [140]. Katzhendler et al. proposed a model for the release of drug from erodible systems in an attempt to rectify shortcomings in Hopfenberg's model. Radial erosion as well as axial erosion are considered in this model [141].

$$\frac{M_t}{M_\infty} = 1 - \left(1 - \frac{k_a t}{c_0 a}\right)^2 \left(1 - \frac{2k_b t}{c_0 b_0}\right) \tag{1.9}$$

In the equation 1.9, k_a and k_b are radial and axial erosion rate constants respectively. Initial radius of tablet is a_0 while b_0 is the thickness of the tablet.

1.14.2 Drug Release from swellable systems

Higuchi equation in its general form is given as

$$M_t = k\sqrt{t} \tag{1.10}$$

Thin film	**Cylinder**	**Sphere**	**Drug release mechanism**
exponent, n			
0.5	0.45	0.43	Fickian diffusion
0.5< n <1.0	0.45< n <0.89	0.43< n <0.85	Anomalous transport
1.0	0.89	0.85	Case-II transport

TABLE 1.1: Values of n for different geometries and drug release mechanisms from polymeric delivery systems [142].

In the equation 1.10 M_t is cumulative amount of drug which is released while k is rate constant which is equal to,

$$k = A\sqrt{2C_{ini}Dc_s} \tag{1.11}$$

In equation 1.11 C_{ini} initial concentration of the drug and c_s is the drug solubility. Mathematical equation based on Fick's second law of diffusion is given in equation 1.3 which governs Fickian diffusional release from polymeric samples. Drug release from swellable systems is not always in- accordance with the Higuchi's or the zero order equation. Majority of drug release processes from glassy polymers is defined by two limiting cases, that is combination of Fickian and case II transport mechanism (specific transport mechanism) [142, 143]. Case-II transport mechanism is given by $M_t = k_2 t$ where k_2 = case II transport rate constant represents how the polymer relaxation will effect the molecules movement with in the matrix [144]. It is based on two assumptions- a boundary is formed between glassy and rubbery phase of the polymer and boundary moves at constant velocity. Mathematically this behaviour is defined by combining diffusional-controlled and visco-elastic relaxation-controlled drug release

$$\frac{M_t}{M_\infty} = k_1\sqrt{t} + k_2 t \tag{1.12}$$

k_1 and k_2 are constants. In more general form this equation can be described as,

$$\frac{M_t}{M_\infty} = kt^n \tag{1.13}$$

In the equation 1.13 k is the rate constant constants and n is the diffusional exponent. when n is equal to 0.5 then drug release is governed by Fickian drug diffusion and n=1 defines the relaxation drug transport. Whereas, the values of n between 0.5 and 1 describe anomalous drug transport.Table 1.1 indicates different values of n for different geometries and drug release mechanisms from polymeric delivery systems [142, 143].

1.14.3 Drug Release from Nanogels

Drug can be released from nanogels as a consequence of diffusion, degradation of nanogel, pH shift, presence of counterions in the environment, external energy responsible for transition, or, due to environmental changes [111].

Chapter 2

Material & Method

2.1 Materials

Iron pentacarbonyl ($Fe(CO)_5$ 99.99%), octadecene (ODE, 90%), oleylamine (OAm, 70%), chloroauric acid (99.999%), sodium citrate, O-[2-(3-Mercaptopropionylamino)ethyl]-O'-methylpolyethylene glycol (PEG−SH) of weight 5000 Da, 3,4-Dihydroxy-L-phenylalanine (L-dopa), Coumarin, Cytochrome C from bovine heart were purchased from Sigma Aldrich, and Hydrogel (pNIPAm/AAC).

Characterization techniques used are ultraviolet visible spectroscopy (UV-vis), Dynamic light scattering (DLS)and scanning transmission electron microscopy (S(T)EM), while mini centrifuge was used for centrifuging particles.

2.2 Methods

2.2.1 Synthesis of Fe@Au

The Fe@Au NPs were synthesized using a method developed by S. Bandyopadhyay [145]. For the synthesis of Fe@Au NPs, stock solution of 10mM sodium citrate was made, (calculations are given in the appendix A). After that 5 mg, of Fe NPs were added in 10ml of 10mM sodium citrate solution in a tube and this mixture was sonicated for 2 hrs at 80 ^{o}C. After 2 hours, most of the Fe NPs were dissolved in sodium citrate solution and this brown coloured solution was removed from sonicator. A 50ml reactor was put in an oil bath, and this citrate stabilized Fe solution was added to the reactor and maintained at 70 ^{o}C with stirring at 200 rpm. Meanwhile stock solution of 1.5mM chloroauric acid was made and 10 mL of this solution was added drop wise in the reactor

containing citrate stabilized Fe NPs solution. Stirring was increased to 500 rpm, and these reactants were allowed to react for 20 minutes. After about 8 minutes reaction, mixture turned into purplish red solution and after 20 minutes reactor was removed from oil bath and the solution was cooled down to room temperature.

This reaction mixture was centrifuged at 14,500 rpm for 10 minutes. Fe@Au NPs were re dispersed in MQ water. Concentration of the produced Fe@Au NPs was calculated using simple concentration measuring technique, and stored for further use. Setup for the formation of Fe@Au NPs is shown in the Figure 2.1.

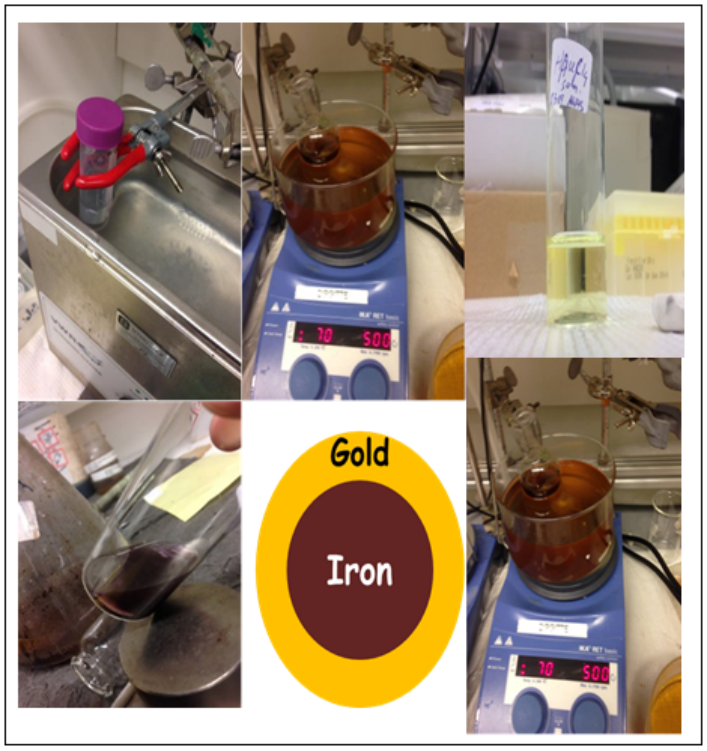

FIGURE 2.1: Setup for the formation of Fe@Au NPs

2.2.2 Coating of Fe@Au NPs

Fe@Au NPs were coated with hydrogel type A by method 1 and 2 and type B by method 2, PEG-SH (term PEG is used throughout this study), and combination of PEG and hydrogel. Coating of Fe@Au with hydrogel will be discussed in the next sub section.

2.2.2.1 Coating of Fe@Au with Hydrogel Type A (Method 1)

Solution of hydrogel having concentration of 1mg/ml was prepared in MQ water. In a separate vial, Fe@Au NPs stock solution was diluted to 10mg/ml concentration. To coat Fe@Au NPs with hydrogel, 500μl of Fe@Au(10mg/ml) was added to 3 ml of hydrogel solution(1mg/ml). After adding Fe@Au NPs to the hydrogel solution, 1.5 ml of MQ water was added to this mixture. Then this mixture was placed on the stirrer at 500 rpm for 2 hours. Reaction solution was removed from the stirrer after 2 hours and centrifuged for 20 minutes at 14,500 rpm. After centrifugation, supernatant were removed and Fe@Au NPs coated with hydrogel was re dispersed in 1 ml of MQ water. This Fe@Au_Hydrogel sample was thereafter stored in the refrigerator for further use.

Safety and precaution relevant to this step is accurate measurement of the hydrogel weight using weighing machine, as it is sometimes difficult to measure the weight of hydrogel due to charging.

It is important that after mixing Fe@Au, Hydrogel and MQ water, the mixture is placed on the stirrer as quickly as possible, because reaction starts immediately after mixing. Magnets used for stirring should always be washed with MQ water before using them.

Special care is needed while removing supernatant, it should be as accurate as possible and supernatant should not contain any Fe@Au_Hydrogel NPs.

2.2.2.2 Coating of Fe@Au with Hydrogel Type A (Method 2)

In order to coat Fe@Au NPs with hydrogel type A (Method 2), 3.3 mg of hydrogel was weighed. Separately, 5 mg/ml of Fe@Au NPs stock solution was made. In the 3.3 mg of hydrogel, 2 ml of 5 mg/ml of Fe@Au NPs solution and 3 ml MQ water were added. After that, the solution was placed on the stirrer at 500 rpm for 2 hours. Reaction solution was removed from the stirrer after 2 hours and the resulting reaction mixture was centrifuged at 14,500 rpm for 20 mins. After centrifugation, supernatant was removed from the Fe@Au_Hydrogel and the formed NPs were re dispersed in 2 ml MQ water and stored in refrigerator for further use.

The main difference between the methods 1 and 2 is the difference in the addition of hydrogel to the Fe@Au NPs solution. In method 1, stock solution of hydrogel in MQ water having 1 mg/ml concentration was first prepared and then this solution of hydrogel was added to the Fe@Au NPs. While in method 2; hydrogel in solid form was mixed with the Fe@Au NPs solution without making its stock solution in MQ water.

Safety and precautions are similar for method 2 as with method 1, however for method 2, it is important that hydrogel should be weighed carefully and exact 3.3 mg should be added to the Fe@Au NPs solution. Higher or lower concentration might affect the results. Figure 2.2 represents the setup for the coating of Fe@Au NPs.

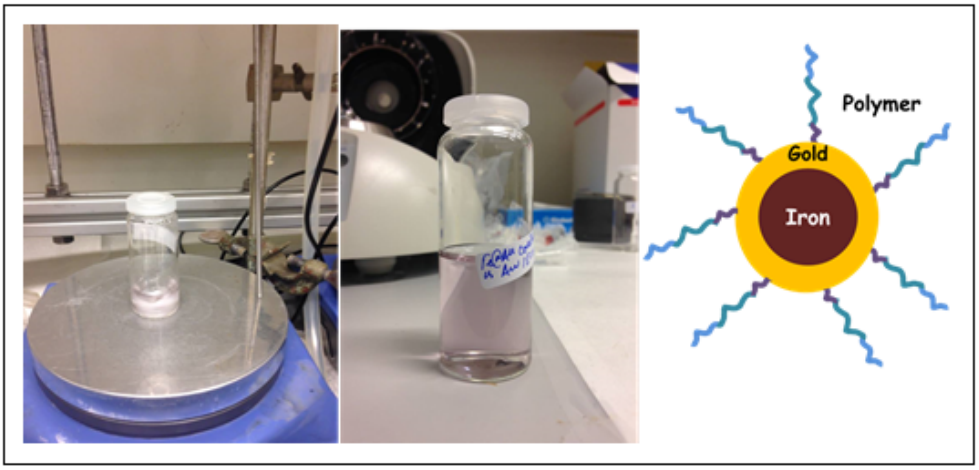

FIGURE 2.2: Setup for the coating Fe@Au NPs

2.2.2.3 Coating of Fe@Au with PEG

PEG coating of Fe@Au was done by adding 500 μl of 10 mg/ml Fe@Au NPs and 4.5 ml MQ water in 2 mg PEG. Afterwards, this solution was placed on the stirrer for 2 hours at 500 rpm. Coating was completed in 2 hours and reaction mixture was removed from the stirrer and centrifuged at 14,500 rpm for 20 mins. After 20 mins of centrifugation, PEG coated Fe@Au NPs were separated from the residual reaction mixture by removing supernatant. Coated NPs were then re- dispersed in 1 ml MQ water and stored in refrigerator for further studies.

Safety and precautions are similar to the hydrogel coating as more or less same procedure was involved in PEG coating. PEG weighing is also tricky as with hydrogel because this white powder is not easy to handle, so extra care should be given during PEG weighing.

2.2.2.4 Coating of Fe@Au with PEG - Hydrogel

Combination of PEG and hydrogel were coated on Fe@Au to exploit combined effects of both PEG and hydrogel. In order to coat PEG and hydrogel on Fe@Au NPs, PEG coating was done on Fe@Au first by adding 500 μl of 10 mg/ml Fe@Au NPs and 4.5 ml MQ water in 2 mg PEG. Two samples of Fe@Au_PEG were made and combined to

give 2 ml of sample. In this 2 ml solution of Fe@Au_PEG, 3.3 mg of hydrogel and 3 ml of MQ water were added. Afterwards this sample was placed on the stirrer for 2 hours at 500 rpm. On completion of coating after 2 hours, the solution was centrifuged using the same conditions and redispersed in 2 ml water. Fe@Au_PEG_Hydrogel sample was thereafter stored in refrigerator.

Safety and precautions are same as for PEG and Hydrogel coating. One important point is the addition of hydrogel to the Fe@Au_PEG as this might cause problem. So, it is important to weigh the hydrogel first and then add Fe@Au_PEG solution to it.

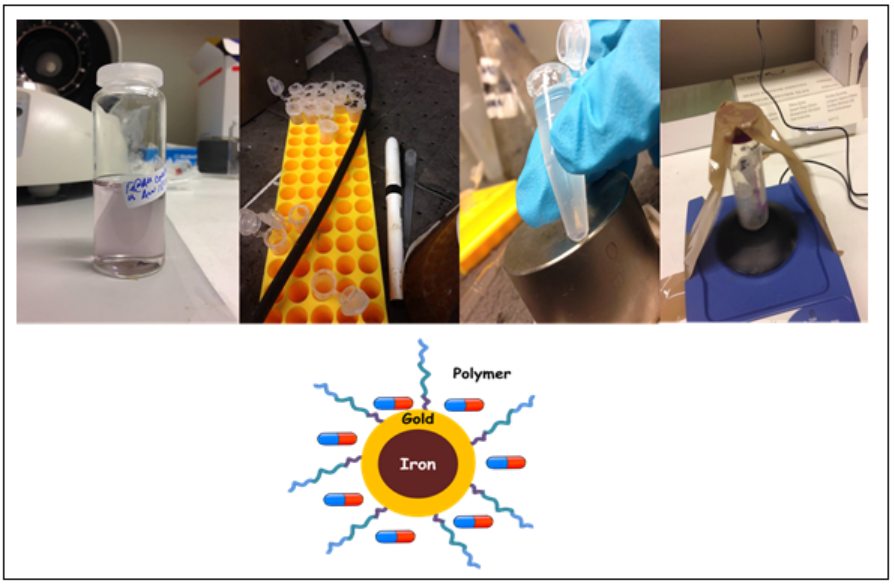

FIGURE 2.3: Steps for the loading of coated Fe@Au NPs

Characterization of the Fe@Au NPs before and after coating were done using DLS, UV-vis spectroscopy, S(T)EM and zeta potential measurements.

2.2.3 Loading

Fe@Au NPs coated with different polymers were loaded with different drugs to use them as drug carriers in therapeutic and theranostics applications. Three drugs namely, L-dopa, Coumarin, and Cytochrome C were employed for loading studies. Procedure used for loading studies is explained in the next section. Results were analysed using UV-vis spectroscopy.

2.2.3.1 L-Dopa

Fe@Au_Hydrogel, Fe@Au_PEG, and Fe@Au_PEG_Hydrogel NPs were loaded with L-Dopa. At first 5 mg/ml Fe@Au particle concentration was used with drug concentration of 0.5 mg/ml. For loading, 1 ml of Fe@Au_Hydrogel having particle of concentration 5 mg/ml was centrifuged at 14,500 rpm for 20 minutes. After centrifugation, supernatant was removed from Fe@Au_Hydrogel NPs. Meanwhile, drug solution having 0.5 mg/ml concentration was prepared. It is important to mention here that L-Dopa has solubility of about 3.2 mg/ml in water at room temperature. L-Dopa is not very soluble in water and requires some time to be completely dissolved. After L-dopa solution was ready, 1 ml of this solution having 0.5 mg/ml concentration was added to the centrifuged Fe@Au_Hydrogel NPs. Similar procedure was used for the loading of Fe@Au_PEG, and Fe@Au_PEG_Hydrogel. After adding drug solution to the coated NPs, three samples were placed on the shaker for 2 hours to complete the loading. After loading, the samples were centrifuged at 14,500 rpm for 20 minutes and the supernatant was measured in the UV-Vis to estimate loading efficiency.

Optimization of Loading Efficiency In order to enhance the loading efficiency, different NP and drug concentrations were used (values of loading efficiencies are given in Appendix C). For instance, in case of Fe@Au_Hydrogel highest loading was achieved for high particle and low drug connection. The optimized results will be discussed in result and discussion section.

Based on the drug and particle concentration used for the L-Dopa, loading studies of Coumarin and Cytochrome c were performed.

2.2.3.2 Coumarin

As mentioned above, Coumarin loading studies were based on the L-dopa loading results. NP concentrations for Fe@Au_Hydrogel, Fe@Au_PEG, and Fe@Au_PEG_Hydrogel which gave best results for L-dopa were used for Coumarin. while drug concentrations used for Coumarin loading were based on the solubility of the Coumarin and highest and lowest concentrations of L-dopa used for loading. Calculations are given in Appendix G.

For Fe@Au_Hydrogel loading, particle concentration of 5 mg/ml and drug concentration of 20 $\mu g/l$ were used. Fe@Au_Hydrogel sample having a volume 1 ml was centrifuged at 14,500 rpm for 20 minutes. After centrifugation, supernatant was removed from the Fe@Au_Hydrogel sample. Drug solution having 20 $\mu g/l$ concentration was prepared and

1 ml of this drug solution was added to Fe@Au_Hydrogel NPs. After adding drug to the NPs, the sample was placed on the shaker for 2 hours at moderate shaking rate. After 2 hours, drug loaded Fe@Au_Hydrogel sample was centrifuged and supernatant was measured in UV-Vis.

Safety and precautions which are important for this step are, handling of coumarin should be done carefully, as it can be toxic or harmful if swallowed. Moreover it is important to place sample as quickly as possible on the shaker after mixing the drug with the Fe@Au_Hydrogel, because loading starts almost immediately after the mixing of drug and Fe@Au_Hydrogel NPs.

2.2.3.3 Cytochrome - C (Cyt-C)

Drug concentration of 0.1 mg/ml and 0.5 mg/ml were used for Cytochrome c loading studies. NP concentrationS for Fe@Au_Hydrogel, Fe@Au_PEG, and Fe@Au_PEG_Hydrogel were same as that for L-dopa and Coumarin loading studies. For Fe@Au_Hydrogel, two samples of 1 ml solution having particle concentration of 5 mg/ml each were centrifuged at 14,500 rpm for 20 minutes. After centrifugation, supernatant was removed and 1 ml of Cytochrome C having a concentration of 0.50 mg/ml was added in one sample while in second sample, drug solution having 0.10 mg/ml concentration was added and samples were placed on the shaker at moderate speed for 2 hours. After 2 hours, samples were removed from shaker and centrifuged and supernatant was measured using UV-Vis. Same procedure was used for the loading of Fe@Au_PEG, and Fe@Au_PEG_Hydrogel.

2.3 Release

Release was performed for Fe@Au_Hydrogel, Fe@Au_PEG, and Fe@Au_PEG_Hydrogel systems loaded with the three drugs (Coumarin, L-Dopa, Cytochrome c) and results were analysed using UV-Vis spectroscopy.

2.3.1 Coumarin Release

Coumarin release studies from Fe@Au_Hydrogel, Fe@Au_PEG, and Fe@Au_PEG_Hydrogel were at first planned under three different conditions, normal pH;high temperature, Low pH;normal temperature, high temperature;low pH. NPs and drug concentrations used for release were same as for the loading studies. Fe@Au_Hydrogel, Fe@Au_PEG, and Fe@Au_PEG_Hydrogel samples (3 samples for each system) loaded with coumarin

were centrifuged at 14,500 rpm for 20 mins. After centrifugation, supernatant was removed from the samples and bottom product for Fe@Au_Hydrogel and Fe@Au_PEG samples were dispersed into 15 ml MQ water respectively (5 ml solution for one study). Fe@Au_PEG sample was measured in the UV-vis, afterwards pH for this sample was measured and it was 6.8. This sample was then divided into two parts. One of 10 ml for high temperature;low pH and normal temperature;low pH (sample 1) and other is of 5 ml for high temperature;normal pH (sample 2), this sample was placed on heating bath at 40 ^{o}C and 500 rpm stirring. For sample 1, solution pH was changed with 0.25mM HCl acid to 3.53. After pH change, this 10 ml solution was divided into 2 parts 5 ml each. One sample was placed onto a heating bath at 40 ^{o}C with stirring at 500 rpm, while to study the effect of low pH other sample was placed on the stirrer at 500 rpm. Similar procedure was repeated with Fe@Au_Hydrogel.

Release study for the above systems did not provide satisfactory results due to low concentrations of the drug. For the third sample, Fe@Au_PEG_Hydrogel, it was decided to increase the concentration by dispersing two loaded samples (1 ml of 100 $\mu g/l$ Coumarin dissolved in 3.75 mg NPs) of Fe@Au_PEG_Hydrogel into 3.5 ml MQ water. Then it was decided to study the release for Fe@Au_Hydrogel and Fe@Au_PEG loaded with Coumarin at high concentrations of drug. For Fe@Au_Hydrogel, three loaded samples were dispersed in 3.5 ml after centrifugation as low drug concentration was used for hydrogel loading. After comparing the results for the three conditions, it was decided to perform the release at high temperature;low pH condition for all the three samples.

High Temperature;Low pH

Two loaded samples each for Fe@Au_PEG and Fe@Au_PEG_Hydrogel were dispersed in 3.5 ml MQ water after centrifugation for 20 minutes at 14,500 rpm. While for Fe@Au_Hydrogel, three loaded samples were dispersed in 3.5 ml water. At time $t_{initial}$, three systems were measured using UV-vis. After that, pH was measured for all the three systems (Fe@Au_Hydrogel, Fe@Au_PEG and Fe@Au_PEG_Hydrogel). For Fe@Au_PEG, Fe@Au_Hydrogel and Fe@Au_PEG_Hydrogel normal pH values were 7.07, 7.04 and 7.02 respectively. To lower the pH, 0.25mM HCl was added to the these three systems. Final pH values for Fe@Au_PEG Fe@Au_Hydrogel and Fe@Au_PEG_Hydrogel were 3.25, 3.22 and 3.16 respectively. Afterwards, these samples were measured in UV-Vis to observe the effect of pH and record t_0. These samples were then placed on the heating bath at 40 ^{o}C with stirring at 500 rpm and measurements were performed using UV-Vis at different time intervals.

2.3.2 L-Dopa Release

L-dopa release was also studied at high temperature;low ph condition. Similar procedure to Coumarin was used for L-dopa release but only single loaded sample for each system was used for L-dopa release.

High Temperature Low pH

One sample each of Fe@Au_PEG, Fe@Au_Hydrogel and Fe@Au_PEG_Hydrogel systems loaded with L-dopa was centrifuged at 14,500 rpm for 20 minutes. After centrifugation, supernatant was removed and loaded NPs were dispersed in 3.5 ml MQ water. As with Coumarin, $t_{initial}$ was measured for these samples using UV-Vis. pH of these samples was then measured using pH meter. Values of pH for Fe@Au_PEG, Fe@Au_Hydrogel and Fe@Au_PEG_Hydrogel were found to be 6.97,7.12 and 7.01 respectively. 0.25mM HCl was added to these samples to lower the pH. After HCL addition, pH for Fe@Au_PEG, Fe@Au_Hydrogel and Fe@Au_PEG_Hydrogel were reduced to 3.50, 3.15 and 3.01 respectively. Effect of pH was observed by measuring samples in UV-vis at time t_0. These samples were then placed on the heating bath at 40 ^{o}C and 500 rpm and change in the absorbance values were observed with UV-Vis at different time intervals.

2.3.3 Cytochrome c

For Cytochrome C release studies procedure similar to Coumarin and L-dopa was adopted. For cyt c two loaded samples each for Fe@Au_PEG Fe@Au_Hydrogel and Fe@Au_PEG_Hydrogel were used for release study.

High Temperature Low pH

Fe@Au_PEG, Fe@Au_Hydrogel and Fe@Au_PEG_Hydrogel loaded with Cyt C (2 samples each for three systems) were centrifuged at 14,500 for 20 minutes. Supernatant was removed from these centrifuged samples and 2 samples for each system (Fe@Au_PEG, Fe@Au_Hydrogel and Fe@Au_PEG_Hydrogel) were dispersed in 3.5 ml MQ water separately. These samples were than measured using UV-Vis to record $t_{initial}$. After measurement, pH was measured for these samples using pH meter. Values of pH for Fe@Au_PEG, Fe@Au_Hydrogel and Fe@Au_PEG_Hydrogel were recorded as 7.05, 7.01 and 7.10 respectively. To make the solution acidic, 0.25mM HCl was added to these samples. After HCl addition, pH for Fe@Au_PEG, Fe@Au_Hydrogel and Fe@Au_PEG_Hydrogel samples changed to 3.21, 3.4 and 3.15 respectively. Effect of pH was then observed by measuring samples in the UV-Vis at time t_0. After measurement, samples were placed on the heating bath at 40 ^{o}C with stirring at 500 rpm to force the drug out of the NPs

carrier. Changes in the absorbance values at different time intervals were recorded with UV-Vis. Release study set up is shown in Figure 2.4.

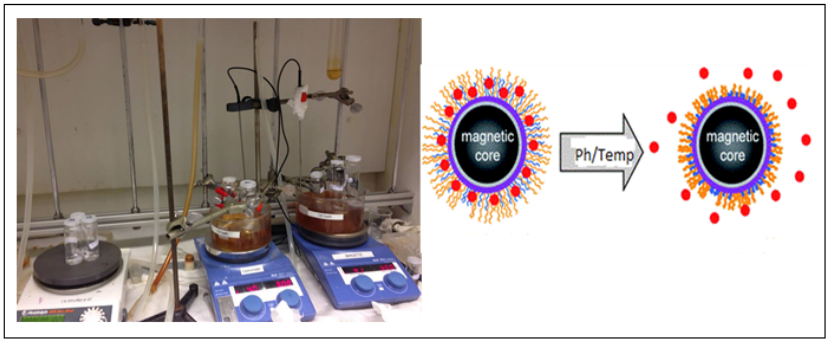

FIGURE 2.4: Release setup for the study of drug release Fe@Au_PEG, Fe@Au_Hydrogel and Fe@Au_PEG_Hydrogel loaded with Coumarin, L-dopa and Cytochrome c

2.4 Characterization techniques

2.4.1 DLS

Size distribution of NPs can be measured with DLS. Brownian motion of suspended particles scatter light in different directions with varying intensities and degrees of polarization after light interacts with particles in the solution[146, 147]. Intensity of scattered light is being measured in this case. Kinetic energy of the particles can cause random motion of particles. This random motion can change the intensity of scattered light with time[148].

Dynamic light scattering measures the diffusion coefficient, size and distribution of particles in colloidal dispersions. Stokes-Einstein equation is used to estimate the hydrodynamic diameter. Diffusion in a dilute dispersion is give as,

$$D = \frac{k_b T}{6\pi\eta R h} \tag{2.1}$$

In this equation k_b is the Boltzmann constant, T is the absolute temperature in K, R_h is the hydrodynamic radius and η is the intrinsic viscosity of the solvent[148].

Nano sizer is the instrument that was used to measure the hydrodynamic sizes of NPs. It can measure size of the particles from lower than nanometers upto microns[149]. Zeta Sizer, which measures both size and zeta potential is shown in Figure 2.5. Principle used to measure samples by this instrument is also explained in Figure 2.5.

2.4.2 Zeta Potential

Zeta potential was also measured using nano sizer. Zeta potential is the amount of electrical charge at the electrical double layer formed by the charged particles. The speed at which charged particles are moving under the influence of an electric field is called electrophoretic mobility [150]. It is measured with the laser doppler micro-electrophoresis which creates an electric field. Electrophoresis is then measured by using phase analysis light scattering [151]. From electrophoretic mobility, zeta potential is calculated using the Smoluchowski equation [152].

$$\upsilon_E = 4\pi\epsilon_0\varepsilon_r \frac{\xi}{6\pi\mu}(1 + kr) \tag{2.2}$$

where υ_E is the mobility of the particles in electric field, k is the Debye-Huckel parameter, ϵ_0 and ε_r are the relative dielectric constants and electrical permittivities of vacuum respectively, r is the radius of the particle and μ is the viscosity of the solution [152].

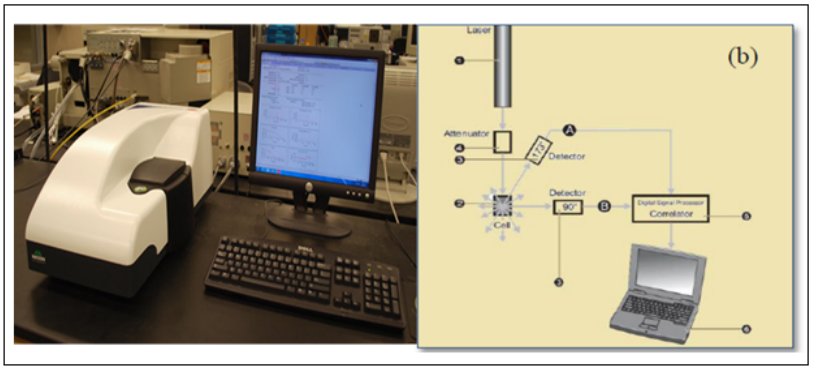

FIGURE 2.5: Zeta sizer and principle of measurement respectively

Instrument was turned on with settings to measure both size and the zeta potential of particles. Size was measured in the plastic size cuvette and zeta potential was measured with zeta cuvette. The cuvettes used for the measurement are shown in Figure 2.6.

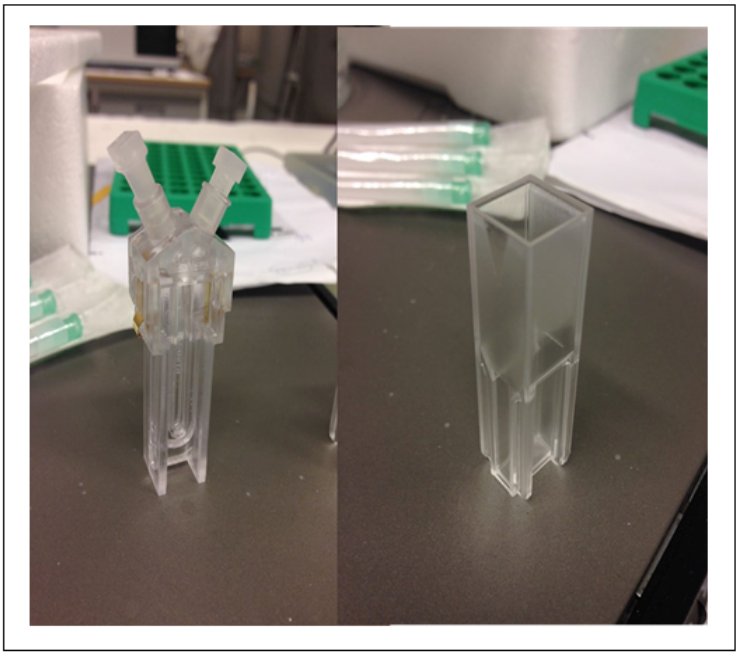

FIGURE 2.6: Zeta and size cuvettes used for measurements

2.4.3 UV-vis Spectroscopy

The instrument is based on the absorption of light by particles in solution, it measures the amount of ultraviolet or visible radiation which is absorbed by substance in solution. Beer Lambert law is used to measure the concentration by using the absorption spectra [153, 154].

$$A = -\left(\frac{I}{I_0}\right) = ecl \tag{2.3}$$

In this equation, A is the absorbance, I_0 and I are the intensities of light before and after the light passes through the sample, c is the concentration of solute in solution, l is the path length of radiation through the sample. Absorbance is measured in UV-vis at specific a wavelength. Normally, wavelength which gives maximum absorbance value is chosen. Three different procedures are used to calculate the absorption. When it is not easy to get a sample of reference substance, standard absorptivity value procedure is used. Second procedure is single or double point standardization while third is calibration which is used when standard solution with known concentration is measured with corresponding measurement of the absorbance [153]. One possible problem with this instrument can be false positive results due to secondary binding or some nonspecific

adsorption [95]. UV-24011PC, which was used for the measurements, is shown in the Figure 2.7.

UV-vis was turned on and baseline with water was done before the measurements of solutions. Cuvette used in the measurements is shown in Figure 2.8.

FIGURE 2.7: Uv-vis instrument used for the measurements

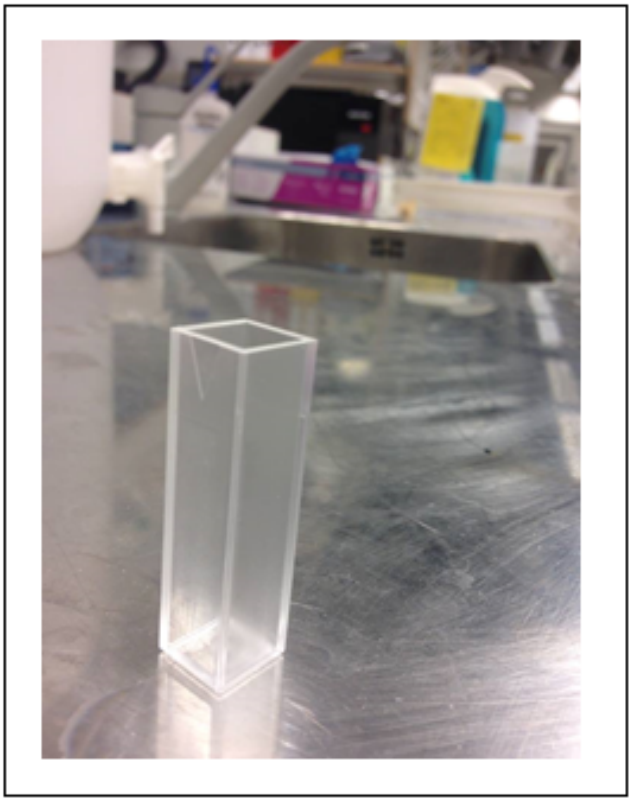

FIGURE 2.8: Cuvette used for the measurements UV-vis

2.4.4 S(T)EM

Scanning transmission electron microscope (S(T)EM) is used for the characterization of nanostructures. S(T)EM is a valuable instrument as it gives electronic structure of single atoms with extreme sensitivity and information for the composition of various elements. Working principle for the S(T)EM is based on scanning of the sample with focussed beam of electrons, and collecting the desired signals to produce an image[155]. Working principle is similar to the SEM, the difference is the use of thin specimens in S(T)EM. Thin specimens are used in S(T)EM to avail the transmission modes of imaging. S(T)EM is a relatively fast means for characterizing nanostructures because there is no need of grinding, polishing or ion milling[156].

Hitachi S-5500 S(T)EM instrument placed in NTNU nanolab was used to study the samples. Samples were deposited on the C-coated copper TEM grids and placed on the sample holder. This sample holder was then placed inside the instrument. Current and voltage were adjusted to get the desired images and information for the samples.

Chapter 3

Results & Discussions

3.1 Synthesis and Characterization of Fe@Au NPs

Fe@Au NPs were synthesized by adding chloroauric acid in the hot citrate stabilized Fe NPs solution. Size of the particles was measured using S(T)EM and DLS. Figure 3.1 a-e) shows a representative S(T)EM image of Fe@Au NPs, DLS sizes and zeta potential values of Fe@Au NPs measured at 25 ^{o}C and 40 ^{o}C, effect of pH on the size and UV-vis spectra of Fe@Au particles at 25 ^{o}C and 40 ^{o}C respectively. Error bars indicate standard deviation from three measurements. S(T)EM measurement provides the average size of Fe@Au NPs as 24±5 nm, while DLS gives an average size of 54.30± 0.52 nm. This difference in the values is because DLS measurement gives the hydrodynamic diameter, the diameter of the dispersed particles in the solution, while size measurement with S(T)EM gives the dry diameter. Further, the difference lies in the fundamental principle of measurement used in the two techniques.

Zeta potential depicts the stability of the Fe@Au NPs, a higher value indicates higher stability. High negative zeta potential (-36.80±0.896 mV) of Fe@Au NPs confirms their stability in aqueous medium. There is no substantial change in the zeta potential values of the NPs on increasing temperature. This indicates that the particles are stable to aggregation at higher temperatures. This stability is provided by the presence of citrate ions on the surface of the NPs that generate Coulombic repulsion among NPs. However, Figure 3.1 d) shows an increase in size of Fe@Au NPs when pH is decreased. This is because of protonation of the citrate groups on Au surface which are formed at lower pH. This results in reduced electrostatic stability leading to agglomeration of NPs. Figure 3.1 e) shows the absorbance peak for Fe@Au NPs at 25 ^{o}C and 40 ^{o}C respectively. LSPR of these NPs is obtained around 524 nm and there is no relative shift of the peak at

increased temperature. This, in addition to the size and zeta potential results, indicates that the synthesized NPs are stable towards aggregation with respect to temperature.

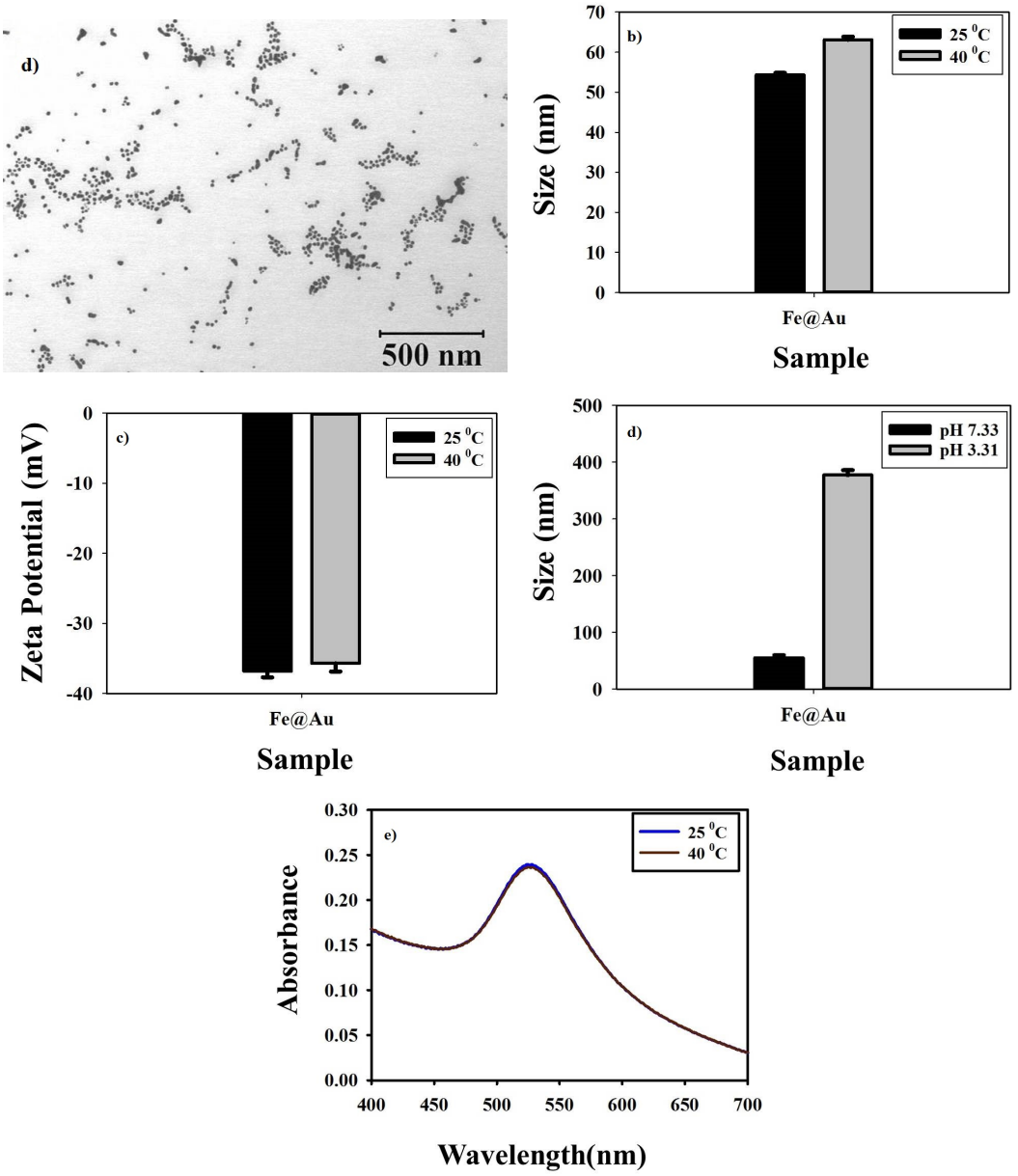

FIGURE 3.1: a) Representative S(T)EM image of Fe@Au NPs b) Variation of DLS sizes of Fe@Au NPs at 25 ^{o}C and 40 ^{o}C c) Variation of Zeta potential of Fe@Au NPs at 25 ^{o}C and 40 ^{o}C d) Variation of DLS sizes of Fe@Au NPs with pH e) UV-vis spectra of Fe@Au NPs at different temperatures

3.2 Coating of Hydrogel

As discussed in the method section 2.2.2, hydrogel samples A and B were used for the coating of Fe@Au NPs. In the preceding section, the physico-chemical properties of both hydrogels, which were used in this study, will be discussed.

3.2.1 Physico-chemical properties of hydrogels

Both hydrogels A and B are pNIPAm/AAc based and were synthesized in Ugelstad laboratory previously [157]. The basic difference between the two is the initial stabilizer concentration (Sodium dodecyl sulphate, SDS)- high SDS concentration is used for hydrogel B.

Hydrogel A Figure 3.2 a) and c) show the sizes and zeta potentials of hydrogel A at 25 ^{o}C and 40 ^{o}C respectively. While 3.2 d) and e) represent the reversibility of the hydrogel in terms of size and volumetric swelling ratios respectively (α). α is defined as $\alpha = \left(\frac{D_H}{D_0}\right)^3$ where D_H = hydrodynamic diameter of the hydrogel at any temperature (T ^{o}C) during heating/cooling and D_0 = hydrodynamic diameter of the hydrogel at room temperature (T ^{o}C) during heating/cooling. It is important to mention here that α values were calculated separately for heating and cooling.

Hydrogel A shows a decrease in the size at higher temperature due to phase transition behaviour, as discussed in section 1.3.3.3. PNIPAm based polymers undergo endothermic phase transition that is driven by entropy. This happens above VPTT, when the hydrogels transit from hydrophilic to hydrophobic state. Figure 3.2 b) shows that decrease in pH causes collapse of the hydrogel owing to protonation of the carboxylic groups from AAc blocks. Dissociated poly AAc segments are more hydrophilic than non-dissociated segments, whereby a transition from lower to higher pH causes a decrease in the free energy of mixing [158]. Zeta potential for hydrogel A is -17.20±0.12 mV at 25 ^{o}C. Zeta potential decreases at higher temperature due to decrease in size at elevated temperature, that leads to increase in the surface charge of the hydrogel. Additionally, carboxyllic groups on the surface of hydrogels are more exposed at higher temperature due to hydrophilic-hydrophobic transition above VPTT. As discussed in section 1.3.3, hydrogel based systems can release the drug owing to environmentally switch-able structures. Hydrogel A has shown substantial reversibility with respect to temperature, as confirmed from Figure 3.2 c). VPTT values for heating and cooling were calculated as 37.7 ^{o}C and 36.7 ^{o}C respectively (using developed procedure given in Appendix E) which further confirm the reversible nature of this system . Volumetric swelling ratios are better representations of the swelling of hydrogels owing to the fact that the hydrogels swell or collapse volumetrically rather than as a single chains.

From the above discussion, it can be concluded that hydrogel A shows collapse at around 37.5 ^{o}C which confirms that it will change its structure at this temperature which is close to body temperature. Increase in the value of zeta potential also indicates decrease in the particle size and no substantial change in stability. Reversibility of the hydrogels

is also confirmed from the volumetric swelling ratios with very minor difference in the heating and cooling collapse temperatures which is very important for drug delivery applications.

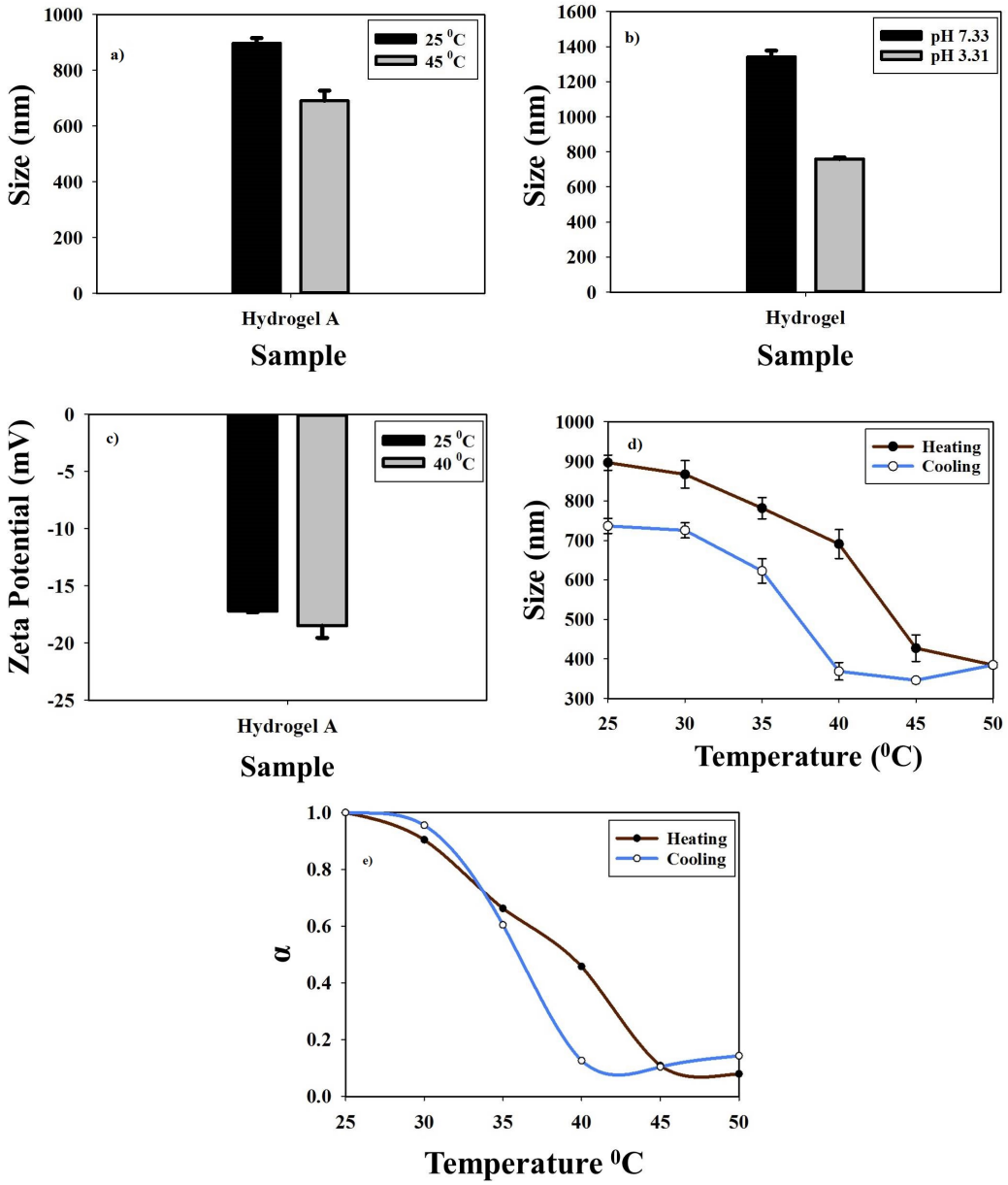

FIGURE 3.2: a) Variation of DLS sizes of hydrogel A at 25 ^{o}C and 40 ^{o}C b) Variation of DLS sizes of hydrogel A with pH c) Variation of Zeta potentials of hydrogel A at 25 ^{o}C and 40 ^{o}C d) Variation of sizes of hydrogel A as function of temperature e) Variation of α as a function of temperature

Figure 3.3 a) and b) represents the STEM images for Hydrogel A at 25 ^{o}C and 50 ^{o}C respectively. It can be observed from these images that at 25 ^{o}C, hydrogels are uniformly distributed and at 50 ^{o}C they from aggregates. This might be due to the effect of drying of nanogels from solution, because the nanogel solution was heated and then a drop of the

heated solution was put on the STEM grid. Moreover, as it is confirmed from the DLS measurements, that there is a decrease in the size of nanogels at higher temperature. It is reasonable to state that DLS is measuring these nanogels individually rather than as an aggregate owing to hydrophilic environment around each particle.

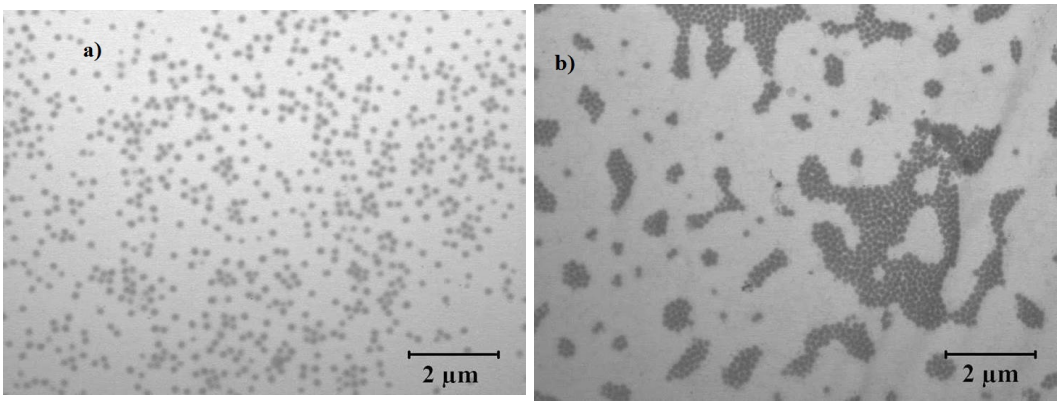

FIGURE 3.3: (a) Representative S(T)EM image of hydrogel A at 25 ^{o}C (b) Representative S(T)EM image of hydrogel A at 50 ^{o}C

Hydrogel B Figure 3.4 a) and c) show the sizes and zeta potentials of hydrogel A at 25 ^{o}C and 40 ^{o}C respectively, while Figures 3.4 d) and e) represent the reversibility of the hydrogel in terms of size and volumetric swelling ratios respectively.

Size and zeta potential trend is similar to hydrogel A with smaller size of gels for hydrogel B, as in this case higher, stabilizer concentration is used compared to that of hydrogel A. Lower values for zeta potential (-12.3 mV$\pm$0.55) are also observed for this hydrogel compared to hydrogel A. Reversibility of the hydrogel B is confirmed as indicated in the Figure 3.4 c. However, hysteresis is observed while cooling down the hydrogels, it not very significant due to the fact that different size values were observed while measuring the same sample twice. Volumetric swelling ratio values also indicate small hysteresis when cooling down. Hydrogel B has better reversibility with not very significant hysteresis as compared to hydrogel A. This is also confirmed from the VPTT calculations for heating and cooling of hydrogel B. For heating and cooling, collapse temperature is 38 ^{o}C for this hydrogel, which indicates reversibility of this nanogel.

For hydrogel B, similar results were observed as with hydrogel A in regards to collapse and reversibility. However, hydrogel B is smaller in size and also shows better reversibility under heating and cooling than hydrogel A as confirmed from VPTT calculations.

S(T)EM images for hydrogel B (not shown here) indicate similar behaviour as shown by hydrogel A.

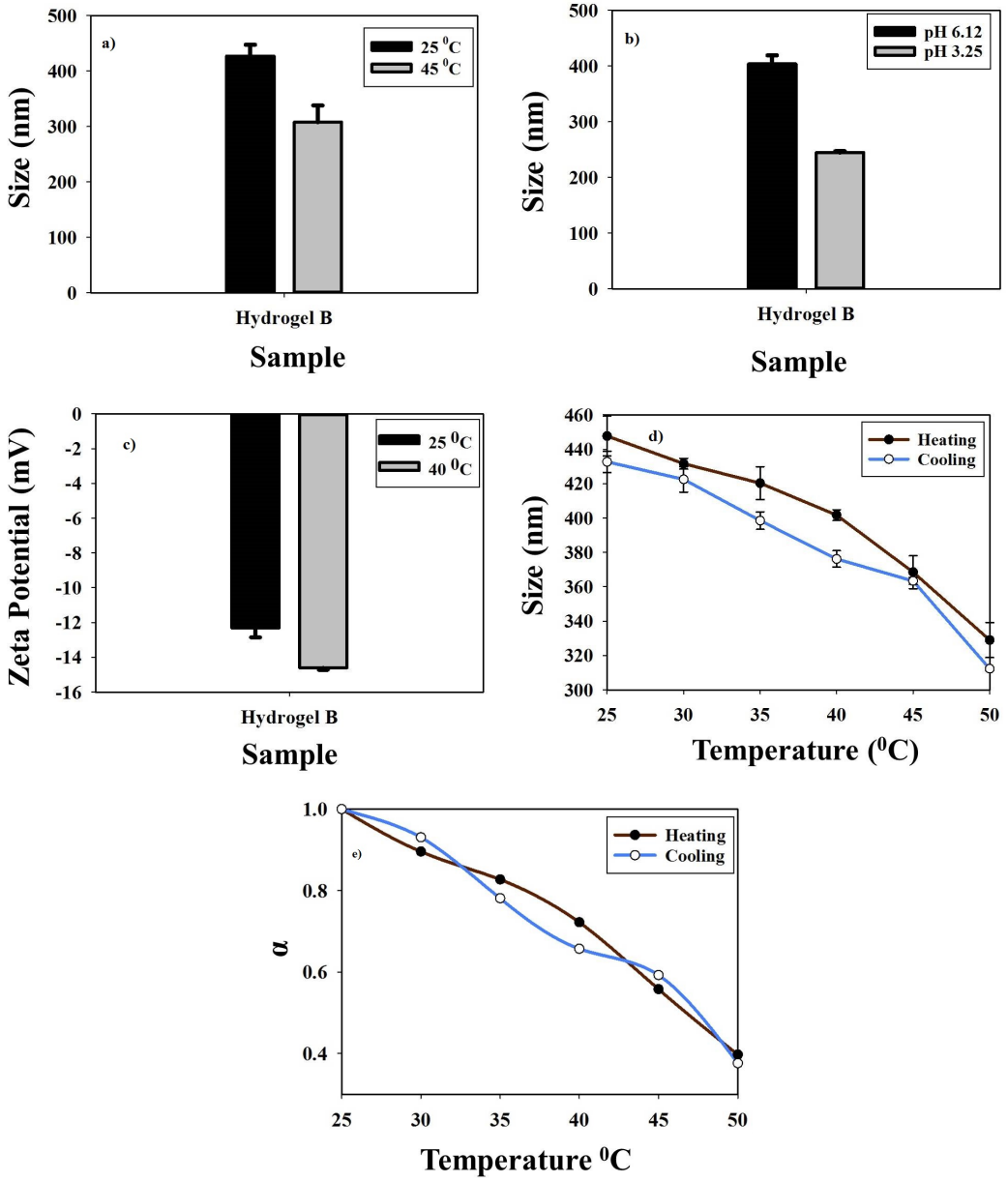

FIGURE 3.4: a) Variation of DLS sizes of hydrogel B at 25 ^{o}C and 40 ^{o}C b) Variation of DLS sizes of hydrogel B with pH c) Variation of Zeta potentials of hydrogel B at 25 ^{o}C and 40 ^{o}C d) Variation of sizes of hydrogel B as function of temperature e) Variation of α as a function of temperature

3.2.2 Fe@Au Hydrogel A

Method 1 As explained in section 2.2.2, Fe@Au NPs were coated with hydrogel A and B by using two different methods. Coating of Fe@Au NPs with hydrogel A by method 1 shows opposite trend for size, zeta potential, reversibility and volumetric swelling ratio values compared to only hydrogel A as shown in the Figure3.5. Figure3.5 a-d) illustrate the size, zeta potential at 25 ^{o}C and 40 ^{o}C and reversibility, volumetric swelling ratios

for Fe@Au_Hydrogel A respectively. Figure 3.5 a) indicates increase in size at 40 ^{o}C for Fe@Au_Hydrogel compared to size at 25 ^{o}C. This increase in size with increasing temperature might be due to the effect of Fe@Au NPs acting as a cross-linker whereby pulling together the gel units. This hypothesis is also supported by the STEM images for this system at 25 ^{o}C and 50 ^{o}C (Figure 3.6). Studies with similar systems also support this assumption [159].

High negative values for zeta potential indicate that coating of hydrogel provides further stability to the Fe@Au NPs as illustrated by Figure 3.5 c), which is significant in drug loading application. Figure 3.5 f) shows that due to higher charge on the surface of Fe@Au NPs, zeta potential of Fe@Au_Hydrogel has larger negative value (zeta potential -34.40±0.42 mV) compared to the hydrogel (zeta potential -17.2±0.12 mV) .The increase in zeta potential of Fe@Au_Hydrogel at higher temperature might be due to increase in the size which ultimately decreases the average charge per unit area of the particles. Reversibility of the Fe@Au_Hydrogel system is confirmed as indicated in Figure 3.5 c). Opposite trend is observed but reversibility of the coated gels provides a platform for their use in drug delivery applications. Hysteresis is not very large and can be explained on the same grounds as with hydrogels. Volumetric swelling ratios also confirms the reversibility of these systems with some hysteresis between 35 ^{o}C to 40 ^{o}C which is not very significant and can be due to cooling and heating effects and error stemming from repeated measurements. VPTT values for this system are around 38.5 ^{o}C and 37.8 ^{o}C for heating and cooling respectively. which confirm that these systems are quite reversible even after addition of Fe@Au to the system. This indicates that coating does not have significant effect on the reversibility of the nanogels, although bare hydrogels are more reversible in terms of swelling-collapse behaviour.

UV-vis spectra of Fe@Au_Hydrogel type A shows their absorbance peak around 518 nm compared to the Fe@Au which shows peak at 524 nm. This shift in the peak can be explained on the basis of increase in the energy required to exit the electron which shifts the wavelength to lower value as explained by Planks equation (E=hc/λ). This behaviour is shown due to the coating of hydrogel on Fe@Au NPs. This further confirms that hydrogel coating does affect the optical signature of the Fe@Au but the peak is still visible. Moreover, at higher temperature, there is not any significant shift in the wavelength for Fe@Au_Hydrogel system. The minor difference at 25 ^{o}C and 40 ^{o}C is attributed to the turbidity of the hydrogels at elevated temperatures.

From the above discussion, it is inferred that Fe@Au_Hydrogel type A shows increase in size at higher temperature but comes back to almost the same size as indicated by reversibility data. Moreover higher stability of the Fe@Au NPs is achieved by their coating with the polymer with minor effects on the optical properties of the Fe@Au after

coating with polymer as indicated by UV-vis absorbance peak. Therefore, Fe@Au coated with hydrogel can act as a unique drug carrier with magnetic, optical and switchable payload release signatures. Figure 3.5 f) shows a comparsion of zeta potential of Fe@Au, hydrogel A and and Fe@Au_Hydrogel A as a function of temperature. Stability of Fe@Au NPs after coating is retained (high negative values of zeta potential for both Fe@Au and Fe@Au_Hydrogel A), while the hydrogel stablity should not be directly interpreted from the data since size changes also affect zeta potential values.

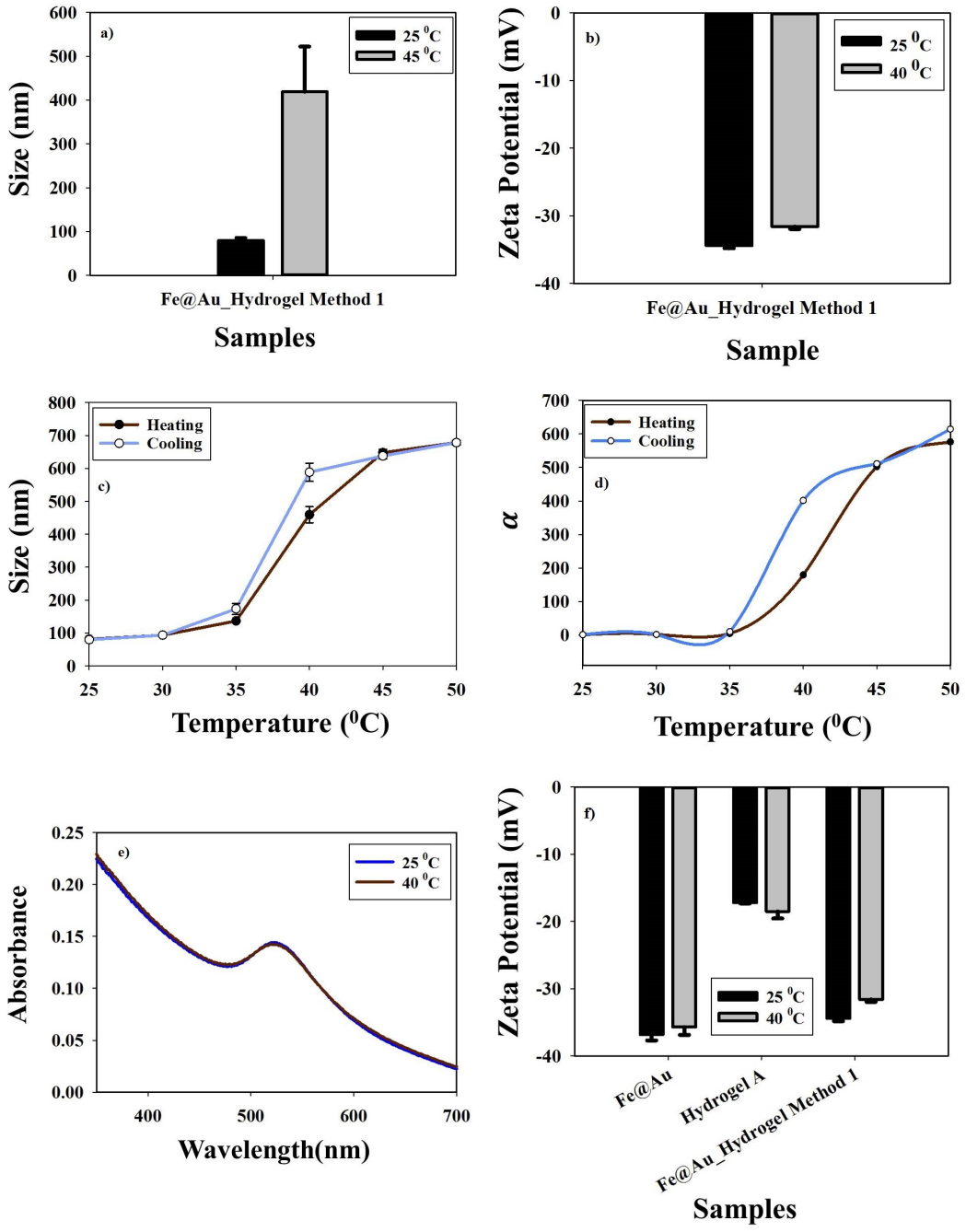

FIGURE 3.5: a) Variation of DLS sizes of Fe@Au_Hydrogel A coated by method 1 at 25 ^{o}C and 40 ^{o}C b) Variation of Zeta potential of Fe@Au_Hydrogel A coated by method 1 at 25 ^{o}C and 40 ^{o}C c) Variation of sizes of Fe@Au_Hydrogel A network coated by method 1 as a function of temperature d) Variation of α as a function of temperature e) UV-vis spectra of Fe@Au_Hydrogel A coated by method 1 at 25 ^{o}C and 40 ^{o}C f) Comparison of zeta potentials of Fe@Au, hydrogel A and and Fe@Au_Hydrogel A at 25 ^{o}C and 40 ^{o}C

S(T)EM images for Fe@Au_Hydrogel A are shown in the Figure 3.6 a) and b). These images confirmed the presence of Fe@Au on the periphery of the nanogel surface which means that enough space is available on the surface of the hydrogels for drug loading.

This indicates that drug will have sufficient chances to interact with the hydrogel structure as well as magnetic and optical properties are provided by the Fe@Au NPs present on the surface of the hydrogel. Moreover, heating of this system at 50 ^{o}C will cause the aggregation of the hydrogel as also shown by hydrogel sample alone. Interesting point here is that NPs are still on the surface of the hydrogels and acting as a cross-linker and pulling the gel structures together. Another interesting observation is the increase in particle number density upon heating, hinting towards collapse of individual hydrogel units. However, DLS data provide increase in sizes which can be attributed to cross-linking effect of NPs acting as bridge molecules between collapsed hydrogel units.

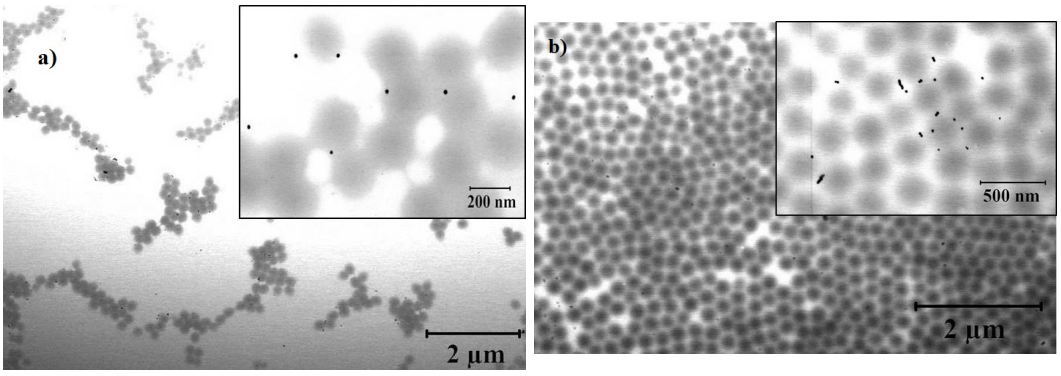

FIGURE 3.6: a) Representative S(T)EM image of Fe@Au_Hydrogel A coated by method 1 at 25 ^{o}C b) Representative S(T)EM image of Fe@Au_Hydrogel A coated by method 1 at 50 ^{o}C

Method 2 Similar set of studies were performed for coating of hydrogel type A by method 2 and more or less similar outcomes were obtained. These results for size, pH effect, zeta potential, swelling de-swelling and volumetric swelling ratios are depicted in Figure 3.7 a-e) while figure f) presents the UV-Vis spectra. Size and Zeta potential measurements shows similar results as for Fe@Au_Hydrogel A coated with method 1. Reversibility studies for Fe@Au_Hydrogel A coated with method 2 shows higher reversibility with VPTT of around 37.9 ^{o}C and 37.7 ^{o}C for heating and cooling respectively. Low hysteresis is indicated by the Figure 3.7 d) and e) compared to the Fe@Au_Hydrogel A coated by method 1. This observation made Fe@Au_Hydrogel A coated with method 2 a better method for coating of Fe@Au NPs. Fe@Au optical signature after coating is also valid for this method. Method 1 and 2 almost provide similar sets of results. However Fe@Au_Hydrogel type A coated by method 2 gave better reversibility of the Fe@Au_Hydrogel as confirmed by VPTT calculations for heating and cooling and also they gave higher loading efficiency, which will be discussed in the loading section. On the basis of these superior qualities of Fe@Au_Hydrogel coated with method 2, it was decided to use it for the loading and release studies in this research.

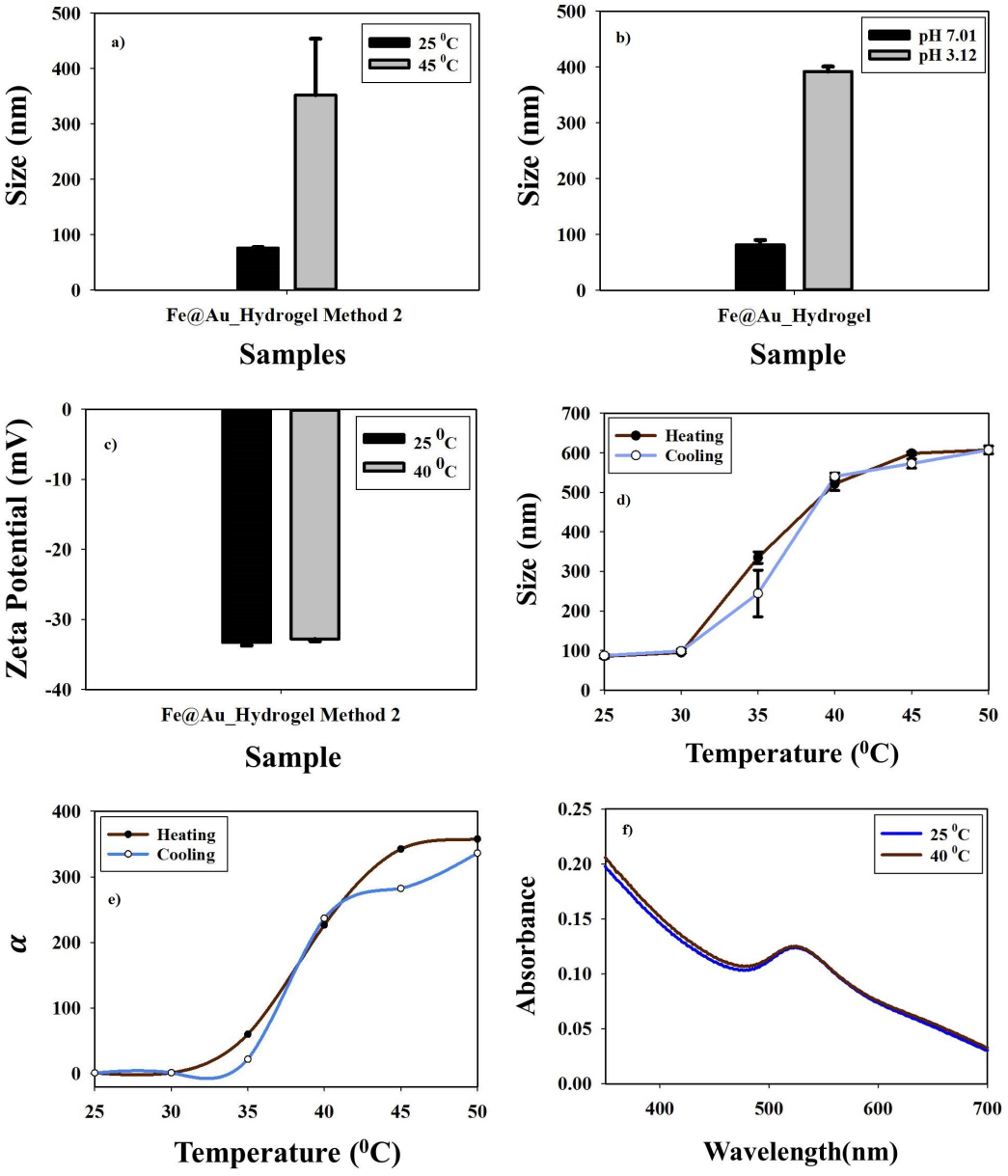

FIGURE 3.7: a) Variation of DLS sizes of Fe@Au_Hydrogel A coated by method 2 at 25 ^{o}C and 40 ^{o}C b) Variation of DLS sizes of Fe@Au_Hydrogel A coated by method 2 with pH c) Variation of Zeta potential of Fe@Au_Hydrogel A coated by method 2 at 25 ^{o}C and 40 ^{o}C d)Variation of sizes of Fe@Au_Hydrogel A network coated by method 2 as a function of temperature e) Variation of α as a function of temperature f) UV-vis spectra of Fe@Au_Hydrogel A coated by method 2 at at 25 ^{o}C and 40 ^{o}C

S(T)EM images for the Fe@Au_Hydrogel A coated with method 2 are represented in the Figure 3.8 a) and b). Similar behaviour to method 1 can be observed for this method as well. Presence of Fe@Au on nanogel surface before and after heating confirms the coating with hydrogel A and also reduction in the size of hydrogels is clear from these images.

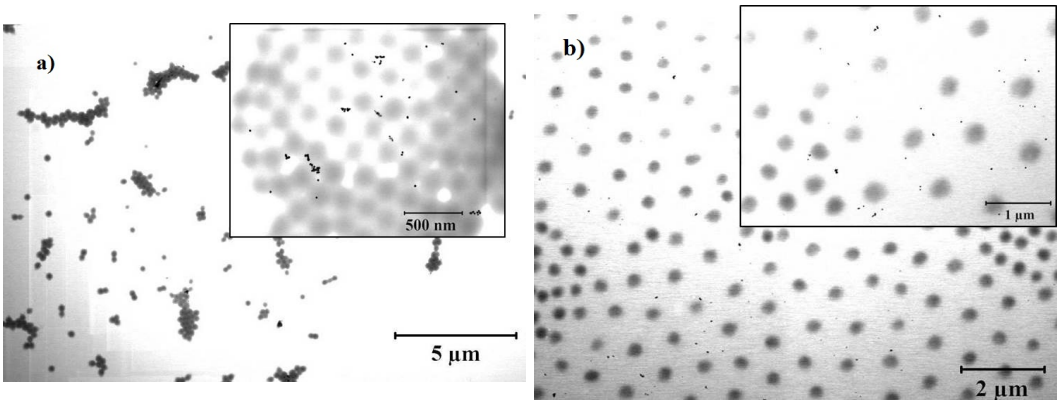

FIGURE 3.8: a) Representative S(T)EM image of Fe@Au_Hydrogel A coated by method 2 at 25 ^{o}C b) Representative S(T)EM image of Fe@Au_Hydrogel A coated by method 2 at 50 ^{o}C

3.2.3 Fe@Au Hydrogel Type B

Fe@Au_Hydrogel B was used to compare it with the hydrogel A. Method 2 was used for type B as it was concluded in the above section that method 2 provides better results compared to that of method 1.

Method 2 Sizes, pH effect on size, Zeta potentials, reversibility and volumetric swelling ratios for heating and cooling of Fe@Au_Hydrogel B coated by method 2 are illustrated in the Figure3.9 a-d) respectively.

Size measurements show increase in size of the hydrogel type B at higher temperature as indicated for the hydrogel type A. Zeta potential of hydrogel has showed higher negative values compared to type A which is advantageous in terms of stability and increase in temperature does not induce large changes in zeta potential values for Fe@Au_Hydrogel B. Reversibility results indicate that Fe@Au_Hydrogel type B system is appreciably reversible with VPTT for heating and cooling at 39.8 ^{o}C and 39.5 ^{o}C respectively and negligible hysteresis.

Better results for reversibility of the Fe@Au_Hydrogel type B coated by method 2 as well as higher loading values as show in the loading section and higher stability of this system are the reasons for their use in this work.

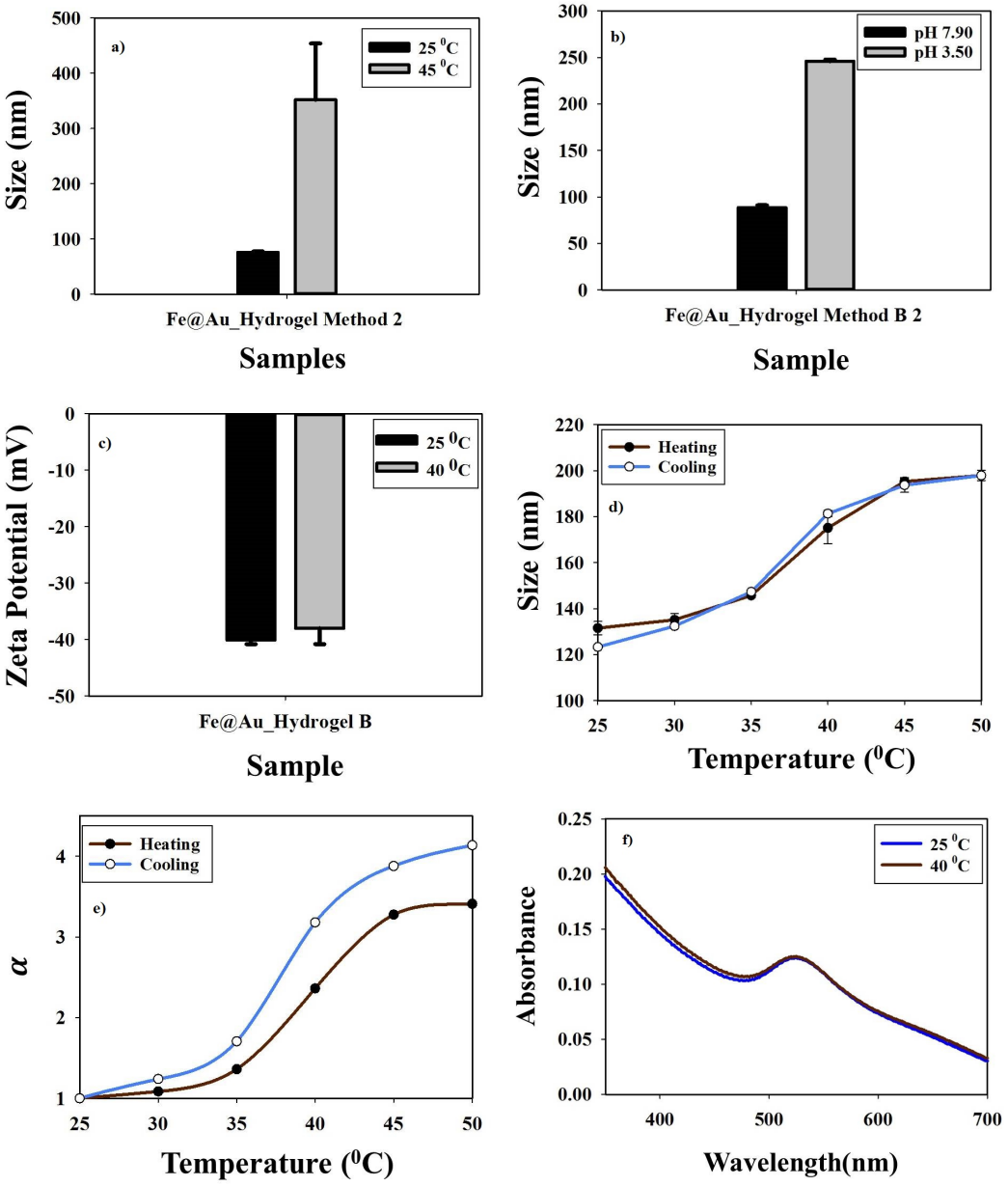

FIGURE 3.9: a) Variation of DLS sizes of Fe@Au_Hydrogel B coated by method 2 at 25 ^{o}C and 40 ^{o}C b) Variation of DLS sizes of Fe@Au_Hydrogel B coated by method 2 with pH c) Variation of Zeta potential of Fe@Au_Hydrogel B coated by method 2 at 25 ^{o}C and 40 ^{o}C d) Variation of sizes of Fe@Au_Hydrogel B network coated by method 2 as a function of temperature e) Variation of α as a function of temperature f) UV-vis spectra of Fe@Au_Hydrogel B coated by method 2 at at 25 ^{o}C and 40 ^{o}C

3.3 Fe@Au PEG

Coating of PEG is done on Fe@Au NPs because of several advantages of PEG coating that includes increase in the half-life time of nanocarriers, through cloaking properties

and steric stabilization. Size and zeta potentials of Fe@Au and Fe@Au_PEG are illustrated in the Figures 3.10 a) and c). It is clear from the Figure 3.10 a) that there is an increase in the size of Fe@Au to 74.81±2.18 nm after they are functionalized with the PEG. S(T)EM images Figure 3.10 d) and e) also illustrate the increase in the size after coating of PEG on Fe@Au. Figure 3.10 b) shows the effect of pH on the size of Fe@Au_PEG.

Increase in DLS size of Fe@Au_PEG to 74.9±2.18 nm is similar to the previous study done at uglestad laboratory [145]. Increase in the size is due to hydrophobic effect of PEG at higher temperature that cause hydrphobic aggregation of NPs. This is also supported by the S(T)EM images Figure 3.10 d) and e). Zeta potential of Fe@Au_PEG NPs is -31.30±2.68 mV compared to Fe@Au -36.80±0.90 mV. The difference is attributed to the increase in the size after PEG coating. Furthermore, there is shift in the zeta potential towards zero at higher temperature also due to slight increase in the size of Fe@Au NPs at higher temperature.

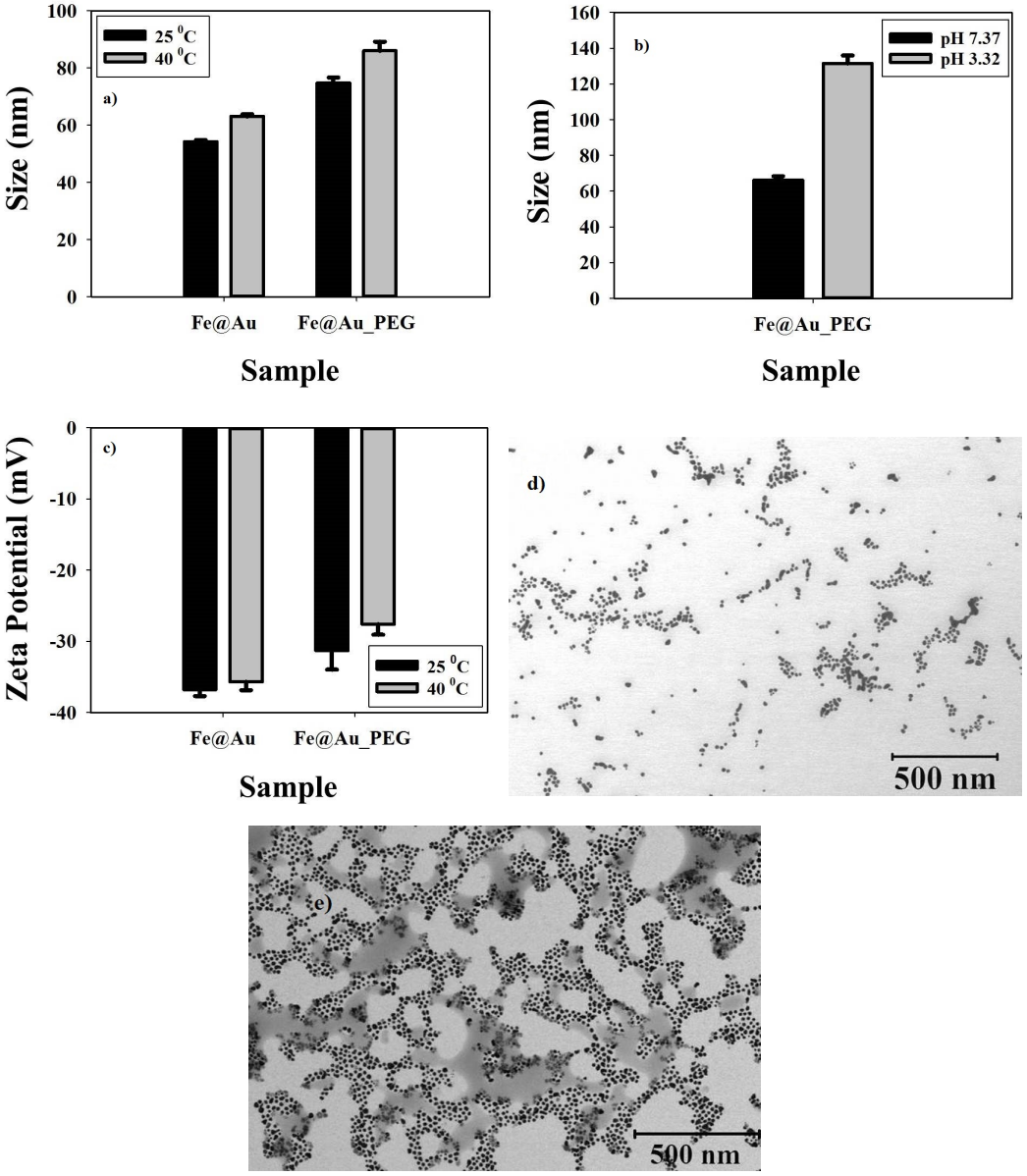

FIGURE 3.10: a) Variation of DLS sizes of Fe@Au_PEG at 25 ^{o}C and 40 ^{o}C b) Variation of DLS sizes of Fe@Au_PEG with pH c) Variation of Zeta potential of Fe@Au_PEG at 25 ^{o}C and 40 ^{o}C d) Representative S(T)EM image of Fe@Au at 25 ^{o}C e) Representative S(T)EM image of Fe@Au_PEG at 50 ^{o}C

UV-Vis Study PEG coating causes a red shift in the absorbance peak (529 nm) for Fe@Au NPs as shown in the Figure 3.11 a) and b), this bathochromic shift caused by the PEG coating is an indication of the increase in the size of NP after coating. This is predicted by Mie-Drude theory [159]. This behaviour is observed at both 25 ^{o}C (Figure 3.11 a)) and 40 ^{o}C (Figure 3.11 b)) and is in conformation with previous studies [145]. Effect of temperature on Fe@Au_PEG is not very significant even at low concentration, which is important for the drug delivery application of this system and also for release of the drug for this kind of carrier that depends on optical signature.

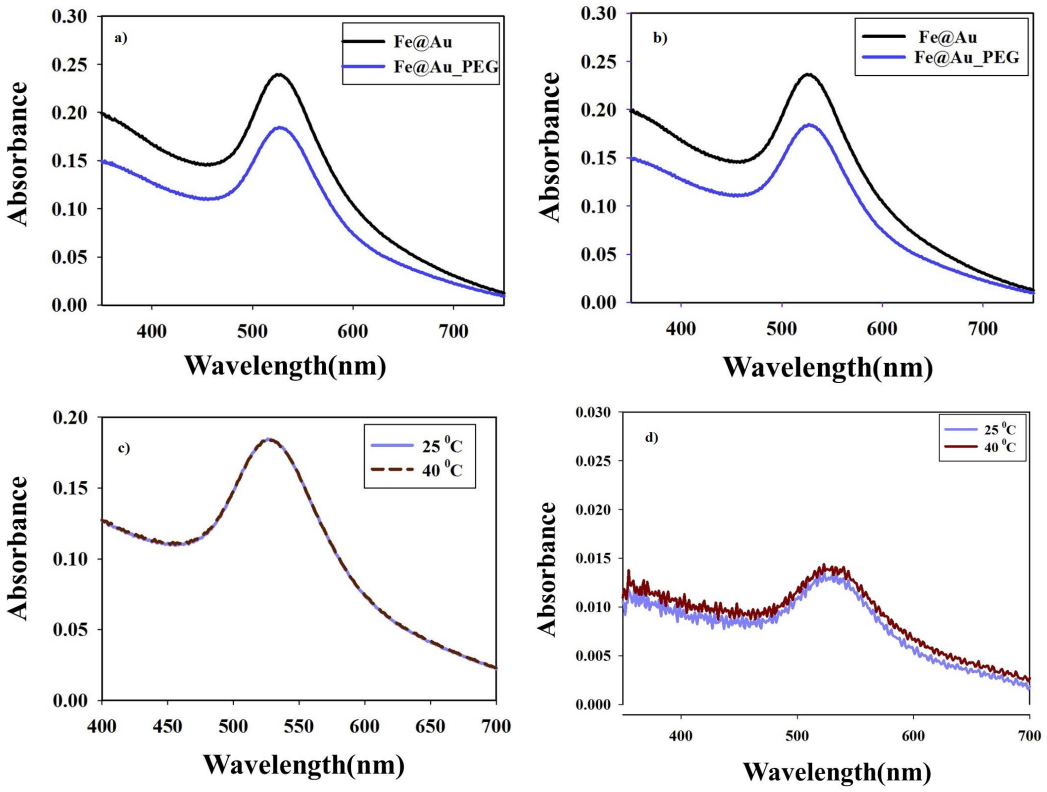

FIGURE 3.11: a) UV-vis spectra of Fe@Au and Fe@Au_PEG at 25 ^{o}C b) UV-vis spectra of Fe@Au and Fe@Au_PEG at 40 ^{o}C c) UV-vis spectra of Fe@Au_PEG at 25 ^{o}C and 40 ^{o}C d) UV-vis spectra of Fe@Au_PEG (low concentration) at 25 ^{o}C and 40 ^{o}C

3.4 Fe@Au_PEG_Hydrogel

Fe@Au NPs were coated with PEG and hydrogel. This system shows properties closer to Fe@Au PEG. Thus these advanced nano-carriers can be significant in the drug delivery due to combined effect of PEG and hydrogel. Combination of PEG and hydrogel showed very promising reversibility. Fe@Au_PEG_Hydrogel also show good stability as illustrated by the zeta potential measurements. Figure 3.12 a-e) represent the size and zeta potential at 25 ^{o}C and 40 ^{o}C, effect of pH on size, temperature induced reversibility and reversibility based on volumetric swelling ratio values for this system.

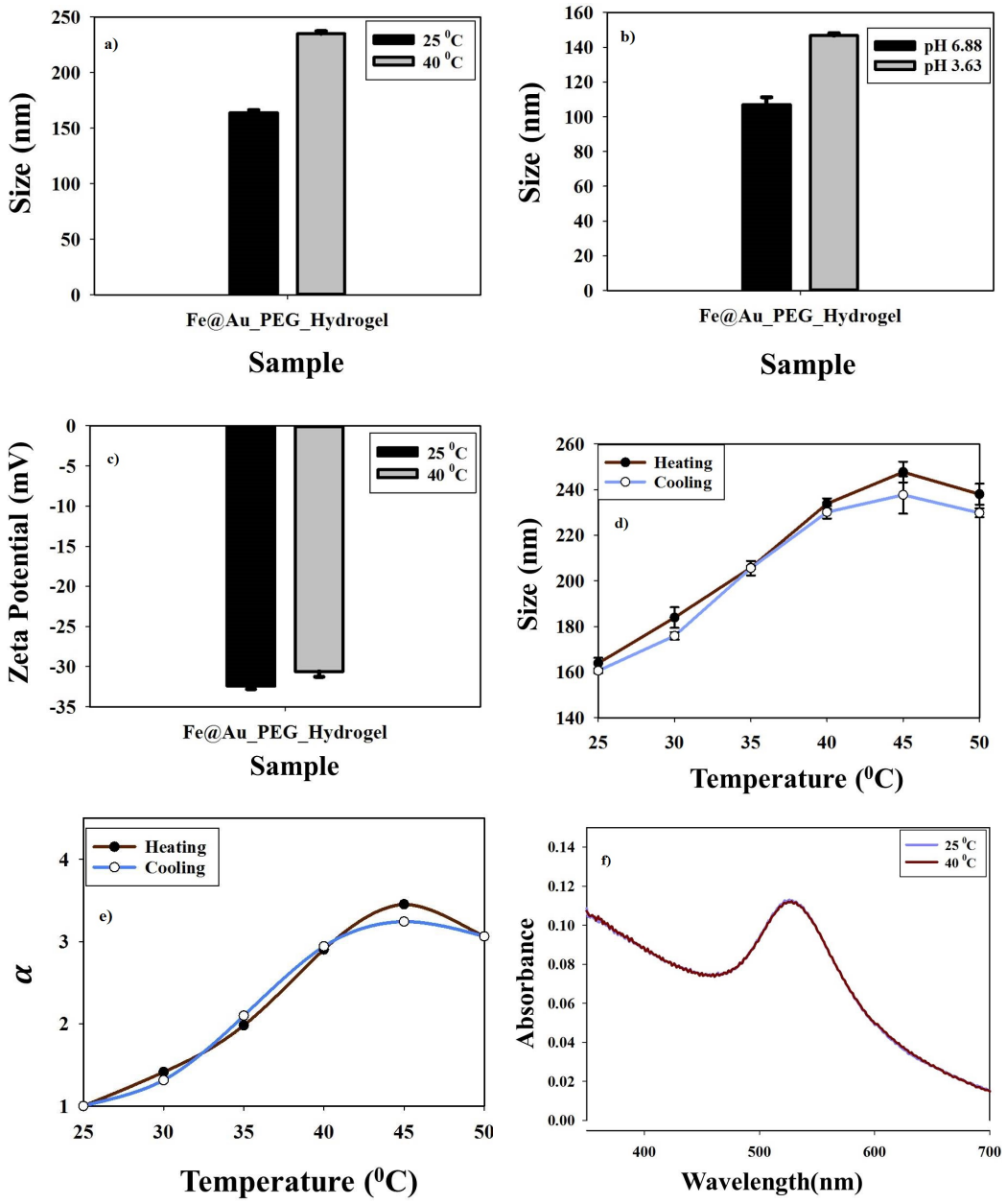

FIGURE 3.12: a) Variation of DLS sizes of Fe@Au_PEG_Hydrogel at 25 ^{o}C and 40 ^{o}C b) Variation of DLS sizes of Fe@Au_PEG_Hydrogel with pH c) Variation of Zeta potential of Fe@Au_PEG_Hydrogel at 25 ^{o}C and 40 ^{o}C d) Variation of sizes of Fe@Au_PEG_Hydrogel network as a function of temperature e) Variation of α as a function of temperature f) UV-vis spectra of Fe@Au_PEG_Hydrogel at 25 ^{o}C and 40 ^{o}C

Size of Fe@Au_PEG_Hydrogel is around 163.9±2.36 nm at 25 ^{o}C, larger size of them compared to Fe@Au_Hydrogel and Fe@Au_PEG is due to coating of both PEG and Hydrogel. It also indicates that outer layer is formed by hydrogel and not PEG owing to order of coating. Reversibility of this system is very promising and it also indicates that outer layer is of hydrogel. Zeta potential value for this carrier is -32.40±0.40 mV and effect of temperature is not very pronounced as illustrated in Figure 3.12. VPTT values

for heating and cooling of this system are reported as 37.1 ^{o}C and 36.7 ^{o}C which are less compared to Hydrogel and Fe@Au_Hydrogel, due to incorporation of PEG which induce hydrophobic effects at higher temperature.

Figure 3.13 a) and b) represents the ST(E)M images for Fe@Au_PEG_Hydrogel at 25 ^{o}C and 50 ^{o}C. It is clear from these images that Fe@Au NPs are present on the periphery of the PEG-Hydrogel surface. As with hydrogel and PEG, this system also shows aggregation at higher temperature, which may be due to drying, while in essence, the collapsed hydrogel particles are being gelled together by Fe@Au NP units.

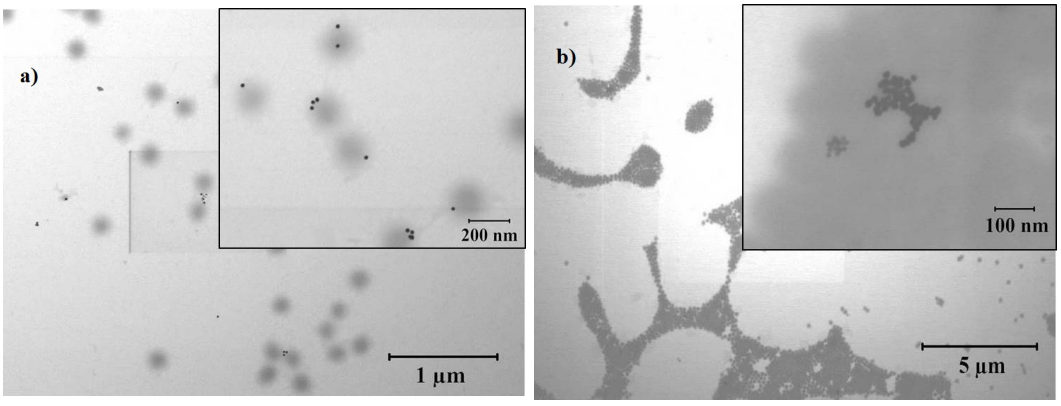

FIGURE 3.13: a) Representative S(T)EM image of Fe@Au_PEG_Hydrogel at 25 ^{o}C b) Representative S(T)EM image of Fe@Au_PEG_Hydrogel at 50 ^{o}C

Three systems Fe@Au_Hydrogel, Fe@Au_PEG and Fe@Au_PEG_Hydrogel which were discussed in the previous sections were used to study the loading of three drugs L-dopa, Coumarin and Cytochrome c. Loading and encapsulation efficiencies results of these system show their effectiveness in drug delivery applications.

3.5 Loading and Encapsulation Efficiencies

Loading and encapsulation efficiency confirms that these systems have potential to be used as a drug carrier with promising results. Loading efficiencies were calculated by using calibration curves given in Appendix B for three drugs.

3.5.1 L-DOPA

Loading results illustrated in figure3.14 a) and b) confirm that, method 2 and sample type B give more promising loading compared to method 1 and sample type A.

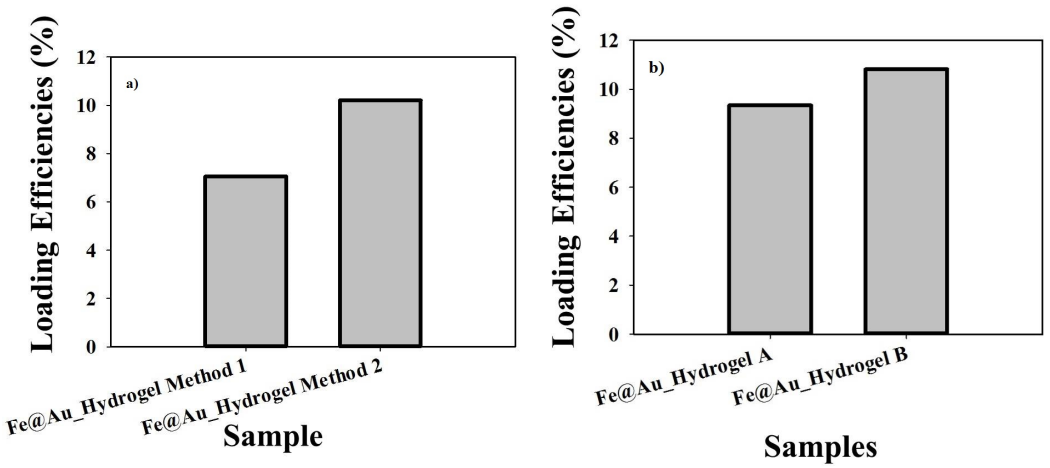

FIGURE 3.14: a) Loading efficiency Fe@Au_Hydrogel A coated by method 1 and 2 b) Loading efficiency Fe@Au_Hydrogel A coated by method 2 and Fe@Au_Hydrogel B coated by method 2

Optimized results for loading and encapsulation of L-dopa on three systems defined above are depicted in Figure 3.15 a) and b). Loading efficiencies for Fe@Au_PEG, Fe@Au_Hydrogel and Fe@Au_PEG_Hydrogel were 8.57 %, 10.20 % and 8.00 % respectively. Loading of L-dopa on Fe@Au_PEG might occur due to the interaction between the methyl group on the L-dopa and the hydroxyl group on the PEG surface, they can from strong bonds as methyl groups prefer to interact with the hydroxyl groups. L-dopa concentration which gave maximum loading on Fe@Au_PEG was 3 mg/ml while the NP concentration was 2.50 mg/ml. Hydrophilic nature of PEG might be the reason for the high values of the loading at high drug concentration.

In case of Fe@Au_Hydrogel, hydrogen bonding between the carboxylic groups on the hydrogel and hydroxyl groups on the L-dopa surface can be responsible for the loading of L-dopa on the surface of the Fe@Au_Hydrogel. It is also possible that hydroxyl and/or amide groups on the surface of L-dopa attach with the acrylic acid present in the hydrogel structure. This interaction can form strong bonds between the drug and Fe@Au_Hydrogel and provide high loading efficiencies. One of these interactions or combination of these can be responsible for the loading of L-dopa on Fe@Au_Hydrogel. In this case, high loading is achieved at high NP concentration for Fe@Au_Hydrogel and low drug concentration.

It is more likely that in case of Fe@Au_PEG_Hydrogel, L-dopa is attached to the hydrogel compared to the PEG because in Fe@Au_PEG_Hydrogel system, it is assumed that hydrogel is on the surface, so drug has more chances to attach with hydrogel. However, it might be possible that drug enters into the polymer structure and can reach the PEG surface. If this might happen then release of the drug from this system might be

slow. For this system, highest loading is achieved for high drug concentration as with Fe@Au_PEG.

Figure 3.15 b) shows the encapsulation efficiencies of the L-dopa on the Fe@Au_PEG, Fe@Au_Hydrogel and Fe@Au_PEG_Hydrogel. It is clear from the Figure that encapsulation is high for the Fe@Au_PEG and Fe@Au_PEG_Hydrogel because in these systems higher drug concentration were used. Low values of encapsulation efficiency for Fe@Au_Hydrogel were obtained due to low concentration of the drug which was used for this particular system.

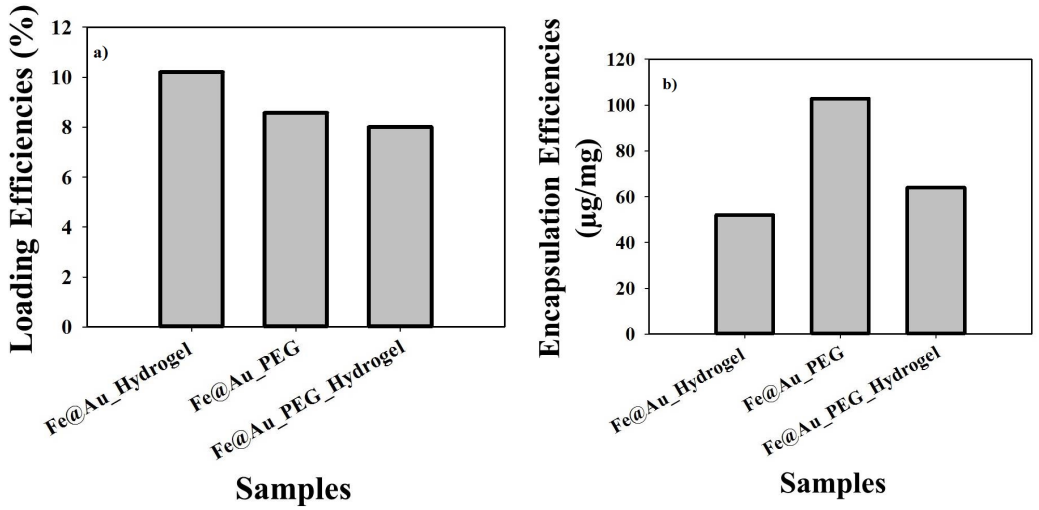

FIGURE 3.15: a) Loading efficiencies of Fe@Au_Hydrogel, Fe@Au_PEG and Fe@Au_PEG_ Hydrogel b) Encapsulation efficiencies of Fe@Au_Hydrogel, Fe@Au_PEG and Fe@Au_PEG_Hydrogel

3.5.2 Coumarin

Coumarin loading was performed on the basis of results obtained from L-dopa loading studies. NP concentrations used for Fe@Au_PEG, Fe@Au_Hydrogel and Fe@Au_PEG_Hydrogel were similar to the ones used for loading studies of L-dopa. Drug concentration for Coumarin was calculated based on the drug concentration used for L-dopa. Loading efficiencies of coumarin on Fe@Au_PEG, Fe@Au_Hydrogel and Fe@Au_PEG_Hydrogel were obtained to be 12.02 %, 8.25 % and 12.10 % respectively as shown in the Figure 3.16 a).

Loading of Coumarin on Fe@Au_PEG is possibly due to the interaction between the charged groups on the coumarin surface. One end of the PEG is anchored with the Fe@Au, because thiol has strong affinity for the Au surface, while the other end on the PEG surface is available to interact with the drug molecule. It is assumed here that

one end of the PEG is attached with the bulky groups of the coumarin most probably -NH group which is the positive center on the PEG surface. Molecular weight of the Coumarin is 146.14 g/mol. It can be assumed that coumarin molecule goes further inside the polymer structure, or else it can stay on the polymer surface due to hydrophobic nature of the drug molecule.

In case of loading of Coumarin on hydrogel, it can be hypothesized that the interaction between the electron donating coumarin structure and positive center on the hydrogel surface is responsible for the loading. Coumarin is more hydrophobic in nature compared to L-dopa and Cyt c due to the presence of the bulky groups, which are not very soluble in water. Therefore in case of loading of coumarin on hydrogel, it can be assumed that the loading is due to the hydrophobic interactions between the drug molecule and nanogel. Drug molecules can be located on the surface of the hydrogel or may be squeezed into the hydrogel surface.

Loading of the Coumarin on the surface of the Fe@Au_PEG_Hydrogel might be due to the hydrophobic interaction as hydrogel is forming the outer layer in the Fe@Au_PEG_Hydrogel system. It is also possible that the drug goes further inside the polymer structure and interacts with the PEG. High loading efficiency indicates that more drug is loaded on the surface of the Fe@Au_PEG_Hydrogel compared to Fe@Au_Hydrogel due to combined effect of nanogel and PEG.

Encapsulation efficiencies for the three systems are depicted in the Figure 3.16 b). Fe@Au_Hydrogel system has lowest encapsulation efficiency due to the fact that low initial drug concentration was used for this particular system, while in case of the Fe@Au_PEG and Fe@Au_PEG_Hydrogel, higher values are indications of high initial drug concentrations. Highest value for the Fe@Au_PEG is because of low NPs concentration for this system, which ultimately increases the ratio of amount of drug loaded to the amount of NPs.

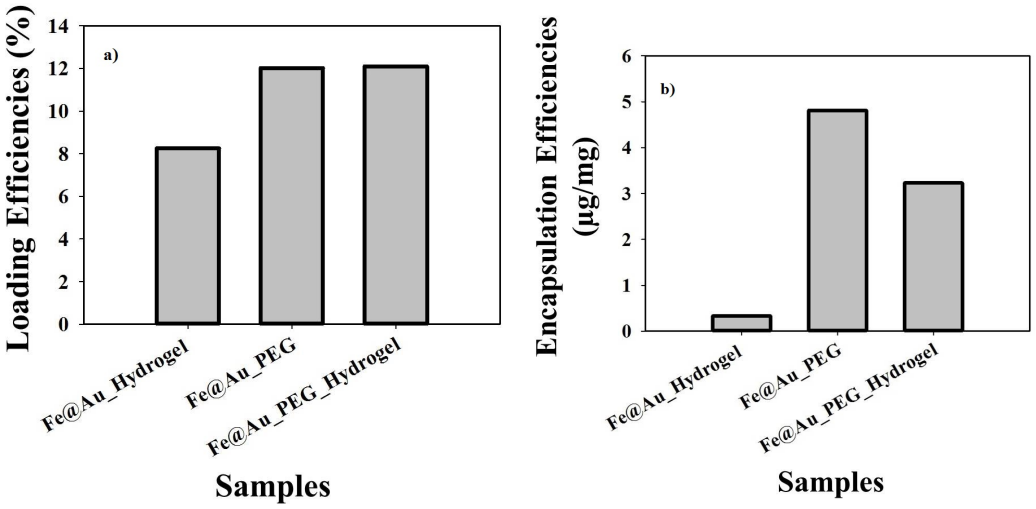

FIGURE 3.16: a) Loading efficiencies of Fe@Au_Hydrogel, Fe@Au_PEG and Fe@Au_PEG_Hydrogel b) Encapsulation efficiencies of Fe@Au_Hydrogel, Fe@Au_PEG and Fe@Au_PEG_Hydrogel

3.5.3 Cytochrome - C (Cyt-C)

Cyt c shows highest loading for Fe@Au-Hydrogel and Fe@Au-PEG-Hydrogel. Cyt c is a small water soluble heme protien having molecular weight of around 12,370 Da. Hydrodynamic diameter of the Cyt c is around 3.5 nm (1.75 R_h measured with DLS). This macromoleucle has a positive charge at pH 7. Studies with similar systems by Smith et al. show that positive charge of the cyt c is responsible for his electrostatic interaction with the negatively charged surface in the hydrogel structure. At neutral pH, this protien has a net charge of +9.3 C, that is why there is a formation of polymer-protien complex due to Coulombic forces between the hydrogel and the cyt c. Net gain in the free energy due to effect of increased entropy through counterion release is responsible for the formation of this cross-linked polyelectrolytes-protien complex. This complex formation is the reason of higher loading efficiency for the Fe@Au-Hydrogel and Fe@Au-PEG-Hydrogel systems. As the hydrodynamic diameter of the protein is around 3.5 nm, so it might be possible that protein diffuses into the polymer surface and goes further inside the hydrogels [160].

Lower values of loading efficiency at higher drug concentration for Fe@Au-Hydrogel and Fe@Au-PEG-Hydrogel might be due to less access of the polymer to the interior of the protein and interaction between the protein and the NPs are not very significant.

While in case of the PEG, lower value of loading efficiency is attributed to hydrophilic nature of both PEG and the protein, so it might be difficult to bind more protein to the surface of the PEG. When protein is attached with the PEG surface, there is a repulsive

force between the PEG and the protein, as PEG chains lose their conformational entropy and available volume for each polymer molecule is then decreased. Moreover, available conformations for the PEG molecules decrease because of their compression owing to osmotic repulsive force generated due to protein chains[161]. Increase in drug loading at higher drug concentration is possibly because of the hydrophillic nature of the PEG, so that when drug concentration is increased, chances of collision between the drug and the PEG are also increased. Figure 3.17 a) and c) shows the loading efficiencies of 0.1 mg/ml and 0.5 mg/ml Cyt c on Fe@Au_Hydrogel, Fe@Au_PEG_Hydrogel and Fe@Au_PEG systems.

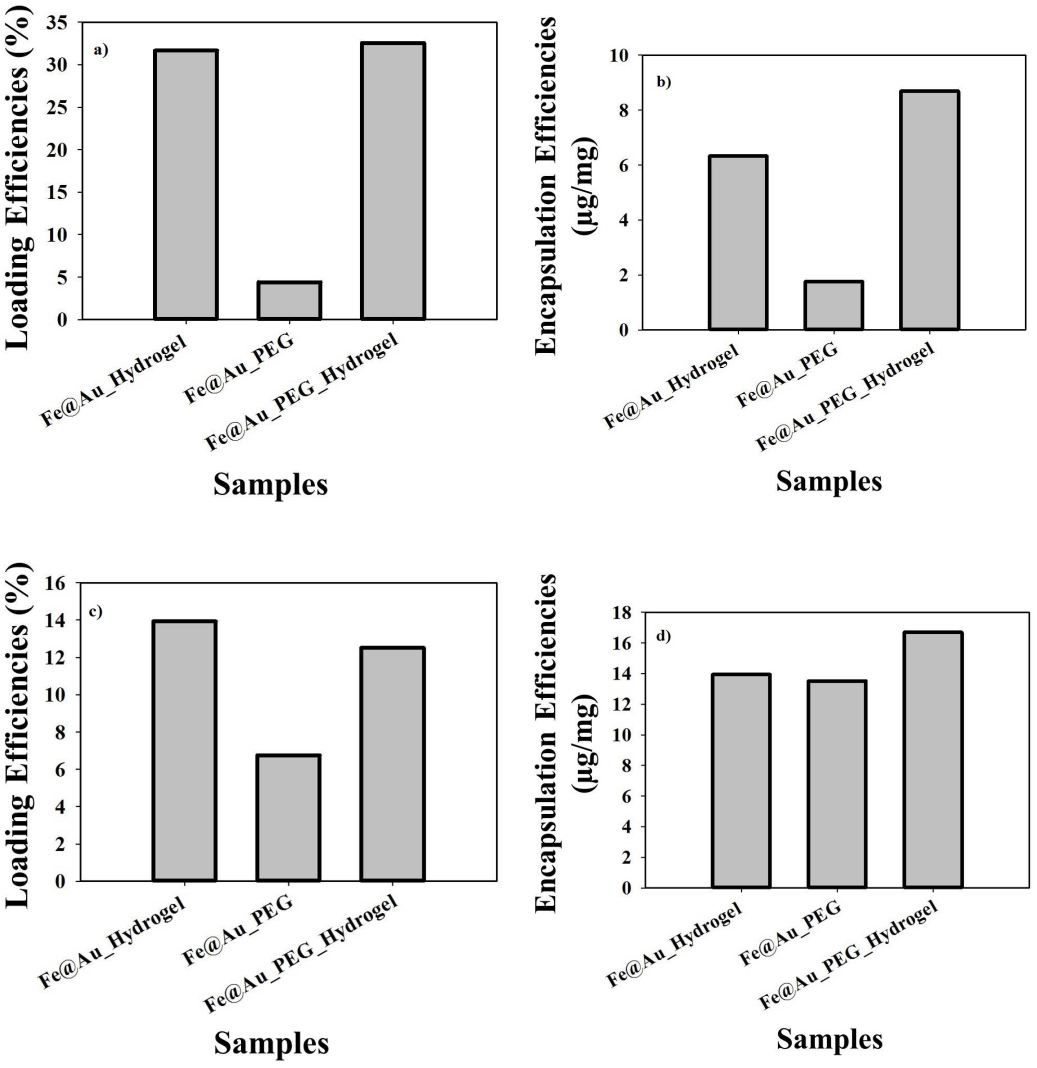

FIGURE 3.17: a) Loading efficiencies of Fe@Au_Hydrogel, Fe@Au_PEG and Fe@Au_PEG_Hydrogel at low drug concentration b) Encapsulation efficiencies of Fe@Au_Hydrogel, Fe@Au_PEG and Fe@Au_PEG_Hydrogel at low drug concentration c) Loading efficiencies of Fe@Au_Hydrogel, Fe@Au_PEG and Fe@Au_PEG_Hydrogel high drug concentration d) Encapsulation efficiencies of Fe@Au_Hydrogel, Fe@Au_PEG and Fe@Au_PEG_Hydrogel high drug concentration

Encapsulation efficiency values are indicated in the Figure 3.17 b) and d) for 0.1 mg/ml and 0.5 mg/ml Cyt c respectively. It is clear form the graphs that as the drug concentration is increased more drug is encapsulated to the NPs.

3.6 Release

Section 1.14 indicates the different factor which govern release of the drug from the nanocarriers. Release study of the three drugs used for the loading studies is done at low-pH (3.5) and high temperature (40 ^{o}C). This condition is used because previous work done with the similar systems provide highest release for this particular condition. [157, 162]. Release (%) calculations are given in the Appendix D.

3.6.1 Coumarin

Release kinetics for the Coumarin for three systems are shown in the Figure 3.18. For Fe@Au_Hydrogel, Fe@Au_PEG and Fe@Au_PEG_Hydrogel systems, release of Coumarin was very unstable and the values were very fluctuating. This is due to the hydrophobic nature of Coumarin and it might not be possible to study the release of this drug by the technique used in this studies (temporal UV-vis study of the NPs and release medium, without separating the particles from free drug). As indicated in Figure 3.18 for Fe@Au_Hydrogel there was a release of about 18.23% in 1 hour, and after 2.03 hours it increased to 46.26%. However, after 3.05 hour there is a decrease in the drug release to 12.10% and increase to 80.78% after 5.03 hours. This is very unusual drug release which indicates that interactions between the drug and the Fe@Au_Hydrogel is very complex and it is suggested that different release setup should be used for Coumarin release. It might be possible to get efficient results by loading the drug to the carriers at high temperature and afterwards study the release at lower or normal temperature.

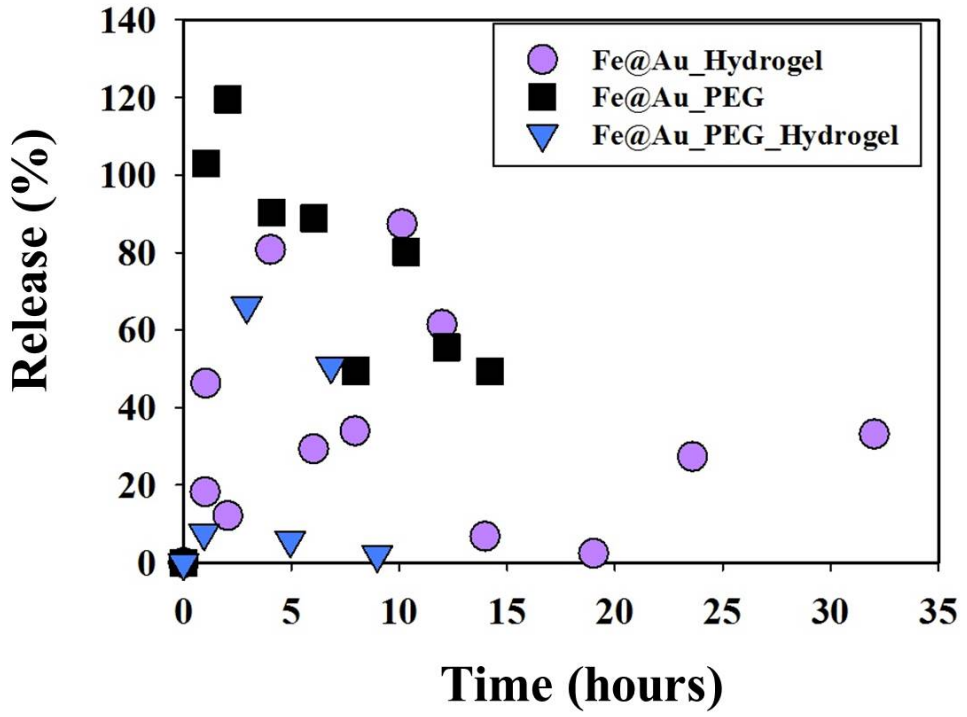

FIGURE 3.18: Release percentage of Drug (Coumarin) from Fe@Au_Hydrogel, Fe@Au_PEG and Fe@Au_PEG_Hydrogel systems

Similar results were observed for the Fe@Au_PEG, Fe@Au_PEG_Hydrogel.

Hence, it is concluded that for Coumarin release form these particular systems, different approach should be used to estimate the release. Additionally, the problems faced during the studies of improper mixing might cause the fluctuated increase and decrease release rates. It is also possible that interaction of the drug with the carriers is such that after changing pH and temperature, there is burst release of the Coumarin during the initial phase of the release, and in the final phase the drug which was located inside the polymeric structure is released at a non-uniform rate. Due to hydrophobic nature of Coumarin, it might be possible that the released drug still remains associated with the hydrophobic (due to increased temperature) hydrogels even after release. Since this drug does not go out into the release medium where the drug concentration is being analysed, random fluctuations in the release percentage are being observed.

3.6.2 L-DOPA

Similar condition was employed for the release of L-dopa from the Fe@Au_PEG, Fe@Au_Hydrogel and Fe@Au_PEG_Hydrogel systems.

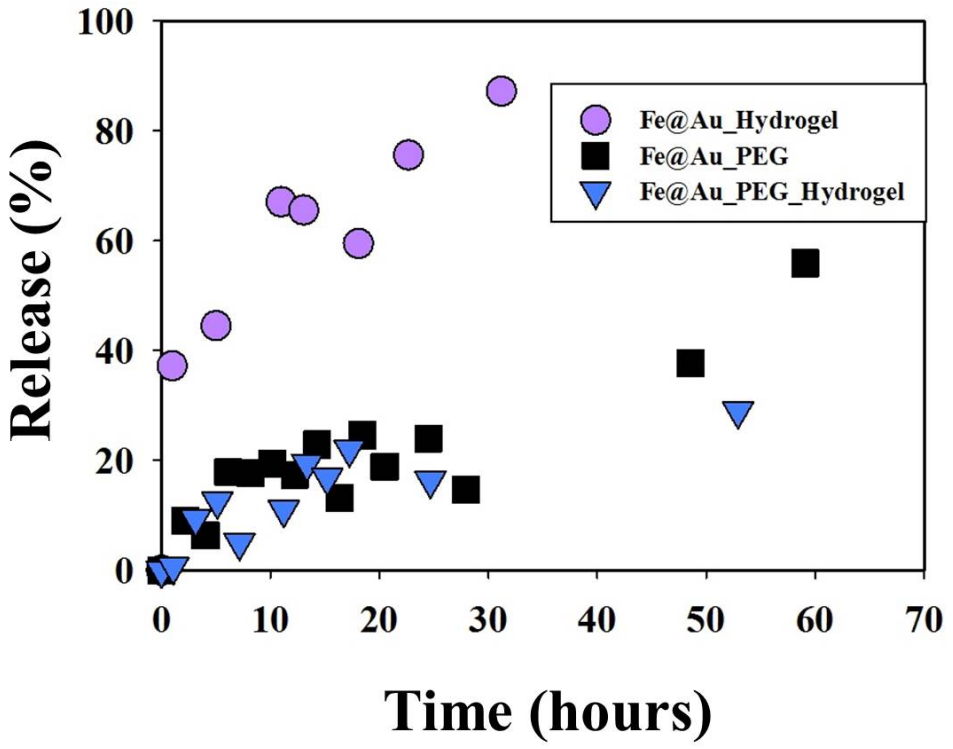

FIGURE 3.19: Release percentage of Drug (L-dopa) from Fe@Au_Hydrogel, Fe@Au_PEG and Fe@Au_PEG_Hydrogel systems

Promising results were observed in case of release of the L-dopa form the Fe@Au_PEG, Fe@Au_Hydrogel and Fe@Au_PEG_Hydrogel systems as illustrated in the Figure 3.19. It is important to mention here that due to the initial problem with the stability of the particles as the pH was reduced by adding 0.25mM HCl to the loaded NPs, t_0 is used which is after 2 to 3 hours from the start. For Fe@Au_Hydrogel loaded with L-dopa 37.20% release of the drug was observed after 0.97 hours. While it increased to 44.51% and 66.07% after 5 and 10 hours respectively. While there is a slight decrease in the release rate after 13.05 and 18.07 hours. This behaviour was observed because of the improper mixing of the Fe@Au_Hydrogel loaded with L-dopa drug system as it was observed during the experiment that NPs are attaching with the magnetic stirrer. Sonication of the sample was done at regular intervals to minimize this effect, which ultimately enhanced the release to 75.61% after 22.67 hours as indicated in the Figure 3.19. After 31.20 hours, 87.20% drug was released from this system. Previous study done with the similar systems during project work [162] gave almost similar results (83% release), which indicates that these results are reproducible and reliable.

Fe@Au_PEG loaded with L-dopa also showed promising results. It can be observed that there is a bit slow release from this system compared to the Fe@Au_Hydrogel owing to

the fact that hydrogel is sensitive to changes in pH and temperature compared to the PEG. For this system 8.98% release was observed after 2.18 hours, while it decreased to 6.27 % after 4.03 hours owing to the same fact of improper mixing as with L-dopa. However, there is a slow increase from 17.70 % after 6.13 hours to 22.87 % in 4.27 hours. Same pattern is shown until 37.69% drug was released after 48.58 hours. After 59.08 hours, 55.93 % drug was released from Fe@Au_PEG. Lower values compared to hydrogel system indicate that drug release from hydrogel system is due to change in its structure with changes in pH and temperature.

Drug release from Fe@Au_PEG_Hydrogel systems show similar trend of slow drug release as with PEG system as illustrated in the figure. After 3.12, hours 9.37 % drug was released which increased to 19.41% after 13.35 hours. Fluctuation in values is attributed to similar reasoning of improper mixing. Drug release further increased to 21.98% after 17.25 hours, ultimately reaching a value of 28.98% after 52.93 hours. Lower release percentage from this system is due to fact that coating of both PEG and hydrogel increase the size of the carrier, and it is possible that drug is entrapped at different layers of PEG and hydrogel structure so it required more time to release.

3.6.3 Cytochrome-C

Cytochrome c release kinetics from the Fe@Au_PEG, Fe@Au_Hydrogel and Fe@Au_PEG_Hydrogel systems are illustrated in Figure 3.20. It can be observed from the figure that drug release profile for this system is very promising and gives very uniform release of the drug. It is necessary to mention here that, the release percentage for cytochrome c is calculated based on the bound cyt c with the NPs. Since it is assumed that cyt c is bound to the polymer and UV-Vis is providing the peak for the bound cyt c with the polymer, decrease in absorbance values for the drug was observed, unlike in case of L-dopa

Fe@Au_Hydrogel loaded with cyt c shows constant release of the drug, 28.3% drug is released after 1.60 hours. As shown in the graph, drug release from this system was uniform and increased at a constant rate. After 7.65 hours, 35.4% drug was released from the Fe@Au_Hydrogel. While after 15.85 hours, there was 41.9% release of the drug from the initial value, however there was a minor decrease in the drug release percentage that can be attributed to the same reason as with drug release from the L-dopa and Coumarin systems. After 43.42 hours, there was 55.4% drug release from this system.

Drug release from the Fe@Au_PEG was faster compared to the Fe@Au_Hydrogel. This might be due to the lower loading efficiency for this system. Also, PEG is hydrophilic therefore, it does not interact very effectively with proteins. After 2.65 hours, there was drug release of 63.2 % while the decrease in the drug release at some time points

indicated the effect of improper mixing. It can be seen from the graph that after 12.10 hours, there was release of 85.9 % which ultimately increases to 89.1 % after 43.40 hours.

In case of the Fe@Au_PEG_Hydrogel, similar trend of constant and relatively slow drug release was observed as with Fe@Au_Hydrogel after release of 30 % in 0.55 hours. 39.6 % drug release occured form this system after 7.52 hours. This drug release percentage increased to 43.6 % after the 15.48 hours. The drug release from Fe@Au_PEG_Hydrogel is not very fast and it slows down. After 33.72 hours there was drug release of 49 % which increase to 50.8 % after 47.73 hours which indicates that there is a slow release of the drug from this system. This might be due to the increase in the structure of the Fe@Au_PEG_Hydrogel as this structure has layers of hydrogel as well as PEG, so drug takes more time to release.

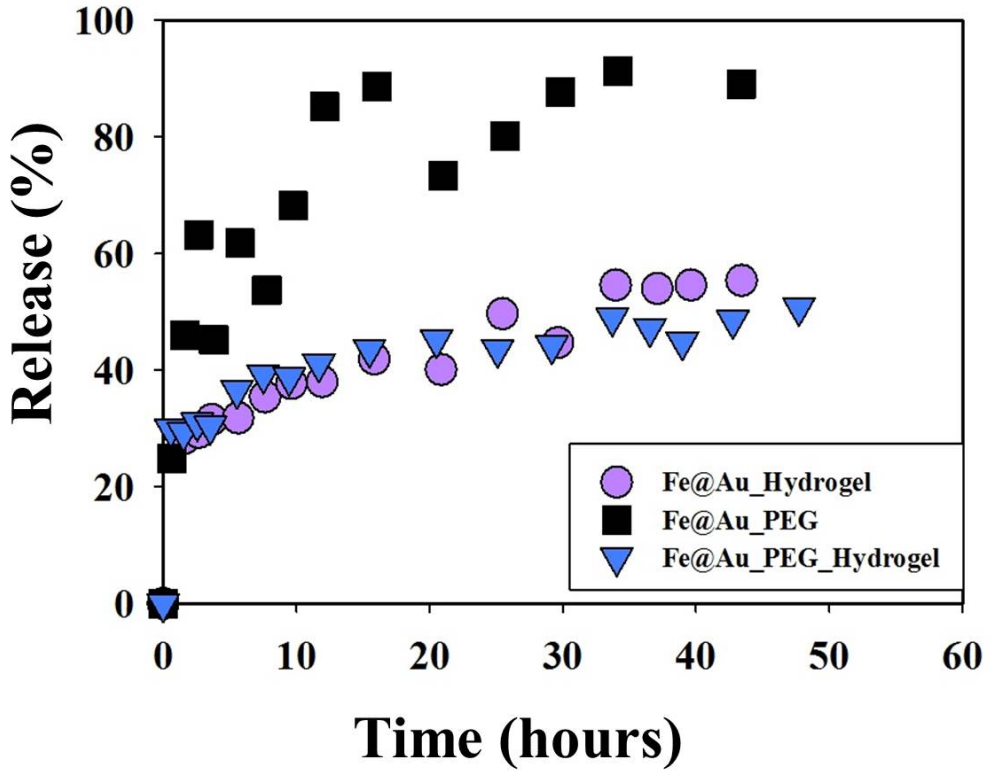

FIGURE 3.20: Release percentage of Drug (Cytochrome-C) from Fe@Au_Hydrogel, Fe@Au_PEG and Fe@Au_PEG_Hydrogel systems

3.6.4 Model-Fitting

Fitting of release data was done by using kinetic models. Four different models zero order, first order, Higuchi and power law were used to estimate the behaviour of Cyt c and

L-dopa release kinetics from Fe@Au_PEG, Fe@Au_Hydrogel and Fe@Au_PEG_Hydrogel systems [142, 163].

3.6.4.1 L-dopa Fe@Au_Hydrogel

Figure 3.21 a-d) illustrate the models zero order, first order, Higuchi, and power law respectively for L-dopa release kinetics from Fe@Au_Hydrogel. Power law model provides the value for n (diffusional exponent for Peppas equation). By examining values for zero order , first order, and Huguichi model fit shown in the graphs a, b and c it is clear that for this system zero order model provides the best linear fit with rate constant of k = 0.0321 hour^{-1}.

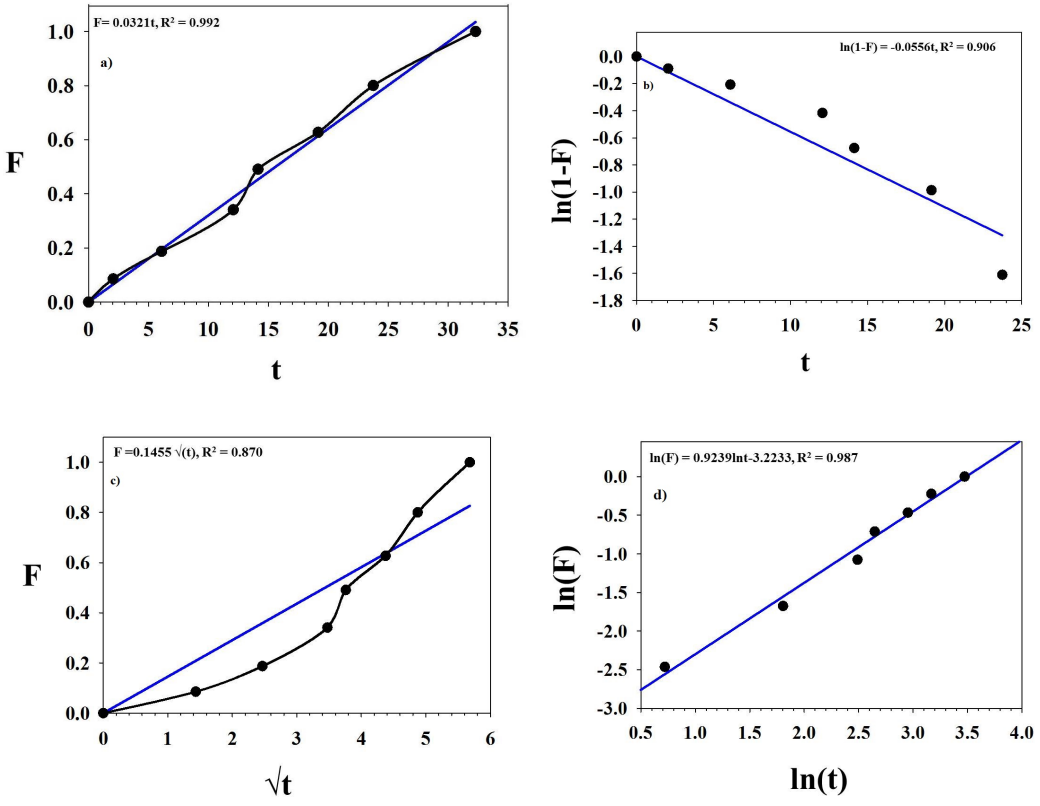

FIGURE 3.21: a) Model Fitting of L-dopa Fe@Au_Hydrogel using zero order model b) Model Fitting of L-dopa Fe@Au_Hydrogel using first order model c) Model Fitting of L-dopa Fe@Au_Hydrogel using Higuchi model d) Model Fitting of L-dopa Fe@Au_Hydrogel using power law model

3.6.4.2 L-dopa Fe@Au_PEG

Figure 3.22 a-d) illustrate the models zero order, first order, Higuchi, and power law respectively for L-dopa release from Fe@Au_PEG. For this system first order model gives the best linear fit having rate constant k = 0.0361 hour^{-1}.

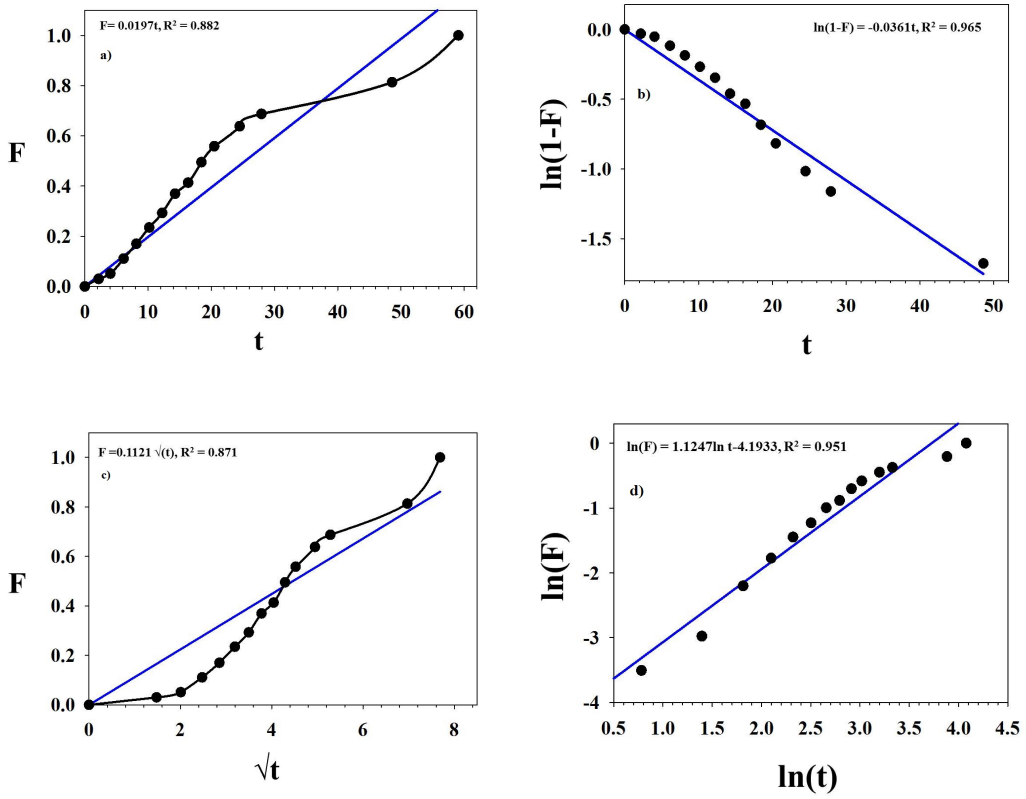

FIGURE 3.22: a) Model Fitting of L-dopa Fe@Au_PEG using zero order model b) Model Fitting of L-dopa Fe@Au_PEG using first order model c) Model Fitting of L-dopa Fe@Au_PEG using Higuchi model d) Model Fitting of L-dopa Fe@Au_PEG using power law model

3.6.4.3 L-dopa Fe@Au_PEG_Hydrogel

Release kinetics for L-dopa from Fe@Au_PEG_Hydrogel is depicted in the Figure 3.23 for the four models used. It is clear from the figure that first order model gives the best linear fit for l-dopa release from the Fe@Au_PEG_Hydrogel. rate constant estimated by using this model give value of k = 0.0546 hour^{-1}.

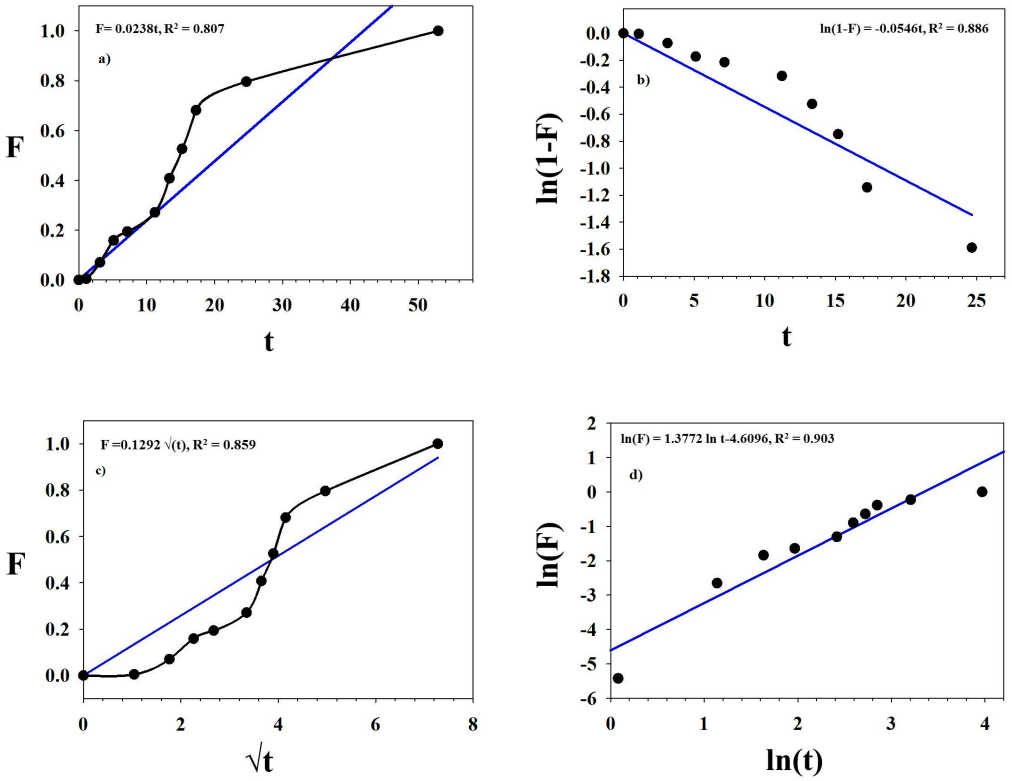

FIGURE 3.23: a) Model Fitting of L-dopa Fe@Au_PEG_Hydrogel using zero order model b) Model Fitting of L-dopa Fe@Au_PEG_Hydrogel using first order model c) Model Fitting of L-dopa Fe@Au_PEG_Hydrogel using Higuchi model d) Model Fitting of Fe@Au_PEG_Hydrogel using power law model

3.6.4.4 Cytochrome - C Fe@Au_Hydrogel

Models used for L-dopa release from Fe@Au_Hydrogel, Fe@Au_PEG, and Fe@Au_PEG_Hydrogel systems also used for the release of cyt c from these systems. Figure depicts 3.24 the release kinetics of cyt c from Fe@Au_Hydrogel using four different models. It can be concluded form the Figures that zero order model provides the better linear fit compared to first order and higuchi model. Value of rate constant K = 0.0232 hour^{-1} is estimated from zero order model.

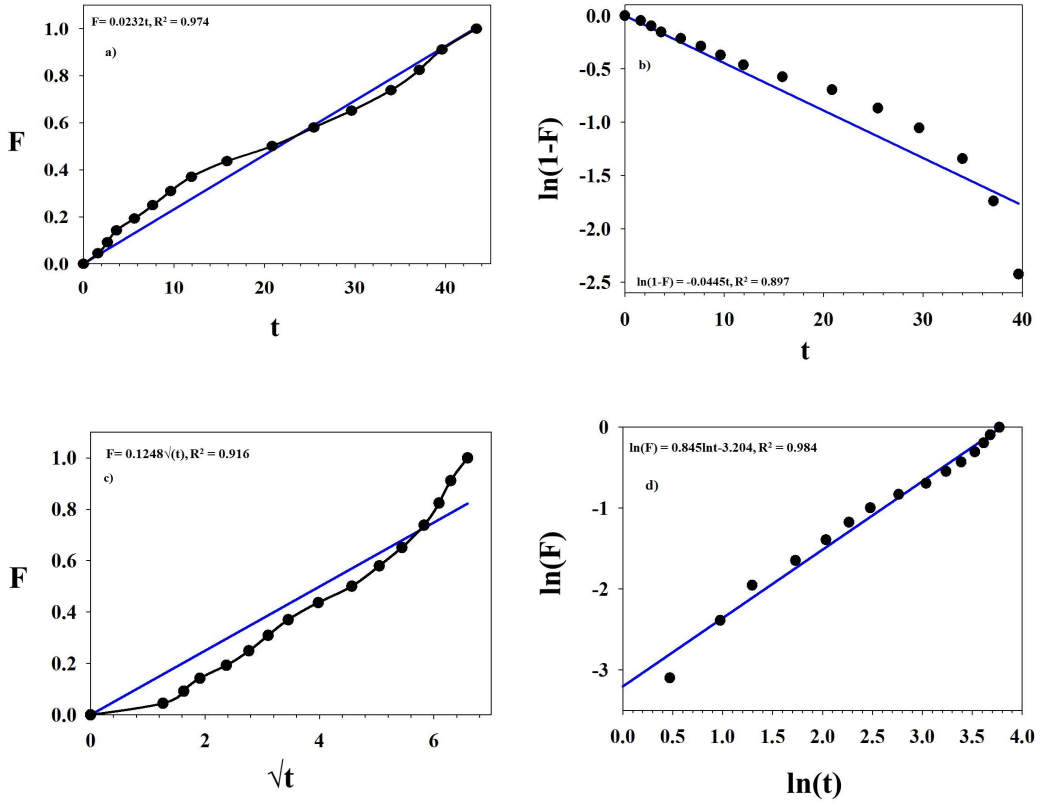

FIGURE 3.24: a) Model Fitting of Cytochrome - C Fe@Au_Hydrogel using zero order model b) Model Fitting of Cytochrome - C Fe@Au_Hydrogel using first order model c) Model Fitting of Cytochrome - C Fe@Au_Hydrogel using Higuchi model d) Model Fitting of Cytochrome - C Fe@Au_Hydrogel using power law model

3.6.4.5 Cytochrome - C Fe@Au_PEG

For release of Fe@Au_PEG from the cyt c similar models as with other systems was used to estimate the release kinetics as illustrated in the Figure. From Figure 3.25 it can be inferred that first order provide superior linear fit compared to zero order model with rate constant k= 0.0573 hour^{-}1.

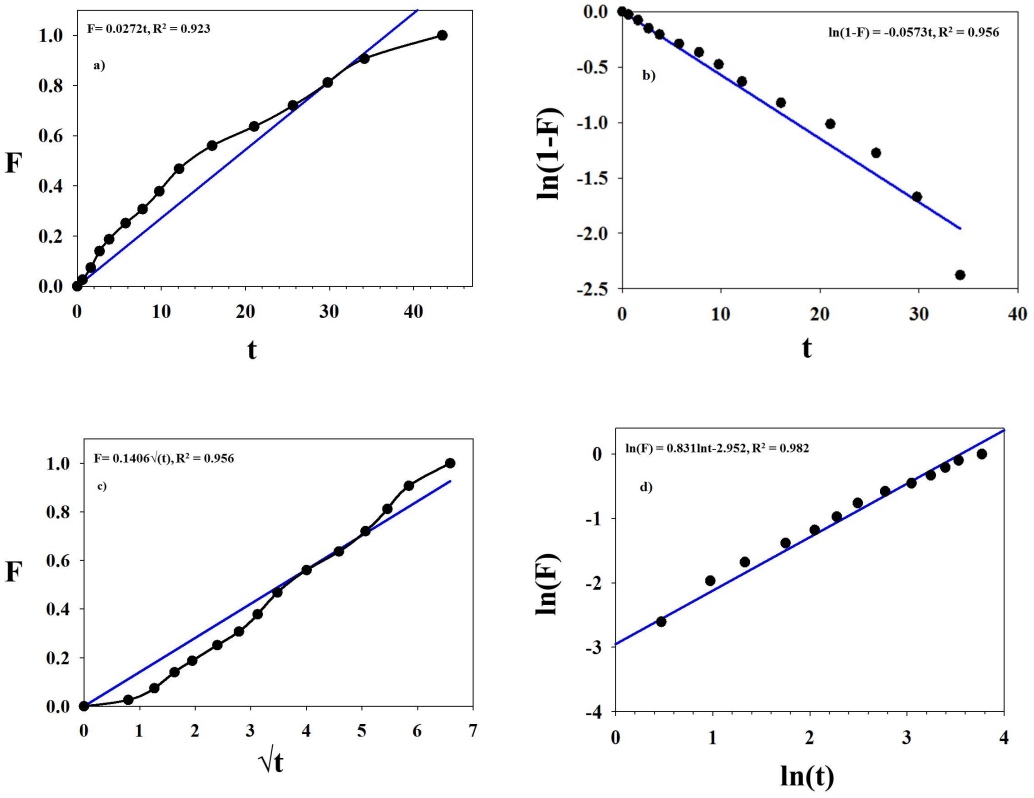

FIGURE 3.25: a) Model Fitting of Cytochrome - C Fe@Au_PEG using zero order model b) Model Fitting of Cytochrome - C Fe@Au_PEG using first order model c) Model Fitting of Cytochrome - C Fe@Au_PEG using Higuchi model d) Model Fitting of Cytochrome - C Fe@Au_PEG using power law model

3.6.4.6 Cytochrome - C Fe@Au_PEG_Hydrogel

Four models which are used to estimate the release kinetics of drug for the systems explained above are also used for this system as shown in the Figure 3.26. Higuchi model is best suited as it provides the best fit for the release kinetics of cyt c from Fe@Au_PEG_Hydrogel with rate constant k = 0.127 hour$^{-1/2}$.

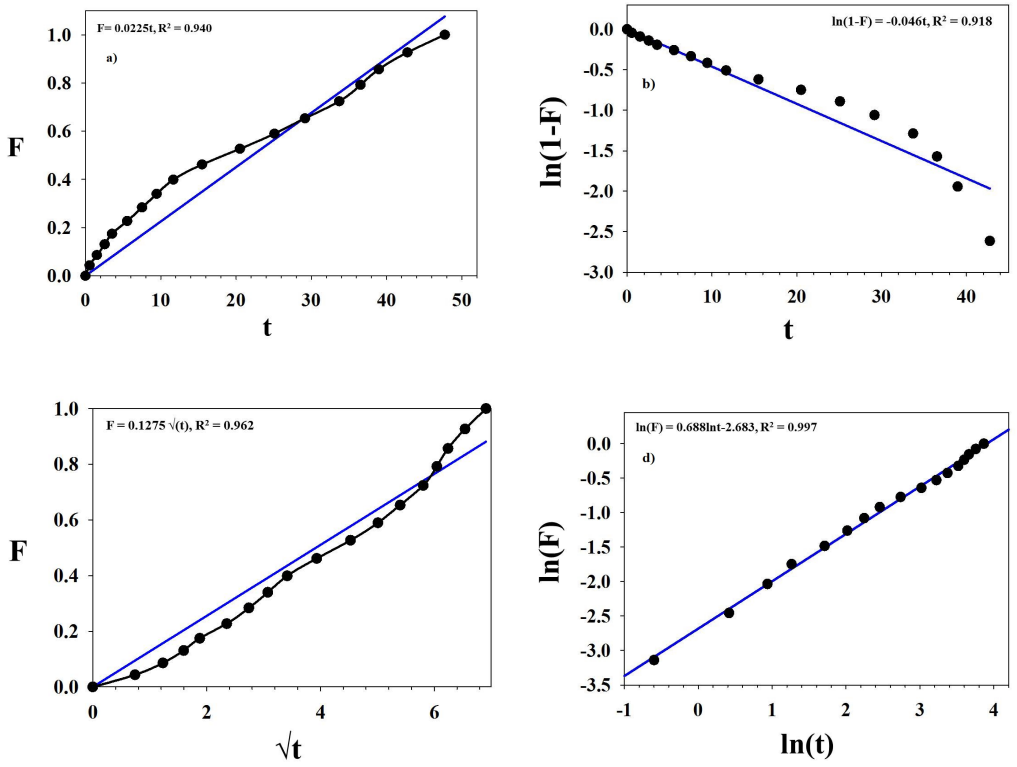

FIGURE 3.26: a) Model Fitting of Cytochrome - C Fe@Au_PEG_Hydrogel using zero order model b) Model Fitting of Cytochrome - C Fe@Au_PEG_Hydrogel using first order model c) Model Fitting of Cytochrome - C Fe@Au_PEG_Hydrogel using Higuchi model d) Model Fitting of Cytochrome - C Fe@Au_PEG_Hydrogel using power law model

Table 3.1 gives the values of diffusion exponent n the peppas equation for Fe@Au_Hydrogel, Fe@Au_PEG and Fe@Au_PEG_Hydrogel loaded with L-dopa and cyt c.

TABLE 3.1: Diffusion exponent n of the peppas equation and drug release mechanism from polymeric systems

Samples	n (Diffusion exponent)	Geometries	Drug release mechanism
L-Dopa drug			
Fe@Au_Hydrogel	0.92	Thin film	Anomalous transport
Fe@Au_PEG	1	Thin film	Case-II transport
Fe@Au_PEG_Hydrogel	1	Thin film	Case-II transport
Cytochrome c drug			
Fe@Au_Hydrogel	0.85	Thin film, Cylinder, Sphere	Anomalous transport, Case-11 transport
Fe@Au_PEG	0.83	Thin film, Cylinder, Sphere	Anomalous transport
Fe@Au_PEG_Hydrogel	0.68	Thin film, Cylinder, Sphere	Anomalous transport

Estimated value of n is 0.92 for release of L-dopa from Fe@Au_Hydrogel which means that system's geometry is thin film and it follows anomalous transport mechanism which is intermediate between Fickian and case-II transport as discussed in the section. Value of n for drug release (L-dopa) from Fe@Au_PEG and Fe@Au_PEG_Hydrogel is equal to 1 which indicates that drug release mechanism is based on the case-II transport mechanism

from a thin film type geometry. It can be stated that drug release from Fe@Au_PEG is based on viscoelastic relaxation-controlled mechanism.

In case of cyt c release from Fe@Au_Hydrogel value of diffusion exponent is equal to 0.85, which means that this system can follow both anomalous and case-II transport mechanism and diffusion exponent value indicates that system can act as thin film, cylinder and sphere. Similarly, cyt c release from Fe@Au_PEG and Fe@Au_PEG_Hydrogel systems can also behave like thin film, cylinder and sphere with diffusion exponent values 0.83 and 0.68 respectively. Drug release mechanism from these systems is anomalous transport that is in between Fickian and case-II transport (viscoelastic relaxation-controlled mechanism).

TABLE 3.2: Release kinetics and maximum release from the drug loaded systems

Sample	**Drug)**	**Maximum Release**	**Model**	**$t_{1/2}$ (hour))**
Fe@Au_Hydrogel	L-dopa	87.20	Zero order	15.60
Fe@Au_PEG	L-dopa	55.93	Ist order	19.2
Fe@Au_PEG_Hydrogel	L-dopa	28.98	Ist order	12.0
Fe@Au_Hydrogel	Cytochrome C	55.40	Zero order	21.6
Fe@Au_PEG	Cytochrome C	89.10	Ist order	12.1
Fe@Au_PEG_Hydrogel	Cytochrome C	50.80	Higuchi	15.4

From table 3.2, it can be concluded that in case of L-dopa, highest release of 87.20 % was obtained from Fe@Au Hydrogel system, whereas fastest release rate (which is calculated based on time required for 50 % cumulative drug release, $t_{1/2}$,, using rate constant values k for all the systems) was shown by Fe@Au PEG Hydrogel. For the Cytochrome C, both highest and fastest release were shown by Fe@Au PEG. However, Fe@Au PEG Hydrogel system also shows similar $t_{1/2}$, when compared to Fe@Au PEG. These results support the collapse hypothesis suggested in the work- hydrogels undergo volumetric collapse with increase in temperature and decrease in pH, however, the Fe@Au NPs act as bridge molecules pulling together the gelling units. Further differences in both release rates and percentages can be linked to the interactions of the drug with the hydrogels- Cytochrome C has stronger interactions with the hydrogel units rather than with PEG. This leads to faster release in case of Fe@Au PEG compared to the other systems, for Cytochrome C. On the other hand, the release rate of L Dopa from Fe@Au PEG Hydrogel is faster as compared to the release rate of Cytochrome C. This can be attributed to stronger interaction of Cytochrome C than L Dopa with the hydrogel units. The data further conform to the fact that both the drugs show a faster release kinetics from Fe@Au PEG Hydrogel than Fe@Au Hydrogel, thereby promoting the need of combination of PEG and hydrogels with the inorganic NPs in one system.

Chapter 4

Conclusion

In this thesis, inorganic and polymeric NPs have been combined to form a single nano drug carrier. This unique system is being studied to exploit the properties such as magnetic, optical, stimuli responsive behavior and biocompatibility, stemming from both the components.

Firstly, Fe@Au NPs were synthesized and their physico-chemical properties mapped using DLS, zeta potential measurements, UV-vis and S(T)EM. Monodisperse population of Fe@Au NPs was obtained having an average DLS size of 54.30± 0.52 nm and zeta potential of -36.8±0.9mV with a characteristic LSPR peak at 524 nm. These NPs were stable in aqeous solution. Afterwards, these inorganic NPs were coated with pNIPAm/AAc based hydrogels, PEG and a combination of the two in order to exploit properties of both the Fe@Au NPs and polymeric NPs. These coated samples were also characterized using the same techniques mentioned above.

Coating was done using two methods, one in which solutions of hydrogel and Fe@Au NPs were mixed together (Method 1). While in the other method, dry hydrogel in solid form was added to the Fe@Au NPs solution (Method 2). Although both the methods showed similar properties (size, zeta potential, UV-vis) of the coated Fe@Au NPs, Method 2 provides better loading efficiencies. Due to this, Method 2 was used for all the experiments in this work. pNIMAm/AAc based hydrogels showed a decrease in size at high temperature due to an entropy driven expulsion of arranged water, when the hydrogels transit from a hydrophilic to a hydrophobic state above VPTT. The VPTT for both heating and cooling for the hydrogel is calculated to be 38^{o}C, indicating reversibility. On the other hand, after coating of Fe@Au NPs with the hydrogels, an increase in size with increasing temperature was observed. This is hypothesized as cross-linking effect provided by Fe@Au NPs which brings together the gelling units at higher temperature.ST(E)M data also support this observation. Additionally, a shift in the VPTT

is observed when compared to only hydrogel, for both heating (39.8^{o}C) and cooling (39.5^{o}C), without significant compromise in hysteresis. As expected, Fe@Au_PEG did not show appreciable temperature induced effects due to absence hydrogel in this system. However, Fe@Au_PEG_Hydrogel system shows appreciable reversibility with VPPT values for heating and cooling reported as 37.1 ^{o}C and 36.7 ^{o}C respectively. Effect of pH on size were also studied for all the system. These results indicates similar outcomes as depicted by temperature effect, in the sense that decrease in size for hydrogels occur at low pH, and increase in size occure in case of Fe@Au coated with the polymers at low pH most probably owing to protonation effect.

Three different drugs were used in these studies for the loading of Fe@Au_PEG_Hydrogel, Fe@Au_PEG and Fe@Au_PEG_Hydrogel systems. Drugs used in this study in order of their decreasing solubilities were Cytochrome C, L-dopa and Coumarin. Loading studies were optimized with different NP and drug concentrations. Highest loading efficiencies for Fe@Au_PEG_Hydrogel, Fe@Au_PEG and Fe@Au_PEG_Hydrogel loaded with L-dopa were reported as 10.20 %, 8.57 % and 8.00 % respectively. In case of Coumarin, maximum loading of 8.25 %, 12.02 % and 12.10 % were obtained for Fe@Au_Hydrogel, Fe@Au_PEG and Fe@Au_PEG_Hydrogel respectively. Cytochrome C loading results depict high loading efficiencies of 31.66 % and 32.57 % for Fe@Au_Hydrogel and Fe@Au_PEG_Hydrogel respectively, whereas, for Fe@Au_PEG maximum loading efficiency of 6.76 % was achieved. The different loading efficiencies can be interpreted in terms of different interactions between the drug and the carrier.

Release studies at high temperature (40 ^{o}C) and low pH (3.5) for the three systems from the drugs mentioned above, were performed after loading. In case of L-dopa, highest release of 87.20 % was acquired from Fe@Au_Hydrogel system, while Fe@Au_PEG_Hydrogel system shows fastest release rate. In case of Cytochrome C, both highest and fastest release were given by Fe@Au_PEG. However, Fe@Au_PEG_Hydrogel system also shows almost identical $t_{1/2}$ in comparison to Fe@Au_PEG. These outcomes support the collapse hypothesis proposed in this research- hydrogels undergoes volumetric collapse at higher temperature and lower pH, however, the Fe@Au NPs act as bridge molecules pulling together the gelling units. Further differences in both release rates and percentages can be linked to the interactions of the drug with the hydrogels. Cytochrome C has stronger interactions with the hydrogel units rather than with PEG. This leads to faster release in case of Fe@Au_PEG compared to the other systems, for Cytochrome C. In contrast, the release rate of L Dopa from Fe@Au_PEG_Hydrogel is faster as compared to the release rate of Cytochrome C. This can be ascribed to stronger interaction of Cytochrome C with the hydrogel units than L Dopa. The results further indicates that both the drugs show a faster release kinetics from Fe@Au_PEG_Hydrogel than Fe@Au_Hydrogel,

thereby boost the need of combination of PEG and hydrogels with the inorganic NPs in single system.

Chapter 5

Future Work

Coumarin showed reasonable loading for all three systems used in this study, but due to its hydrophobic nature, it shows unstable release kinetics under the conditions employed. In future it would be quite interesting to use some other techniques to estimate the release kinetics for this system. It might be possible that under the conditions which were utlized in this study, Coumarin release is not being effected. Therefore, it is suggested that the loading study of Coumarin be done at higher temperature, while its release be performed at normal or lower temperature.

One more suggestion which might provide interesting results is to study the release of drug from Fe@Au coated NPs at normal temperature, because results observed in this study indicate that there was decrease in size of coated NPs at 25 ^{o}C, and these systems are almost attaining the same size after heating and cooling cycles at 25 ^{o}C and 50 ^{o}C.

Furthermore, the coating of Fe@Au NPs with a cationic and anionic polymer separately can be done. The idea is to coat Fe@Au NPs with anionic polymer and then load this system with drug 1. Separately, coating of cationic polymer on the Fe@Au NPs can be done followed by subsequent loading of this system with drug 2. Difference in loading and release kinetics from these systems can provide further insights for the application of these nanocarriers in drug delivery. Also, High Performance Liquid Chromatography (HPLC) technique can be utilized to estimate the loading and release of two drugs on a single nanocarrier. For example, the system which is suggested above can be modified by mixing drug 1 loaded on Fe@Au NPs coated with anionic polymer and drug 2 loaded on Fe@Au NPs coated with cationic polymer. After mixing these systems, their loading and release studies can be performed with HPLC column.

Future work can also be based on loading of the drug by adding drug during the coating stage to Fe@Au and polymer solution. This experimental design might provide higher

loading of drugs on these systems. Release of the drug from this system can be compared with the drug release study in this work.

Bibliography

[1] Q. A. Pankhurst, J. Connolly, S. K. Jones, J. Dobson, Applications of magnetic nanoparticles in biomedicine, Journal of Physics D: Applied Physics 36 (13) (2003) R167.
URL http://stacks.iop.org/0022-3727/36/i=13/a=201

[2] B. Mukherjee, N. S. Dey, R. Maji, P. Bhowmik, P. J. Das, P. Paul, Current status and future scope for nanomaterials in drug delivery.

[3] V. I. Shubayev, T. R. Pisanic, S. Jin, Magnetic nanoparticles for theragnostics, Advanced drug delivery reviews 61 (6) (2009) 467–477.

[4] Superparamagnetic iron oxide nanoparticles (spions): Development, surface modification and applications in chemotherapy, Advanced Drug Delivery Reviews 63 (1–2) (2011) 24 – 46, 2011 Editors' Collection.
URL http://www.sciencedirect.com/science/article/pii/S0169409X1000133X

[5] World drug delivery summit, accessed: 2015-07-02.
URL http://drugdelivery.pharmaceuticalconferences.com

[6] Lexinnova (2012) nanoparticles smart drug delivery systems for cancer, accessed: 2015-07-02.
URL http://wipo.int/export/sites/www/patentscope/en/programs/patent_landscapes/documents/lexinnova_nanoparticles_smart_delivery_system_for_tumors.pdf

[7] P. Tartaj, M. del Puerto Morales, S. Veintemillas-Verdaguer, T. Gonzalez-Carreno, C. J. Serna, The preparation of magnetic nanoparticles for applications in biomedicine, Journal of Physics D: Applied Physics 36 (13) (2003) R182.

[8] R. Ghosh Chaudhuri, S. Paria, Core/shell nanoparticles: classes, properties, synthesis mechanisms, characterization, and applications, Chemical reviews 112 (4) (2011) 2373–2433.

[9] M. Ethayaraja, C. Ravikumar, D. Muthukumaran, K. Dutta, R. Bandyopadhyaya, Cds-zns core-shell nanoparticle formation: Experiment, mechanism, and simulation, The Journal of Physical Chemistry C 111 (8) (2007) 3246–3252.
URL http://dx.doi.org/10.1021/jp066066j

[10] G. Cao, Synthesis, properties and applications.

[11] A. Kraynov, T. E. Müller, Concepts for the stabilization of metal nanoparticles in ionic liquids, INTECH Open Access Publisher, 2011.

[12] H. I. Schlesinger, H. C. Brown, B. Abraham, A. C. Bond, N. Davidson, A. E. Finholt, J. R. Gilbreath, H. Hoekstra, L. Horvitz, E. K. Hyde, J. J. Katz, J. Knight, R. A. Lad, D. L. Mayfield, L. Rapp, D. M. Ritter, A. M. Schwartz, I. Sheft, L. D. Tuck, A. O. Walker, New developments in the chemistry of diborane and the borohydrides. i. general summary1, Journal of the American Chemical Society 75 (1) (1953) 186–190.
URL http://dx.doi.org/10.1021/ja01097a049

[13] K. Naka, Y. Chujo, Nanohybridized synthesis of metal nanoparticles and their organization, in: Nanohybridization of Organic-Inorganic Materials, Springer, 2009, pp. 3–40.

[14] A. S. Teja, P.-Y. Koh, Synthesis, properties, and applications of magnetic iron oxide nanoparticles, Progress in Crystal Growth and Characterization of Materials 55 (1–2) (2009) 22 – 45.
URL http://www.sciencedirect.com/science/article/pii/S0960897408000168

[15] K. T. Lee, Y. S. Jung, S. M. Oh, Synthesis of tin-encapsulated spherical hollow carbon for anode material in lithium secondary batteries, Journal of the American Chemical Society 125 (19) (2003) 5652–5653.

[16] A. Tavakoli, M. Sohrabi, A. Kargari, A review of methods for synthesis of nanostructured metals with emphasis on iron compounds, Chemical Papers 61 (3) (2007) 151–170.

[17] M. Tadić, D. Marković, V. Spasojević, V. Kusigerski, M. Remškar, J. Pirnat, Z. Jagličić, Synthesis and magnetic properties of concentrated α-fe 2 o 3 nanoparticles in a silica matrix, Journal of alloys and compounds 441 (1) (2007) 291–296.

[18] M. Sedlar, The preparation and magnetic properties of sodium-modified iron oxide thin films by a sol gel method, Ceramics International 20 (1) (1994) 73 – 78.
URL http://sciencedirect.com/science/article/pii/0272884294900116

[19] B. Samiey, C.-H. Cheng, J. Wu, Organic-inorganic hybrid polymers as adsorbents for removal of heavy metal ions from solutions: A review, Materials 7 (2) (2014) 673–726.

[20] D. Langevin, Micelles and microemulsions, Annual Review of Physical Chemistry 43 (1) (1992) 341–369.
URL http://dx.doi.org/10.1146/annurev.pc.43.100192.002013

[21] B. K. Paul, S. P. Moulik, Uses and applications of microemulsions, CURRENT SCIENCE-BANGALORE- 80 (8) (2001) 990–1001.

[22] A. K. Gupta, M. Gupta, Synthesis and surface engineering of iron oxide nanoparticles for biomedical applications, Biomaterials 26 (18) (2005) 3995 – 4021.
URL http://sciencedirect.com/science/article/pii/S0142961204009317

[23] A.-H. Lu, E. Salabas, F. Schüth, Magnetic nanoparticles: Synthesis, protection, functionalization, and application, Angewandte Chemie International Edition 46 (8) (2007) 1222–1244.
URL http://dx.doi.org/10.1002/anie.200602866

[24] C. Bréchignac, P. Houdy, M. Lahmani, Nanomaterials and nanochemistry, Springer Science & Business Media, 2008.

[25] E. E. Carpenter, C. T. Seip, C. J. O'Connor, Magnetism of nanophase metal and metal alloy particles formed in ordered phases, Journal of Applied Physics 85 (8) (1999) 5184–5186.
URL http://scitation.aip.org/content/aip/journal/jap/85/8/10.1063/1.369118

[26] J. R. McCarthy, R. Weissleder, Multifunctional magnetic nanoparticles for targeted imaging and therapy, Advanced Drug Delivery Reviews 60 (11) (2008) 1241 – 1251, inorganic Nanoparticles in Drug Delivery.
URL http://sciencedirect.com/science/article/pii/S0169409X08000963

[27] R. Krahne, G. Morello, A. Figuerola, C. George, S. Deka, L. Manna, Physical properties of elongated inorganic nanoparticles, Physics Reports 501 (3–5) (2011) 75 – 221.
URL http://www.sciencedirect.com/science/article/pii/S037015731100010X

[28] Y.-Q. Song, Focus on the physics of magnetic resonance on porous media, New Journal of Physics 14 (5) (2012) 055017.
URL http://stacks.iop.org/1367-2630/14/i=5/a=055017

[29] C. Sun, J. S. Lee, M. Zhang, Magnetic nanoparticles in {MR} imaging and drug delivery, Advanced Drug Delivery Reviews 60 (11) (2008) 1252 – 1265, inorganic Nanoparticles in Drug Delivery.
URL http://www.sciencedirect.com/science/article/pii/S0169409X08001014

[30] S. Horikoshi, N. Serpone, Nanoparticle Synthesis through Microwave Heating, Wiley-VCH Verlag GmbH & Co. KGaA, 2013, pp. 75–105.
URL http://dx.doi.org/10.1002/9783527648122.ch5

[31] Nanoparticle plasmonics, accessed: 2015-07-24.
URL http://physics.aalto.fi/groups/comp/msp/research/plasmonics/

[32] J. Panyam, V. Labhasetwar, Biodegradable nanoparticles for drug and gene delivery to cells and tissue, Advanced drug delivery reviews 55 (3) (2003) 329–347.

[33] A. Mahapatro, D. K. Singh, Biodegradable nanoparticles are excellent vehicle for site directed in-vivo delivery of drugs and vaccines, J. Nanobiotechnol 9 (55) (2011) 1–11.

[34] . Albertsson, Ann-Christine, Degradable aliphatic polyestersIncludes bibliographical references and indexes.

[35] S. Gelperina, K. Kisich, M. D. Iseman, L. Heifets, The potential advantages of nanoparticle drug delivery systems in chemotherapy of tuberculosis, American journal of respiratory and critical care medicine 172 (12) (2005) 1487–1490.

[36] R. Singh, J. W. Lillard, Nanoparticle-based targeted drug delivery, Experimental and molecular pathology 86 (3) (2009) 215–223.

[37] A. Prokop, J. M. Davidson, Nanovehicular intracellular delivery systems, Journal of Pharmaceutical Sciences 97 (9) (2008) 3518–3590.
URL http://dx.doi.org/10.1002/jps.21270

[38] V. Lassalle, M. L. Ferreira, Pla nano- and microparticles for drug delivery: An overview of the methods of preparation, Macromolecular Bioscience 7 (6) (2007) 767–783.
URL http://dx.doi.org/10.1002/mabi.200700022

[39] T. Görner, R. Gref, D. Michenot, F. Sommer, M. Tran, E. Dellacherie, Lidocaine-loaded biodegradable nanospheres. i. optimization of the drug incorporation into the polymer matrix, Journal of controlled release 57 (3) (1999) 259–268.

[40] S. Bontha, A. V. Kabanov, T. K. Bronich, Polymer micelles with cross-linked ionic cores for delivery of anticancer drugs, Journal of controlled release 114 (2) (2006) 163–174.

[41] V. P. Torchilin, Structure and design of polymeric surfactant-based drug delivery systems, Journal of controlled release 73 (2) (2001) 137–172.

[42] A. M. Jhaveri, V. P. Torchilin, Multifunctional polymeric micelles for delivery of drugs and sirna, Frontiers in pharmacology 5.

[43] K. D. Sattler, Handbook of nanophysics: nanomedicine and nanorobotics, CRC Press, 2010.

[44] S. Ganta, H. Devalapally, A. Shahiwala, M. Amiji, A review of stimuli-responsive nanocarriers for drug and gene delivery, Journal of Controlled Release 126 (3) (2008) 187–204.

[45] C. C. Lee, J. A. MacKay, J. M. Fréchet, F. C. Szoka, Designing dendrimers for biological applications, Nature biotechnology 23 (12) (2005) 1517–1526.

[46] A. D. Wong, M. A. DeWit, E. R. Gillies, Amplified release through the stimulus triggered degradation of self-immolative oligomers, dendrimers, and linear polymers, Advanced drug delivery reviews 64 (11) (2012) 1031–1045.

[47] W. Yang, Y. Cheng, T. Xu, X. Wang, L.-p. Wen, Targeting cancer cells with biotin–dendrimer conjugates, European journal of medicinal chemistry 44 (2) (2009) 862–868.

[48] A. S. Hoffman, Hydrogels for biomedical applications, Advanced Drug Delivery Reviews 54 (1) (2002) 3–12.

[49] S. Gehrke, Synthesis, equilibrium swelling, kinetics, permeability and applications of environmentally responsive gels 110 (1993) 81–144.
URL http://dx.doi.org/10.1007/BFb0021130

[50] S. Nayak, L. A. Lyon, Soft nanotechnology with soft nanoparticles, Angewandte chemie international edition 44 (47) (2005) 7686–7708.

[51] W. R. Gombotz, S. Wee, Protein release from alginate matrices, Advanced Drug Delivery Reviews 31 (3) (1998) 267–285.

[52] M. P. Lutolf, G. P. Raeber, A. H. Zisch, N. Tirelli, J. A. Hubbell, Cell-responsive synthetic hydrogels, Advanced Materials 15 (11) (2003) 888–892.

[53] W. Hennink, C. Van Nostrum, Novel crosslinking methods to design hydrogels, Advanced drug delivery reviews 64 (2012) 223–236.

[54] Y. Li, T. Tanaka, Study of the universality class of the gel network system, The Journal of Chemical Physics 90 (9) (1989) 5161–5166.
URL http://scitation.aip.org/content/aip/journal/jcp/90/9/10.1063/1.456559

[55] Y. Li, T. Tanaka, Kinetics of swelling and shrinking of gels, The Journal of Chemical Physics 92 (2) (1990) 1365–1371.
URL http://scitation.aip.org/content/aip/journal/jcp/92/2/10.1063/1.458148

[56] D. Gan, L. A. Lyon, Tunable swelling kinetics in core shell hydrogel nanoparticles, Journal of the American Chemical Society 123 (31) (2001) 7511–7517, pMID: 11480971.
URL http://dx.doi.org/10.1021/ja010609f

[57] C. D. Jones, L. A. Lyon, Synthesis and characterization of multiresponsive core shell microgels, Macromolecules 33 (22) (2000) 8301–8306.
URL http://dx.doi.org/10.1021/ma001398m

[58] K. Dušek, D. Patterson, Transition in swollen polymer networks induced by intramolecular condensation, Journal of Polymer Science Part A-2: Polymer Physics 6 (7) (1968) 1209–1216.

[59] T. Tanaka, Collapse of gels and the critical endpoint, Physical Review Letters 40 (12) (1978) 820.

[60] H. Schild, Poly(n-isopropylacrylamide): experiment, theory and application, Progress in Polymer Science 17 (2) (1992) 163 – 249.
URL http://www.sciencedirect.com/science/article/pii/007967009290023R

[61] M.Heskins, J. E. Guillet, Solution properties of poly(n-isopropylacrylamide), Journal of Macromolecular Science: Part A - Chemistry 2 (8) (1968) 1441–1455.
URL http://dx.doi.org/10.1080/10601326808051910

[62] C. Wu, X. Wang, Globule to coil transition of a single homopolymer chain in solution, Physical review letters 80 (18) (1998) 4092.

[63] X. Wang, X. Qiu, C. Wu, Comparison of the coil to globule and the globule to coil transitions of a single poly(n-isopropylacrylamide) homopolymer chain in water, Macromolecules 31 (9) (1998) 2972–2976.
URL http://dx.doi.org/10.1021/ma971873p

[64] C. Wu, S. Zhou, Volume phase transition of swollen gels: discontinuous or continuous?, Macromolecules 30 (3) (1997) 574–576.

[65] D. Gan, L. A. Lyon, Interfacial nonradiative energy transfer in responsive core shell hydrogel nanoparticles, Journal of the American Chemical Society 123 (34) (2001) 8203–8209, pMID: 11516270.
URL http://dx.doi.org/10.1021/ja0159741

[66] M. J. Snowden, B. Z. Chowdhry, B. Vincent, G. E. Morris.

[67] J. D. Debord, L. A. Lyon, Synthesis and characterization of ph responsive copolymer microgels with tunable volume phase transition temperatures, Langmuir 19 (18) (2003) 7662–7664.

[68] Berndt, Doubly temperature sensitive core shell microgels, Macromolecules 36 (23) (2003) 8780–8785.
URL http://dx.doi.org/10.1021/ma034771+

[69] I. Berndt, J. S. Pedersen, W. Richtering, Structure of multiresponsive intelligent core shell microgels, Journal of the American Chemical Society 127 (26) (2005) 9372–9373, pMID: 15984856.
URL http://dx.doi.org/10.1021/ja051825h

[70] M. Shibayama, T. Tanaka, Volume phase transition and related phenomena of polymer gels, in: Responsive gels: volume transitions I, Springer, 1993, pp. 1–62.

[71] K. Dušek, W. Prins, Structure and elasticity of non-crystalline polymer networks, in: Fortschritte der Hochpolymeren-Forschung, Vol. 6/1 of Advances in Polymer Science, Springer Berlin Heidelberg, 1969, pp. 1–102.
URL http://dx.doi.org/10.1007/BFb0051042

[72] C. Chakraborty, S. Pal, G. P. C. Doss, Z.-H. Wen, C.-S. Lin, Nanoparticles as 'smart' pharmaceutical delivery, Frontiers in bioscience (Landmark edition) 18 (2013) 1030—1050.
URL http://dx.doi.org/10.2741/4161

[73] S. H. Choi, J. J. Yoon, T. G. Park, Galactosylated poly (n-isopropylacrylamide) hydrogel submicrometer particles for specific cellular uptake within hepatocytes, Journal of colloid and interface science 251 (1) (2002) 57–63.

[74] A. S. de Dios, M. E. Díaz-García, Multifunctional nanoparticles: Analytical prospects, Analytica Chimica Acta 666 (1–2) (2010) 1 – 22.
URL http://www.sciencedirect.com/science/article/pii/S0003267010003211

[75] M. Liong, J. Lu, M. Kovochich, T. Xia, S. G. Ruehm, A. E. Nel, F. Tamanoi, J. I. Zink, Multifunctional inorganic nanoparticles for imaging, targeting, and drug delivery, ACS Nano 2 (5) (2008) 889–896, pMID: 19206485.
URL http://dx.doi.org/10.1021/nn800072t

[76] Y. Cao, B. Wang, D. Lou, Y. Wang, S. Hao, L. Zhang, Nanoscale delivery systems for multiple drug combinations in cancer, Future Oncology 7 (11) (2011) 1347–1357.

[77] T. Bronich, Multifunctional polymeric carriers for gene and drug delivery, Pharmaceutical Research 27 (11) (2010) 2257–2259.
URL http://dx.doi.org/10.1007/s11095-010-0270-z

[78] H. Maeda, Tumor-selective delivery of macromolecular drugs via the epr effect: Background and future prospects, Bioconjugate Chemistry 21 (5) (2010) 797–802, pMID: 20397686.
URL http://dx.doi.org/10.1021/bc100070g

[79] H. Maeda, Macromolecular therapeutics in cancer treatment: The epr effect and beyond, Journal of Controlled Release 164 (2) (2012) 138–144, cited By 138.
URL http://www.scopus.com/inward/record.url?eid=2-s2.0-84869496799&partnerID=40&md5=1b3edc8c30868f26c2b9af4c621bae27

[80] V. Torchilin, Targeted polymeric micelles for delivery of poorly soluble drugs, Cellular and Molecular Life Sciences CMLS 61 (19-20) (2004) 2549–2559.
URL http://dx.doi.org/10.1007/s00018-004-4153-5

[81] N. Nasongkla, E. Bey, J. Ren, H. Ai, C. Khemtong, J. S. Guthi, S.-F. Chin, A. D. Sherry, D. A. Boothman, J. Gao, Multifunctional polymeric micelles as cancer-targeted, mri-ultrasensitive drug delivery systems, Nano Letters 6 (11) (2006) 2427–2430, pMID: 17090068.
URL http://dx.doi.org/10.1021/nl061412u

[82] S. T. Selvan, Multifunctional fluorescent and magnetic nanoparticles for biomedical applications, Proc. SPIE 8232 (2012) 823211–823211–6.
URL http://dx.doi.org/10.1117/12.915811

[83] Z. Ali, A. Z. Abbasi, F. Zhang, P. Arosio, A. Lascialfari, M. F. Casula, A. Wenk, W. Kreyling, R. Plapper, M. Seidel, R. Niessner, J. Knöll, A. Seubert, W. J. Parak, Multifunctional nanoparticles for dual imaging, Analytical Chemistry 83 (8) (2011) 2877–2882, pMID: 21413785.
URL http://dx.doi.org/10.1021/ac103261y

[84] H. Koo, M. S. Huh, I.-C. Sun, S. H. Yuk, K. Choi, K. Kim, I. C. Kwon, In vivo targeted delivery of nanoparticles for theranosis, Accounts of Chemical Research 44 (10) (2011) 1018–1028, pMID: 21851104.
URL http://dx.doi.org/10.1021/ar2000138

[85] L. Vannucci, E. Falvo, M. Fornara, P. Di Micco, O. Benada, J. Krizan, J. Svoboda, K. Hulikova-Capkova, V. Morea, A. Boffi, P. Ceci, Selective targeting of melanoma by peg-masked protein-based multifunctional nanoparticles, International Journal of Nanomedicine 7 (2012) 1489–1509, cited By 18.
URL http://www.scopus.com/inward/record.url?eid=2-s2.0-84866769573&partnerID=40&md5=3f05df84f81bab0b85e22d8ea740a527

[86] M. K. Yu, J. Park, S. Jon, Targeting strategies for multifunctional nanoparticles in cancer imaging and therapy, Theranostics 2 (1) (2012) 3.

[87] J. Kreuter, Nanoparticulate systems for brain delivery of drugs, Advanced Drug Delivery Reviews 47 (1) (2001) 65–81, cited By 689.
URL http://www.scopus.com/inward/record.url?eid=2-s2.0-0035937595&partnerID=40&md5=22bfcbbb74765632dedd1c5b8eb49b29

[88] G. Bao, S. Mitragotri, S. Tong, Multifunctional nanoparticles for drug delivery and molecular imaging, Annual Review of Biomedical Engineering 15 (1) (2013) 253–282, pMID: 23642243.
URL http://dx.doi.org/10.1146/annurev-bioeng-071812-152409

[89] F. Jia, X. Liu, L. Li, S. Mallapragada, B. Narasimhan, Q. Wang, Multifunctional nanoparticles for targeted delivery of immune activating and cancer therapeutic agents, Journal of Controlled Release 172 (3) (2013) 1020 – 1034.
URL http://www.sciencedirect.com/science/article/pii/S0168365913008420

[90] J. Conniot, J. M. Silva, J. G. Fernandes, L. C. Silva, R. Gaspar, S. Brocchini, H. F. Florindo, T. S. Barata, Cancer immunotherapy: nanodelivery approaches for immune cell targeting and tracking, Frontiers in Chemistry 2 (105).
URL http://www.frontiersin.org/chemical_engineering/10.3389/fchem.2014.00105/abstract

[91] F. Benyettou, J. Hardouin, J. H. Marc Lecouvey, L. Motte, Pegylate d versus non-pegylated γ-Fe_2O_3 @ alendronate nanoparticles, J Bioanal Biomed 4 (2012) 39–45.

[92] V. I. Shubayev, T. R. P. II, S. Jin, Magnetic nanoparticles for theragnostics, Advanced Drug Delivery Reviews 61 (6) (2009) 467 – 477, identifying and

Assessing Biomaterial Nanotoxicity in Translational Research for Preclinical Drug Development.
URL http://www.sciencedirect.com/science/article/pii/S0169409X09001045

[93] C. Chakraborty, S. Pal, G. P. C. Doss, Z.-H. Wen, C.-S. Lin, Nanoparticles as 'smart' pharmaceutical delivery, Frontiers in bioscience (Landmark edition) 18 (2013) 1030—1050.
URL http://dx.doi.org/10.2741/4161

[94] H. Bysell, R. Månsson, P. Hansson, M. Malmsten, Microgels and microcapsules in peptide and protein drug delivery, Advanced Drug Delivery Reviews 63 (13) (2011) 1172 – 1185, formulating biomolecules: mechanistics insights in molecular interactions.
URL http://www.sciencedirect.com/science/article/pii/S0169409X11002304

[95] G. R. Hendrickson, M. H. Smith, A. B. South, L. A. Lyon, Design of multiresponsive hydrogel particles and assemblies, Advanced Functional Materials 20 (11) (2010) 1697–1712.
URL http://dx.doi.org/10.1002/adfm.200902429

[96] X. Li, L. Wang, Y. Fan, Q. Feng, F.-z. Cui, Biocompatibility and toxicity of nanoparticles and nanotubes, J. Nanomaterials 2012 (2012) 6:6–6:6.
URL http://dx.doi.org/10.1155/2012/548389

[97] M. Malmsten, Soft drug delivery systems, Soft Matter 2 (2006) 760–769.
URL http://dx.doi.org/10.1039/B608348J

[98] J. Panyam, V. Labhasetwar, Biodegradable nanoparticles for drug and gene delivery to cells and tissue, Advanced Drug Delivery Reviews 55 (3) (2003) 329–347.
URL http://www.scopus.com/inward/record.url?eid=2-s2.0-0037462997&partnerID=40&md5=4113bffd4fb23080a8285686a4f8af6d

[99] A. Kumar, F. Chen, A. Mozhi, X. Zhang, Y. Zhao, X. Xue, Y. Hao, X. Zhang, P. C. Wang, X.-J. Liang, Innovative pharmaceutical development based on unique properties of nanoscale delivery formulation, Nanoscale 5 (18) (2013) 8307–8325.

[100] T. Fan, M. Li, X. Wu, M. Li, Y. Wu, Preparation of thermoresponsive and ph-sensitivity polymer magnetic hydrogel nanospheres as anticancer drug carriers, Colloids and Surfaces B: Biointerfaces 88 (2) (2011) 593 – 600.
URL http://sciencedirect.com/science/article/pii/S0927776511004516

[101] L-dopa effects, side effects and dosages, accessed: 2015-07-05.
URL http://nootriment.com/l-dopa/

[102] D9628 sigma 3,4-dihydroxy-l-phenylalanine, accessed: 2015-07-06.
URL http://sigmaaldrich.com/catalog/product/sigma/d9628?lang=en&region=NO

[103] Uniprotkb - p99999, accessed: 2015-07-23.
URL http://uniprot.org/uniprot/P99999

[104] Cytochrome, accessed: 2015-07-24.
URL https://en.wikipedia.org/wiki/Cytochrome

[105] N. Mirkin, J. Jaconcic, V. Stojanoff, A. Moreno, High resolution x-ray crystallographic structure of bovine heart cytochrome c and its application to the design of an electron transfer biosensor, Proteins: Structure, Function, and Bioinformatics 70 (1) (2008) 83–92.
URL http://dx.doi.org/10.1002/prot.21452

[106] C2037 sigma cytochrome c from bovine heart, accessed: 2015-07-23.
URL http://sigmaaldrich.com/catalog/product/sigma/c2037?lang=en&region=NO

[107] X. Jiang, X. Wang, Cytochrome c-mediated apoptosis, Annual Review of Biochemistry 73 (1) (2004) 87–106, pMID: 15189137.
URL http://dx.doi.org/10.1146/annurev.biochem.73.011303.073706

[108] Partial purification of cytochrome c from bovine heart, accessed: 2015-07-23.
URL http://sigmaaldrich.com/catalog/product/sigma/c2037?lang=en&region=NO

[109] C4261 sigma coumarin, accessed: 2015-07-23.
URL http://www.sigmaaldrich.com/catalog/product/sigma/c4261?lang=en&region=NO

[110] M. A. Musa, J. S. Cooperwood, M. O. F. Khan, A review of coumarin derivatives in pharmacotherapy of breast cancer, Current medicinal chemistry 15 (26) (2008) 2664.

[111] J. L. Arias, Nanotechnology and Drug Delivery, Volume One: Nanoplatforms in Drug Delivery, Vol. 1, CRC Press, 2014.

[112] M. M. De Villiers, P. Aramwit, G. S. Kwon, Nanotechnology in drug delivery, Springer Science & Business Media, 2008.

[113] V. Lehto, J. Riikonen, H. Santos, Drug loading and characterisation of porous silicon materials, Porous silicon for biomedical applications. Woodhead Publishing, Cambridge, UK (2014) 337–355.

[114] R. Singh, J. W. Lillard, Nanoparticle-based targeted drug delivery, Experimental and molecular pathology 86 (3) (2009) 215–223.
URL http://www.sciencedirect.com/science/article/pii/S001448000800141X

[115] Biodegradable polymeric nanoparticles as drug delivery devices, Journal of Controlled Release 70 (1–2) (2001) 1 – 20.

[116] H. Yoo, J. Oh, K. Lee, T. Park, Biodegradable nanoparticles containing doxorubicin-plga conjugate for sustained release, Pharmaceutical Research 16 (7) (1999) 1114–1118.
URL http://dx.doi.org/10.1023/A%3A1018908421434

[117] T. Govender, T. Riley, T. Ehtezazi, M. C. Garnett, S. Stolnik, L. Illum, S. S. Davis, Defining the drug incorporation properties of pla–peg nanoparticles, International Journal of Pharmaceutics 199 (1) (2000) 95 – 110.
URL http://www.sciencedirect.com/science/article/pii/S0378517300003756

[118] T. Govender, S. Stolnik, M. Garnett, L. Illum, S. Davis, Plga nanoparticles prepared by nanoprecipitation: Drug loading and release studies of a water soluble drug, Journal of Controlled Release 57 (2) (1999) 171–185, cited By 439.
URL http://scopus.com/inward/record.url?eid=2-s2.0-0032952283&partnerID=40&md5=b4b29b85ed8140fe8427a92bf7ada000

[119] J. Panyam, D. William, A. Dash, D. Leslie-Pelecky, V. Labhasetwar, Solid-state solubility influences encapsulation and release of hydrophobic drugs from plga/pla nanoparticles, Journal of Pharmaceutical Sciences 93 (7) (2004) 1804–1814, cited By 105.
URL http://scopus.com/inward/record.url?eid=2-s2.0-3042601972&partnerID=40&md5=1083ef9f82c28885e604985cc258a96b

[120] K. S. Soppimath, T. M. Aminabhavi, A. R. Kulkarni, W. E. Rudzinski, Biodegradable polymeric nanoparticles as drug delivery devices, Journal of Controlled Release 70 (1–2) (2001) 1 – 20.
URL http://sciencedirect.com/science/article/pii/S0168365900003394

[121] M. Egea, F. Gamisans, J. Valero, M. Garcia, M. Garcia, Entrapment of cisplatin into biodegradable polyalkylcyanoacrylate nanoparticles, Farmaco 49 (3) (1994)

211–217, cited By 16.
URL http://scopus.com/inward/record.url?eid=2-s2.0-0028225711&partnerID=40&md5=4639adbd75f2b25d215adae586d1394f

[122] T. Tanaka, D. J. Fillmore, Kinetics of swelling of gels, The Journal of Chemical Physics 70 (3) (1979) 1214–1218.
URL http://scitation.aip.org/content/aip/journal/jcp/70/3/10.1063/1.437602

[123] D. Dupin, S. Fujii, S. Armes, P. Reeve, S. Baxter, Efficient synthesis of sterically stabilized ph-responsive microgels of controllable particle diameter by emulsion polymerization, Langmuir 22 (7) (2006) 3381–3387, cited By 104.
URL http://scopus.com/inward/record.url?eid=2-s2.0-33645509526&partnerID=40&md5=03e5491bc432297b418087c7ccf133ac

[124] L. Bromberg, M. Temchenko, T. Hatton, Dually responsive microgels from polyether-modified poly(acrylic acid): Swelling and drug loading, Langmuir 18 (12) (2002) 4944–4952, cited By 108.
URL http://scopus.com/inward/record.url?eid=2-s2.0-0037062824&partnerID=40&md5=30be496c0b4616850422012a107b308b

[125] K. Plunkett, M. Kraft, Q. Yu, J. Moore, Swelling kinetics of disulfide cross-linked microgels, Macromolecules 36 (11) (2003) 3960–3966, cited By 44.
URL http://www.scopus.com/inward/record.url?eid=2-s2.0-0038069217&partnerID=40&md5=07462a60f55a493ee5a40e2777e24cac

[126] D. Gan, L. Lyon, Tunable swelling kinetics in core - shell hydrogel nanoparticles, Journal of the American Chemical Society 123 (31) (2001) 7511–7517, cited By 183.
URL http://www.scopus.com/inward/record.url?eid=2-s2.0-0034813654&partnerID=40&md5=c76bc325806d9f54ea14bcdf26954e7d

[127] R. Shah, J.-W. Kim, J. Agresti, D. Weitz, L.-Y. Chu, Fabrication of monodisperse thermosensitive microgels and gel capsules in microfluidic devices, Soft Matter 4 (12) (2008) 2303–2309, cited By 93.
URL http://www.scopus.com/inward/record.url?eid=2-s2.0-56149119048&partnerID=40&md5=94318f94642ae8283007369e69995893

[128] L.-Y. Chu, J.-W. Kim, R. Shah, D. Weitz, Monodisperse thermoresponsive microgels with tunable volume-phase transition kinetics, Advanced Functional Materials 17 (17) (2007) 3499–3504, cited By 85.
URL http://www.scopus.com/inward/record.url?eid=2-s2.0-36849044613&partnerID=40&md5=e60549534fd707cf603e184d1e28a078

[129] A. Kumari, S. K. Yadav, S. C. Yadav, Biodegradable polymeric nanoparticles based drug delivery systems, Colloids and Surfaces B: Biointerfaces 75 (1) (2010) 1 – 18.
URL http://www.sciencedirect.com/science/article/pii/S0927776509004111

[130] B. Magenheim, M. Levy, S. Benita, A new in vitro technique for the evaluation of drug release profile from colloidal carriers - ultrafiltration technique at low pressure, International Journal of Pharmaceutics 94 (1–3) (1993) 115 – 123.
URL http://www.sciencedirect.com/science/article/pii/0378517393900158

[131] M. Fresta, G. Puglisi, G. Giammona, G. Cavallaro, N. Micali, P. M. Furneri, Pefloxacine mesilate- and ofloxacin-loaded polyethylcyanoacrylate nanoparticles: Characterization of the colloidal drug carrier formulation, Journal of Pharmaceutical Sciences 84 (7) (1995) 895–902.
URL http://dx.doi.org/10.1002/jps.2600840721

[132] Y. Chen, R. McCulloch, B. Gray, Synthesis of albumin-dextran sulfate microspheres possessing favourable loading and release characteristics for the anticancer drug doxorubicin, Journal of controlled release 31 (1) (1994) 49–54.

[133] J. Siepmann, N. Peppas, Mathematical modeling of controlled drug delivery, Advanced drug delivery reviews 48 (2-3) (2001) 137—138.
URL http://dx.doi.org/10.1016/S0169-409X(01)00111-9

[134] Y. Fu, W. J. Kao, Drug release kinetics and transport mechanisms of non-degradable and degradable polymeric delivery systems, Expert opinion on drug delivery 7 (4) (2010) 429–444.

[135] J. Siepmann, A. Göpferich, Mathematical modeling of bioerodible, polymeric drug delivery systems, Advanced Drug Delivery Reviews 48 (2–3) (2001) 229 – 247, mathematical Modeling of Controlled Drug Delivery.
URL http://www.sciencedirect.com/science/article/pii/S0169409X01001168

[136] G. Modesti, B. Zimmermann, M. Börsch, A. Herrmann, K. Saalwächter, Diffusion in model networks as studied by nmr and fluorescence correlation spectroscopy, Macromolecules 42 (13) (2009) 4681–4689, pMID: 19812716.
URL http://dx.doi.org/10.1021/ma900614j

[137] B. Narasimhan, Mathematical models describing polymer dissolution: consequences for drug delivery, Advanced Drug Delivery Reviews 48 (2) (2001) 195–210.

[138] B. Narasimhan, N. A. Peppas, Molecular analysis of drug delivery systems controlled by dissolution of the polymer carrier, Journal of Pharmaceutical Sciences 86 (3) (1997) 297–304.
URL http://dx.doi.org/10.1021/js960372z

[139] H. Hopfenberg, Controlled release from erodible slabs, cylinders, and spheres, Controlled release polymeric formulations 33 (1976) 26–32.

[140] H. Karasulu, G. Ertan, T. Köse, Modeling of theophylline release from different geometrical erodible tablets, European journal of pharmaceutics and biopharmaceutics 49 (2) (2000) 177–182.

[141] I. Katzhendler, A. Hoffman, A. Goldberger, M. Friedman, Modeling of drug release from erodible tablets, Journal of Pharmaceutical Sciences 86 (1) (1997) 110–115.
URL http://dx.doi.org/10.1021/js9600538

[142] J. Siepmann, N. A. Peppas, Higuchi equation: derivation, applications, use and misuse, International journal of pharmaceutics 418 (1) (2011) 6–12.

[143] C. S. Brazel, N. A. Peppas, Modeling of drug release from swellable polymers, European journal of pharmaceutics and biopharmaceutics 49 (1) (2000) 47–58.

[144] D. Enscore, H. Hopfenberg, V. Stannett, Effect of particle size on the mechanism controlling n-hexane sorption in glassy polystyrene microspheres, Polymer 18 (8) (977) 793 – 800.
URL http://www.sciencedirect.com/science/article/pii/0032386177901835

[145] S. Bandyopadhyay, G. Singh, I. Sandvig, A. Sandvig, R. Mathieu, P. A. Kumar, W. R. Glomm, Synthesis and in vitro cellular interactions of superparamagnetic iron nanoparticles with a crystalline gold shell, Applied Surface Science 316 (2014) 171 – 178.
URL http://www.sciencedirect.com/science/article/pii/S0169433214016092

[146] B. J. Berne, R. Pecora, Dynamic light scattering: with applications to chemistry, biology, and physics, Courier Corporation, 2000.

[147] K. Kratz, T. Hellweg, W. Eimer, Influence of charge density on the swelling of colloidal poly (n-isopropylacrylamide-co-acrylic acid) microgels, Colloids and Surfaces A: Physicochemical and Engineering Aspects 170 (2) (2000) 137–149.

[148] P. C. Hiemenz, R. Rajagopalan, Principles of Colloid and Surface Chemistry, revised and expanded, Vol. 14, CRC press, 1997.

[149] Zetasizer nano range, accessed: 2015-07-24.
URL http://malvern.com/en/products/product-range/zetasizer-range/zetasizer-nano-range/

[150] J. Lyklema, Fundamentals of interface and colloid science: soft colloids, Vol. 5, Academic press, 2005.

[151] Zetasizer nano range, accessed: 2015-07-24.
URL http://malvern.com/en/products/product-range/zetasizer-range/zetasizer-nano-range/

[152] A. Sze, D. Erickson, L. Ren, D. Li, Zeta-potential measurement using the smoluchowski equation and the slope of the current–time relationship in electroosmotic flow, Journal of colloid and interface science 261 (2) (2003) 402–410.

[153] S. Behera, S. Ghanty, F. Ahmad, S. Santra, S. Banerjee, Uv-visible spectrophotometric method development and validation of assay of paracetamol tablet formulation, J Anal Bioanal Techniques 3 (151) (2012) 2.

[154] F.-X. Schmid, Biological Macromolecules: UV-visible Spectrophotometry, John Wiley & Sons, Ltd, 2001.
URL http://dx.doi.org/10.1038/npg.els.0003142

[155] A. V. Crewe, J. Wall, J. Langmore, Visibility of single atoms, Science 168 (3937) (1970) 1338–1340.

[156] S. Pennycook, A. Lupini, M. Varela, A. Borisevich, Y. Peng, M. Oxley, K. Van Benthem, M. Chisholm, Scanning transmission electron microscopy for nanostructure characterization, in: Scanning Microscopy for Nanotechnology, Springer, 2007, pp. 152–191.

[157] M. K. Anderson, Polymeric hydrogels for drug delivery, marte kee anderson, master thesis ntnu, 2014.

[158] J. Kost, Pulsed and self-regulated drug delivery, CRC Press, 1990.

[159] S. Volden, A.-L. Kjøniksen, K. Zhu, J. Genzer, B. Nyström, W. R. Glomm, Temperature-dependent optical properties of gold nanoparticles coated with a charged diblock copolymer and an uncharged triblock copolymer, ACS Nano 4 (2) (2010) 1187–1201, pMID: 20078133.
URL http://dx.doi.org/10.1021/nn901517u

[160] M. H. Smith, L. A. Lyon, Tunable encapsulation of proteins within charged microgels, Macromolecules 44 (20) (2011) 8154–8160, pMID: 22058574.
URL http://dx.doi.org/10.1021/ma201365p

[161] S. Sharma, K. C. Popat, T. A. Desai, Controlling nonspecific protein interactions in silicon biomicrosystems with nanostructured poly(ethylene glycol) films, Langmuir 18 (23) (2002) 8728–8731.
URL http://dx.doi.org/10.1021/la026097f

[162] M. A. Ashfaq, Specilization project on controlled release from nanoparticles (nps) for theranostic applications, 2014.

[163] M. Barzegar-Jalali, K. Adibkia, H. Valizadeh, M. R. S. Shadbad, A. Nokhodchi, Y. Omidi, G. Mohammadi, S. H. Nezhadi, M. Hasan, Kinetic analysis of drug release from nanoparticles, Journal of Pharmacy and Pharmaceutical Sciences 11 (1) (2008) 167–177.

Appendix A

Fe@Au Synthesis

A.1 Calculation for Fe@Au Synthesis

10 mM sodium citrate

$$\left(\frac{10\times10^{-3}moles}{1000ml}\times 100ml\right)\times 294 = 294mg$$

Here 294 is the molecular weight of sodium citrate

1.5mM chloroauric acid

$$= 1.5\times10^{-3}mole\times 393.8g = 0.5907g0.5907\times 10g$$

$$\frac{0.5907}{1000}\times 10g = 5.9mgofchloroauricacid$$

Here 393.8 g is the molecular weight chloroauric acid Dilution of Fe@Au solution

Concentration of Fe@Au were 32.6 mg/ml it was diluted to 10 mg/ml concentration

To prepare 4 ml solution

$Requiredvolume\times requiredconcentration = x\times concentrationofsolution4ml\times 10mg/ml = x\times 32.6mg/ml$

$x = 1.22mlofsolutiondissolvedin2.77mlofmilliQwater$

Appendix B

Calibration curves

B.1 Calibration curve of Coumarin

Figure B.1 shows the calibaration curve for Coumarin.

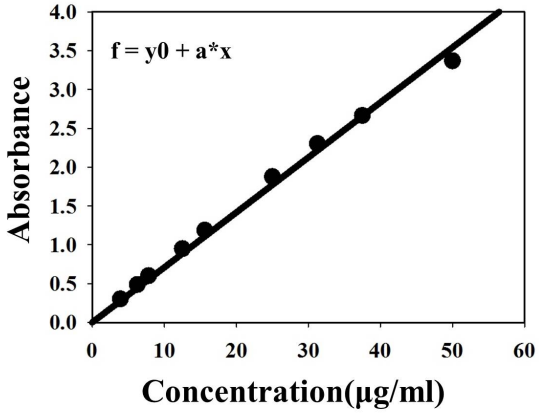

FIGURE B.1: Calibration curve of Coumarin

B.2 Calibration curve of L-dopa

Figure B.2 is showing Calibration curve for L-dopa.

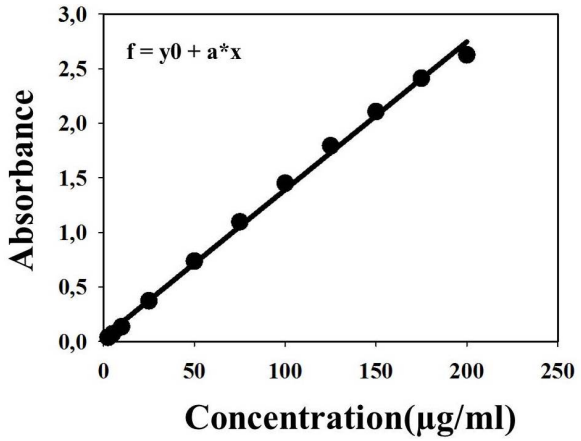

FIGURE B.2: Calibration curve of L-dopa

B.3 Calibration curve of Cytochrome-C

Figure B.3 is showing Calibration curve for Cytochrome-C.

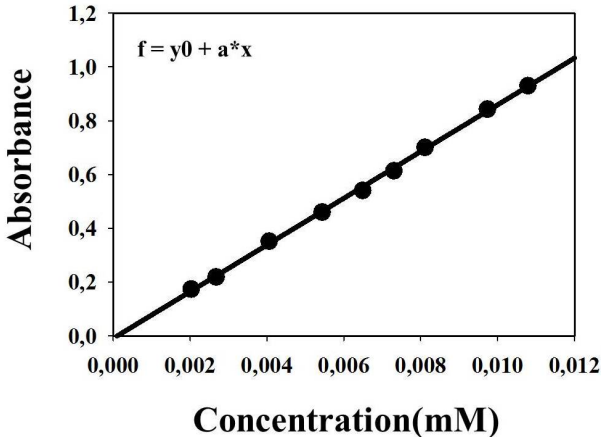

FIGURE B.3: Different Steps in coating

Appendix C

Loading Efficiencies and Encapsulation Efficiencies

C.1 Loading Efficiency

Loading efficiencies were calculated by using calibration curve of L-dopa at 281 nm and absorbance values for different systems as follows,

$$\text{Concentration} = \frac{Abs - y_0}{a^*} \tag{C.1}$$

$$= \frac{0.240 - 0.0375}{0.0135} \tag{C.2}$$

Concentration = 15.01 mg/ml

$$\text{Dilution factor} = 15.01 \times 30 = 450.22 \tag{C.3}$$

$$= \frac{450.22}{1000} = 0.45 \tag{C.4}$$

Corrected concentration before loading = 0.45 mg/ml

Concentration After loading = 0.40 mg/ml

$$\text{Loading efficiency} = \frac{\text{Mass of drug loaded}}{\text{intial mass of drug}} \times 100 \tag{C.5}$$

$$\text{Loading efficiency} = \frac{C_0 - C_1}{C_0} \times 100 \tag{C.6}$$

$$\text{Loading efficiency} = \frac{0.450 - 0.404}{0.450} \times 100 = 10.20\% \tag{C.7}$$

Loading efficiencies for Coumarin and Cytochrome C were calculated at 277 nm and 409 nm respectively using the similar procedure as used for L-dopa.

C.2 Encapsulation Efficiency

Encapsulation efficiency is calculated by using this formula

$$\text{Encapsulationefficiency} = \frac{\text{Mass of Drug loaded}}{\text{Mass of NPs}} \tag{C.8}$$

NP concentration = 5 mg/ml Drug concentration = 0.5 mg/ml

$$\text{Encapsulation efficiency} = \frac{10.22}{100} \times \frac{5}{0.50} = 0.01 mg/mg \tag{C.9}$$

$0.01 \times 1000 = 10.20 \mu g/ml$

C.3 Loading and Encapsulation efficiencies for different NPs and drug concentrations-L-dopa

TABLE C.1: Loading and Encapsulation efficiencies for different NPs and drug concentrations-L-dopa

NPs concentration (mg/ml)	n Drug concentration (mg/ml)	Loading Efficiency (%)	Encapsulation Efficiency (μg/mg)
Fe@Au_Hydrogel	**L-dopa**		
5	0.50	10.20	10.02
2.50	0.50	7.95	15.90
5.00	3	1.58	9.48
2.50	3	4.33	51.96
Fe@Au_PEG			
5	0.50	8.73	9.73
2.50	0.50	2.70	5.40
5	3	5.95	35.70
2.50	3	8.57	102.84
Fe@Au_PEG_Hydrogel			
5	0.50	2.16	2.16
2.50	0.50	5.30	10.60
5	3	7.74	46.44
2.50	3	6.08	72.96
3.75	0.50	2.14	2.85
3.75	3	8	64
10	3	5.77	17.31

C.4 Loading and Encapsulation efficiencies for different NPs and drug concentrations-Cytochrom C

TABLE C.2: Loading and Encapsulation efficiencies for different NPs and drug concentrations-Cytochrom C

NPs concentration (mg/ml)	n Drug concentration (mg/ml)	Loading Efficiency (%)	Encapsulation Efficiency (μg/mg)
Fe@Au_Hydrogel	**Cytochrome c**		
5	0.10	31.66	6.33
5	0.50	13.94	13.94
Fe@Au_PEG			
2.50	0.10	4.41	1.76
2.50	0.50	6.76	13.52
Fe@Au_PEG_Hydrogel			
3.75	0.10	32.57	8.69
3.75	0.50	12.52	16.69

C.5 Loading and Encapsulation efficiencies for different NPs and drug concentrations-Coumarin

TABLE C.3: Loading and Encapsulation efficiencies for different NPs and drug concentrations-Coumarin

NPs concentration (mg/ml)	n Drug concentration (mg/ml)	Loading Efficiency (%)	Encapsulation Efficiency (μg/mg)
Fe@Au_Hydrogel	**Coumarine**		
5	0.02	8.25	0.33
Fe@Au_PEG			
2.50	0.10	12.02	4.81
Fe@Au_PEG_Hydrogel			
3.75	0.10	12.10	3.23

Appendix D

(%) Release and Model Fitting

D.1 (%) Release

(%) Release is calculated as follows,

$$(\%)\ \text{Release} = \left(\frac{\text{Asorbance at time t initial - Absrobance at time t final}}{\text{Absorbance at time t initial}}\right) \times 100 \quad \text{(D.1)}$$

$$(\%)\ \text{Release} = \left(\frac{0.187 - 0.132}{0.187}\right) \times 100 = 29.3 \quad \text{(D.2)}$$

D.2 Mass Released (mg)

Mass release mg at time t = 2.65 is calculated by using equation below,

$$\text{Mass Released(mg)} = (\%\text{Release}) \times (\%\ \text{Loading efficiency}) \times \left(\frac{\text{Drug concentration (mg/ml)}}{100}\right) \quad \text{(D.3)}$$

$$\frac{\left((29.3) \times (31.66) \times \left(\frac{0.1}{100}\right)\right)}{100} = 0.009 \quad \text{(D.4)}$$

M_t is the cumulative drug release calculated at t = 2.65 by adding all the values of drug release up to this time point. For this case it is calculated by adding mass release at t0 and t1 and t2.

$$M_t = 0 + 0.90 + 0.93 = 1.82 \tag{D.5}$$

cumulative fraction of drug release at t = 2.65 is calculated by using following equation

$$F = \frac{M_t}{M_\infty} F = \frac{1.82}{19.85} \tag{D.6}$$

In this equation M_t is mass release at time = 2.65 while M_∞ is the mass of drug released at final time which in this case is t = 43.42.

D.3 Release modelling calculation

L-dopa Fe@Au_Hydrogel

TABLE D.1: L-dopa Fe@Au_Hydrogel

t	% Release	Mass released (mg)	Mt (mg)	F	ln(1-F)	$t^{0.5}$	ln(F)	ln(t)
0.00	0.0	0.000	0.000	0.000	0	0		
2.05	37.2	0.019	0.019	0.085	-0.089	1.4329	-2.463	0.7195
6.09	44.5	0.023	0.042	0.187	-0.207	2.4671	-1.676	1.8061
12.07	67.1	0.034	0.076	0.341	-0.417	3.4742	-1.077	2.4907
14.14	65.6	0.033	0.109	0.491	-0.675	3.7599	-0.711	2.6488
19.15	59.5	0.030	0.140	0.627	-0.987	4.3765	-0.467	2.9525
23.75	75.6	0.039	0.178	0.800	-1.611	4.8737	-0.223	3.1677
32.29	87.2	0.044	0.223	1.000		5.6821	0	3.4747

L-dopa Fe@Au_PEG

Table D.2: L-dopa Fe@Au_PEG

t	% Release	Mass released (mg)	Mt (mg)	F	ln(1-F)	$t^{0.5}$	ln(F)	ln(t)
0.00	0.0	0.000	0.000	0.000	0	0		
2.18	9.0	2.309	2.309	0.030	-0.03	1.4776	-3.506	0.7809
4.03	6.3	1.612	3.921	0.051	-0.052	2.0083	-2.977	1.3946
6.13	17.9	4.595	8.515	0.111	-0.117	2.4766	-2.201	1.8137
8.15	17.7	4.551	13.067	0.170	-0.186	2.8548	-1.773	2.098
10.18	19.4	4.999	18.065	0.235	-0.268	3.1911	-1.449	2.3208
12.23	17.3	4.460	22.525	0.293	-0.346	3.4976	-1.229	2.5042
14.27	22.9	5.879	28.404	0.369	-0.461	3.7771	-0.997	2.6579
16.33	13.2	3.392	31.796	0.413	-0.533	4.0415	-0.884	2.7932
18.43	24.6	6.317	38.113	0.495	-0.684	4.2934	-0.703	2.9142
20.47	18.9	4.849	42.962	0.558	-0.817	4.524	-0.583	3.0188
24.48	24.0	6.158	49.120	0.638	-1.017	4.9481	-0.449	3.198
27.93	14.7	3.777	52.897	0.687	-1.162	5.2852	-0.375	3.3298
48.58	37.7	9.689	62.586	0.813	-1.678	6.9702	-0.207	3.8833
59.08	55.9	14.380	76.966	1.000		7.6866	0	4.0789

L-dopa Fe@Au_PEG_Hydrogel

Table D.3: L-dopa Fe@Au_PEG_Hydrogel

t	% Release	Mass released (mg)	Mt (mg)	F	ln(1-F)	$t^{0.5}$	ln(F)	ln(t)
0.00	0.0	0.000	0.000	0.000	0	0		
1.08	0.6	0.002	0.002	0.004	-0.004427	1.0408	-5.422	0.08
3.12	9.4	0.022	0.024	0.070	-0.072951	1.7654	-2.654	1.1368
5.12	12.5	0.030	0.054	0.159	-0.172812	2.262	-1.841	1.6325
7.15	5.0	0.012	0.066	0.194	-0.215321	2.6739	-1.641	1.9671
11.22	11.0	0.026	0.092	0.271	-0.316227	3.3491	-1.305	2.4174
13.35	19.4	0.047	0.139	0.408	-0.52378	3.6538	-0.897	2.5915
15.20	16.8	0.040	0.179	0.526	-0.747269	3.8987	-0.642	2.7213
17.25	22.0	0.053	0.232	0.681	-1.142938	4.1533	-0.384	2.8478
24.67	16.3	0.039	0.271	0.796	-1.589513	4.9666	-0.228	3.2055
52.93	29.0	0.070	0.341	1.000		7.2755	0	3.969

Cytochrome c Fe@Au_Hydrogel

TABLE D.4: Cytochrome c Fe@Au_Hydrogel

t	% Release	Mass released (mg)	Mt (mg)	F	ln(1-F)	$t^{0.5}$	ln(F)	ln(t)
0	0	0.000	0.000	0.000	0	0		
1.6	28.3	0.009	0.009	0.045	-0.04619	1.2649	-3.098	0.47
2.65	29.3	0.009	0.018	0.092	-0.09636	1.6279	-2.387	0.9746
3.65	31.5	0.010	0.028	0.142	-0.15327	1.9105	-1.951	1.2947
5.63	31.8	0.010	0.038	0.193	-0.21421	2.3728	-1.646	1.7281
7.65	35.4	0.011	0.049	0.249	-0.28673	2.7659	-1.389	2.0347
9.63	37.7	0.012	0.061	0.309	-0.37021	3.1032	-1.173	2.2649
11.93	38	0.012	0.073	0.370	-0.46206	3.454	-0.994	2.4791
15.85	41.9	0.013	0.087	0.437	-0.5742	3.9812	-0.828	2.7632
20.85	40.1	0.013	0.099	0.501	-0.69474	4.5662	-0.692	3.0374
25.47	49.7	0.016	0.115	0.580	-0.86765	5.0468	-0.545	3.2375
29.62	44.7	0.014	0.129	0.651	-1.0537	5.4424	-0.429	3.3884
33.98	54.6	0.017	0.147	0.738	-1.34108	5.8292	-0.303	3.5258
37.1	54	0.017	0.164	0.825	-1.74047	6.091	-0.193	3.6136
39.62	54.6	0.017	0.181	0.912	-2.42637	6.2944	-0.093	3.6793
43.42	55.4	0.018	0.199	1.000		6.5894	0	3.7709

Cytochrome c Fe@Au_PEG

Table D.5: Cytochrome c Fe@Au_PEG

t	% Release	Mass released (mg)	Mt	F	ln(1-F)	$t^{0.5}$	ln(F)	ln(t)
0.00	0.00	0.000	0.000	0	0	0.00		
0.63	24.88	0.008	0.008	0.0259	-0.0263	0.80	-3.652	-0.457
1.60	45.98	0.016	0.024	0.0739	-0.0768	1.26	-2.605	0.47
2.65	63.15	0.021	0.045	0.1397	-0.1505	1.63	-1.968	0.9746
3.78	45.15	0.015	0.061	0.1868	-0.2068	1.95	-1.678	1.3306
5.75	61.78	0.021	0.081	0.2512	-0.2893	2.40	-1.381	1.7492
7.77	53.70	0.018	0.100	0.3072	-0.367	2.79	-1.18	2.0498
9.75	68.21	0.023	0.123	0.3783	-0.4754	3.12	-0.972	2.2773
12.10	85.95	0.029	0.152	0.468	-0.631	3.48	-0.759	2.4932
16.03	88.61	0.030	0.182	0.5604	-0.8218	4.00	-0.579	2.7747
21.03	73.34	0.025	0.206	0.6368	-1.0129	4.59	-0.451	3.0461
25.65	80.16	0.027	0.234	0.7204	-1.2744	5.06	-0.328	3.2445
29.78	87.75	0.030	0.263	0.8119	-1.6708	5.46	-0.208	3.3939
34.15	91.26	0.031	0.294	0.9071	-2.3757	5.84	-0.098	3.5308
43.40	89.14	0.030	0.324	1		6.59	0	3.7705

Cytochrome c Fe@Au_PEG_Hydrogel

Please add the following required packages to your document preamble: booktabs graphicx

Table D.6: Cytochrome c Fe@Au_PEG_Hydrogel

t	% Release	Mass released (mg)	Mt	F	ln(1-F)	$t^{0.5}$	ln(F)	ln(t)
0.00	0.00	0.000	0.000	0	0	0.00		
0.55	30.05	0.010	0.010	0.0433	-0.044	0.74	-3.139	-0.598
1.52	29.49	0.010	0.019	0.0858	-0.09	1.23	-2.456	0.4165
2.55	31.04	0.010	0.030	0.1306	-0.14	1.60	-2.036	0.9361
3.53	30.42	0.010	0.039	0.1744	-0.192	1.88	-1.746	1.2622
5.53	36.55	0.012	0.051	0.2271	-0.258	2.35	-1.482	1.7108
7.52	39.19	0.013	0.064	0.2836	-0.333	2.74	-1.26	2.0171
9.45	38.80	0.013	0.077	0.3395	-0.415	3.07	-1.08	2.246
11.67	41.08	0.013	0.090	0.3987	-0.509	3.42	-0.92	2.4567
15.48	43.56	0.014	0.104	0.4615	-0.619	3.93	-0.773	2.7398
20.50	45.28	0.015	0.119	0.5268	-0.748	4.53	-0.641	3.0204
25.10	43.57	0.014	0.133	0.5896	-0.891	5.01	-0.528	3.2229
29.17	44.23	0.014	0.148	0.6533	-1.059	5.40	-0.426	3.373
33.72	49.02	0.016	0.164	0.724	-1.287	5.81	-0.323	3.518
36.53	47.21	0.015	0.179	0.792	-1.57	6.04	-0.233	3.5982
38.97	44.8790637	0.015	0.194	0.8567	-1.943	6.24	-0.155	3.6627
42.77	48.5825748	0.016	0.209	0.9267	-2.614	6.54	-0.076	3.7558
47.73	50.8296489	0.017	0.226	1		6.91	0	3.8656

Appendix E

VPTT Calculations

E.1 Procedure used to calculate VPTT

Developed approach, which was used to evaluate collapse temperature involves plotting a spectroscopic parameter along with temperature. The following plot E.1 represents the variation of Optical Density along with Absolute Temperature;

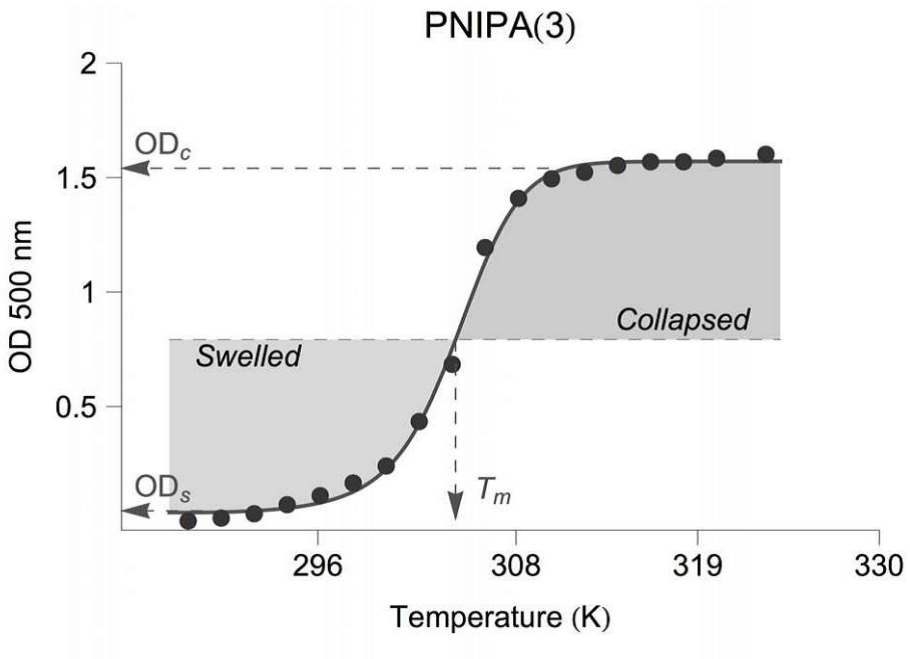

FIGURE E.1: variation of Optical Density along with Absolute Temperature

The experimental parameter taken into account for our studies is 'Alpha', which is defined as,

$$\alpha = \left(\frac{D_H}{D_0}\right)^3 \tag{E.1}$$

Hydrogel is a mixture of moieties with different sizes. As a result of which, the hydrogel doesn't have a distinctive value of collapse temperature, but varies over a range. Alpha is plotted against temperature. At any point on the curve, the hydrogel exists in a partially collapsed state. Therefore, we can assume that at the mean collapse temperature, denoted by (T_m), of the complete hydrogel, the collapsed state lies in equilibrium with the swelled state. The swelled state area lies to the left of Tm on the swelling curve, whereas the collapsed state area lies to the right of Tm.

The program tries to find out the probable value of collapse temperature by equating the swelling and the collapsed state areas. Therefore, at the ideal situation, both these areas should be equal. The area is calculated by integrating the curve and the method applied here is the "Simpson's 1/3rd Rule" which calculates the area under the curve by integrating the function as follows,

$$\int_a^b f(x)\,dx \approx \tfrac{h}{3}\Big[f(x_0) + 2\sum_{j=1}^{n/2-1} f(x_{2j}) + 4\sum_{j=1}^{n/2} f(x_{2j-1}) + f(x_n)\Big],$$

FIGURE E.2: Equation used to estimate area under the curve

For the first part of the curve, measured from the lower temperature (T_a), the system integrates between the limits T_a to T_m. Similarly, for the next part of the curve, the limits vary from Tm to the higher temperature limit, i.e. (T_b). SigmaPlotTM version 12.5 is used as a tool to plot the data points and obtain a smooth curve fit using the Equation Category – 'Sigmoidal' and in it the Equation Name – 'Sigmoid, 5 Parameter'. The fit, shown by equation below, provides the user the value of 5 parameters which the user needs to input into the MATLAB code.

$$y = y_0 + \frac{a}{\left(1 + e^{-\left(\frac{x - x_0}{b}\right)}\right)^c}$$

FIGURE E.3: 'Sigmoid, 5 Parameter' equation

The user then runs the code and enters these parameters along with the value of relative tolerance as well as the number of iterations desired by the user. The program calculates the collapse temperature by calculating the relative difference in the areas of the collapsed as well as the swelled state up to the input tolerance value. The program, automatically adjusts the value of the number of iterations, if the desired tolerance is not reached within the iterations provided by the user. At the end of the program run, it also generates the curve, thereby confirming with the SigmaPlotTM curve about the

dependency as well as the reliability of the MATLABTM code. The point, marked with a red circle on the curve, depicts the collapse temperature of the entire system. It is to be noted that the user is free to enter the temperature in the absolute, as well as the Celsius scale. The program can be used to study both, the heating as well as the cooling curves.

The choice of the tolerance and the number of iterations has been left with the user. A higher degree of precision has been observed by choosing a lower value of tolerance or a higher number of iterations. For this particular study case, the value of tolerance has been set to 0.001 and collapse temperature has been calculated by changing the number of iterations. A mean value of all these collapse temperatures is then selected as the overall collapse temperature of the system (separately for heating and cooling).

Appendix F

UV-vis and DLS Plots

F.1 UV-vis spectra for step wise coating of Hydrogel on Fe@Au

This Figure F.1 is showing UV-vis spectra for step wise coating of Hydrogel on Fe@Au.

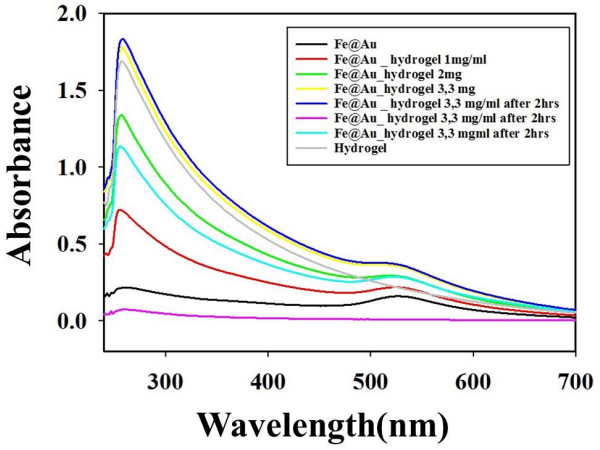

FIGURE F.1: UV-vis spectra for step wise coating of Hydrogel on Fe@Au

F.2 UV-vis spectra of Fe@Au, Hydrogel, Fe@Au_Hydrogel M1 and M2

UV-vis spectra for effect of coating of Hydrogel with method 1 and method 2 is shown in the Figure F.2,

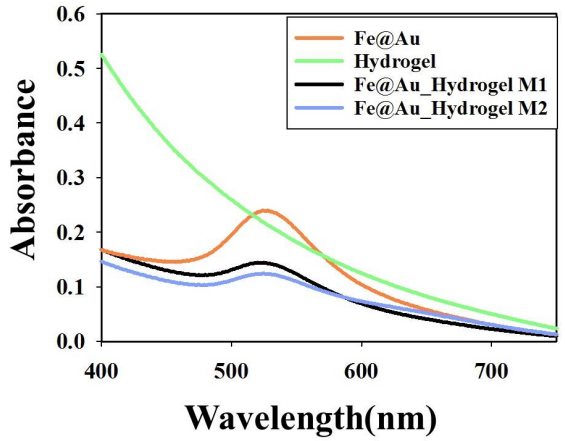

FIGURE F.2: UV-vis spectra of Fe@Au, Hydrogel, Fe@Au_Hydrogel M1 and M2

F.3 UV-vis spectra of Fe@Au, Fe@Au_Hydrogel M1 and M2

Figure F.3 UV-vis spectra of Fe@Au and coating of Fe@Au by method 1 and 2.

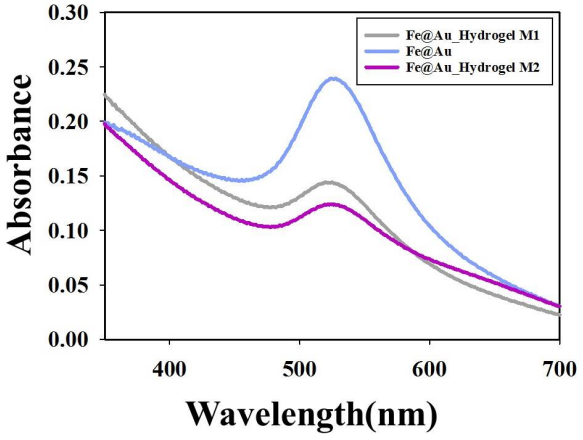

FIGURE F.3: UV-vis spectra of Fe@Au, Fe@Au_Hydrogel M1 and M2

F.4 Reversibility of Fe@Au_Hydrogel M1

Reversibility of Fe@Au_Hydrogel caoted by method 1 at a heating rate of 10 C is shown in the Figure F.4

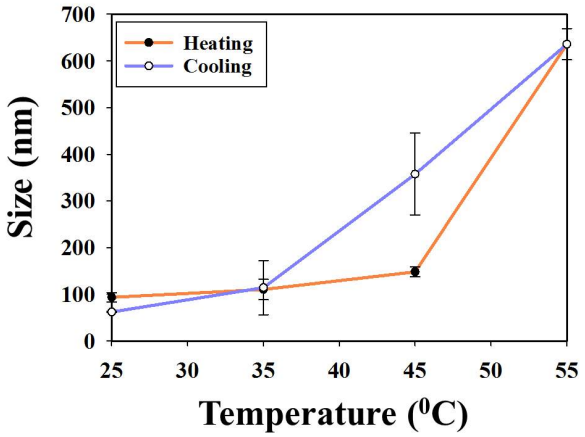

FIGURE F.4: Reversibility of Fe@Au_Hydrogel M1 at a heating rate of 10 C

F.5 Reversibility of Fe@Au_Hydrogel M2

Reversibility of Fe@Au_Hydrogel caoted by method 1 at a heating rate of 10 C is F.5.

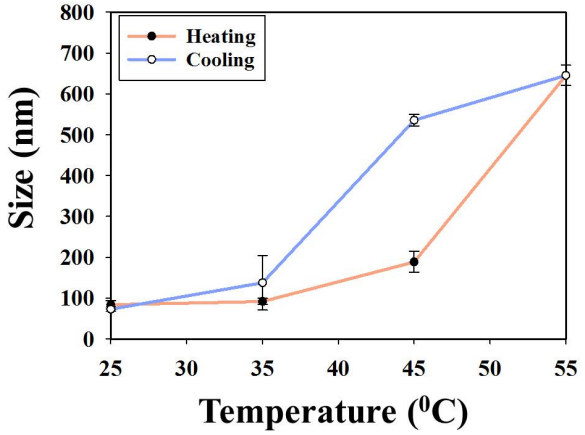

FIGURE F.5: Reversibility of Fe@Au_Hydrogel M1 at a heating rate of 10 C

F.6 Variation in size at different hydrogel concentrations

The Figure F.6 is showing Variation of Size with the concentration of hydrogel

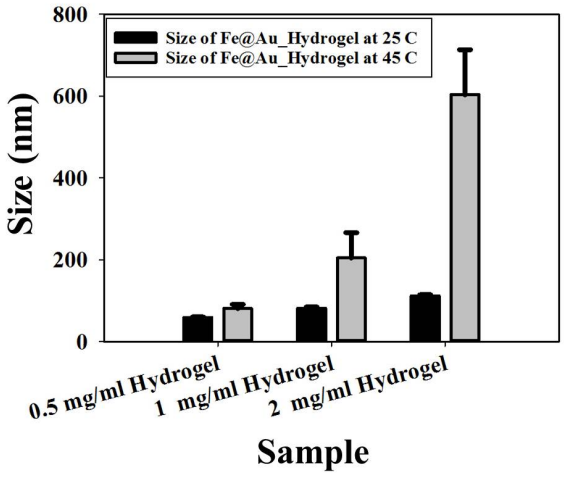

FIGURE F.6: Variation in size at different hydrogel concentrations

F.7 Cyclic measurements of Hydrogel at 25 ^{o}C and 40 ^{o}C

The Figure F.6 is showing cyclic size measurements for hydrogel at 25 ^{o}C and 40 ^{o}C

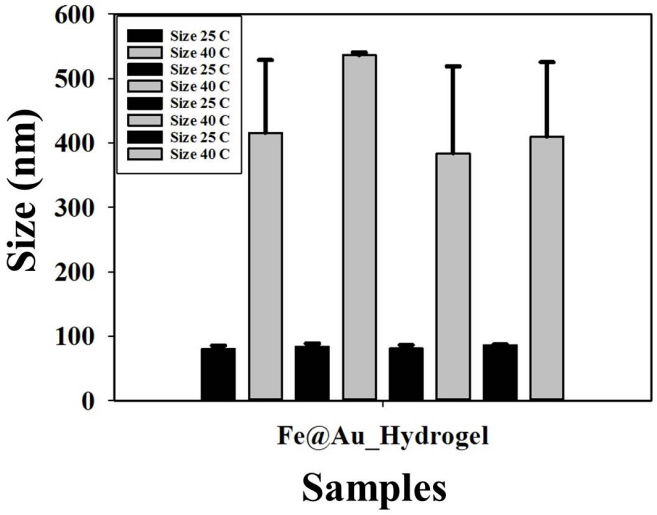

FIGURE F.7: Cyclic measurements of Hydrogel at 25 ^{o}C and 40 ^{o}C

Appendix G

Choice of drug concentrations

G.1 Coumarin

Coumarin Drug concentration

L-Dopa minimum concentration used = 0.50 mg/ml L-Dopa maximum concentration used = 3.00 mg/ml L-Dopa solubility = 3.20 mg/ml coumarine solubility (y) = 0.10 mg/ml

x for 0,5 mg/ml drug concentration = $\frac{0.50}{3.20} \times 100 = 15.63$

x (%) of y = $\frac{15.63}{100} \times 0.10 = 0.015625$

x for 3 mg/ml drug concentration = $\frac{3}{3.20} \times 100 = 93.75$

x (%) of y = $\frac{93.75}{100} \times 0.10 = 0.09375$

Coumarin Drug concentration used

= 0.02 mg/ml and 0.1 mg/ml